Journal of the European Ceramic Society 35 (2015) 4327–4369

Contents lists available at www.sciencedirect.com

Journal of the European Ceramic Society

journal homepage: www.elsevier.com/locate/jeurceramsoc

Ceramics and ceramic coatings in orthopaedics

B.J. McEntire[a,*], B.S. Bal[a,b], M.N. Rahaman[c], J. Chevalier[d], G. Pezzotti[e,**]

[a] Amedica Corporation, 1885 West 2100 South, Salt Lake City, UT 84119, United States
[b] Department of Orthopaedic Surgery, University of Missouri, Columbia, MO 65212, United States
[c] Department of Materials Science and Engineering, Missouri University of Science and Technology, Rolla, MO 65409, United States
[d] University of Lyon, INSA-Lyon, MATEIS UMR CNRS 5510, 20 Avenue Albert Einstien, Villeurbanne 69621, France
[e] Ceramic Physics Laboratory, Kyoto Institute of Technology, Sakyo-ku, Matsugasaki, 606-8126 Kyoto, Japan

ARTICLE INFO

Article history:
Received 20 April 2015
Received in revised form 28 July 2015
Accepted 29 July 2015
Available online 2 October 2015

Keywords:
Bioceramics
Ceramic coatings
Implants
Orthopaedics
Arthroplasty

ABSTRACT

Advanced bioceramics have played integral roles in treatment modalities for damaged or diseased human joints and osseous defects. This paper reviews the uses and properties of ceramics and ceramic coatings variously employed as articulation devices in hip, knee, shoulder, and other joints, either as self-mated surfaces, or against polyethylene (both conventional and highly cross-linked versions), or for osseous- fixation as arthrodesis devices, bone scaffolds, and substitutes in the spine or extremities. The modern uses of oxide and non-oxide materials in these applications will be discussed, followed by an assessment and comparison of their mechanical and physicochemical properties. Recent developments in new bioceramic materials and composites along with advanced processing and testing methods are presented. Advanced bioceramics and coatings are expected to have increasing use in orthopaedics because of their unique combination and range of properties including strength and toughness, hardness and wear resistance, biocompatibility, bacteriostasis, and osseointegration.

1. Introduction

Orthopaedic reconstructive surgery typically involves the use of prosthetic biomaterials to repair or replace damaged or diseased musculoskeletal tissue in order to relieve pain and restore function for patients suffering from bone fractures, tumors, congenital deformities, arthritis, osteoporosis, scoliosis, infection, and other etiologies coincident with an ageing population. While these procedures were envisioned by medical practitioners for a long time, it was not until the advent of safe anesthesia techniques, sterility, and improved biomaterials in the 20th century that prosthetic correction of bone defects and replacement of diseased or damaged joints became practical [1]. The pioneering work in total hip arthroplasty by Sir John Charnley in the 1960s [2,3] paved the way for reconstructive procedures in other areas, including spine, knee, shoulder, ankle, wrist, and phalanges. Worldwide, the number of people affected from bone and joint disorders was estimated to be 1.78 billion in 2012, with spinal and lower extremity disabilities being the most prevalent [4]. In 2010–2011, the number of musculoskeletal surgeries in the US alone was 3.79 million [5], with joint arthroplasty accounting for more than half of this total [6–10]. Further, from a global perspective, approximately 2.9 million joint replacement surgeries take place annually, including more than 1.4 million hip, 1.1 million knee, and over 100,000 shoulder replacements [11].

Ceramics and ceramic coated devices have been incorporated into various prostheses almost from inception either for osseous-fixation or articulation devices. Current ceramics include alumina (Al_2O_3), zirconia (ZrO_2), zirconia-toughened alumina (ZTA), alumina matrix composites (AMC), alumina-toughened zirconia (ATZ), silicon nitride (Si_3N_4), and hydroxyapatite (HAp); whereas ceramic coatings encompass diamond-like carbon (DLC), titanium nitride (TiN), zirconium nitride (ZrN), titanium–niobium-nitride (TiNbN), calcium phosphates ($Ca_3(PO_4)_2$), and also hydroxyapatite ($Ca_{10}(PO_4)_6(OH)_2$). Although not strictly regarded as a coating (but as a native oxide layer), another popular metallic-ceramic composite is an *in situ* grown monoclinic zirconia onto a zirconium niobium alloy (*i.e.*, oxidized zirconia, OxZr). All of these materials have found various applications in orthopaedic surgery during the late 20th and early 21st centuries. The purpose of this review is to discuss the uses of these ceramics and ceramic coatings, provide comparative analyses of their physical and mechanical properties, present their *in vitro* and *in vivo* performance, and correlate these to physicochemical observations.

* Corresponding author. Fax: +1 801 539 3605.
** Corresponding author. Fax: +81 75 724 7568.
E-mail addresses: bmcentire@amedica.com (B.J. McEntire), Pezzotti@kit.ac.jp (G. Pezzotti).

http://dx.doi.org/10.1016/j.jeurceramsoc.2015.07.034
0955-2219/

2. Modern uses of orthopaedic ceramics and coatings

An excellent review of the early history of arthroplasty including the use of ceramics was provided by Steinberg et al [1]. This section will not retrace their effort but instead focus on developments during the past century. There has been explosive growth in the science and application of biomaterials in joint replacement during the past 50 years. In fact, total hip arthroplasty has been referred to as the most successful operation of the 20th century [12]; and its success has led to the development of arthroplastic procedures for other human joints. Ceramic materials have been integral to this evolution. They were first considered for use as prostheses in the 1920s when hip reconstructive procedures were devised using hollow hemispherical molded glass as femoral heads. However, these devices lacked sufficient strength and toughness to withstand acetabular loads and many fractured *in vivo* [13]. A nearly 50 year hiatus ensued during which physicians turned principally to metals and polymers. However, in the latter third of the 20th century, orthopedists returned to ceramics because of favorable properties such as biocompatibility, strength, hardness, wear, and corrosion resistance. This period saw the introduction and proliferation of alumina, hydroxyapatite, zirconia, silicon nitride, ceramic-coated metals, and zirconia-toughened alumina. For an in-depth treatise on the physicochemical characteristics of most of these biomaterials, the interested reader is referred to a recently published work by Pezzotti [14].

2.1. Alumina

Interest in polycrystalline bioceramics started in 1970 when Dr. Pierre Boutin implanted the first hip prostheses with Al_2O_3 ceramic bearings [15,16]. His success led to a string of ceramic biomaterial innovations, with patents appearing shortly thereafter claiming various ceramics, including Al_2O_3, as viable orthopedic materials [17–20]. Recognizing a potential for limb reconstruction and correction of skeletal defects in veterans, the US Defense Department investigated and demonstrated the usefulness of porous Al_2O_3 as a bone scaffold in 1972 [21], and a similar Scandinavian study in 1973 established its osseointegration effectiveness [22]. Al_2O_3 has been the most widely used structural ceramic in total hip arthroplasty (THA) for the past approximately 50 years, typically in articulation against polyethylene [23] or itself [24,25]. Its success in THA led to its adoption in other joints including knee [26,27], elbow [28], ankle [29], wrist [30], phalanges [31], spine [32,33], and also bone reconstruction [34]. Industrial specifications for its composition, processing, and properties have been issued [35,36]. It has been repeatedly shown to be biocompatible [16,37], possessing high hardness and a low coefficient of friction, all of which significantly reduce the occurrence of wear debris [38]. However, it also has relatively modest fracture strength and toughness, both of which increase the risk of brittle failure [39,40]. Yet, enhanced reliability has been realized with three generations of processing improvements, including increased raw material purity, refinement of its microstructure, use of hot- isostatic pressing (HIP), and inclusion of post-manufacturing proof testing [41].

2.2. Hydroxyapatite and calcium phosphates

Apatite-based ceramics were investigated and introduced in the 1960–70s concurrent with Al_2O_3 [42], although their therapeutic bone remodeling benefits have been known for centuries [43]. β-Tri-calcium phosphate ($Ca_3(PO_4)_2$, TCP) and its close chemical cousin, calcium hydroxyapatite ($Ca_{10}(PO_4)_6(OH)_2$, HAp), in granular, porous and dense forms, were suggested as corrective therapies for various bone defects, such as tooth repair and replacement, alveolar ridge augmentation, maxillofacial reconstruction, ossicles bone repair, or as burr-hole buttons, orbital implants, spinal fusion devices, and bone scaffolds [44–46]. Their early use in dental procedures resulted in marked improvement in osseointegration [47]. This success provided incentives to other researchers to apply hydroxyapatite coatings onto femoral stems and cups in total hip arthroplasty. Clinical trials of coated hip stems were initiated by the mid-1980s [48], with follow-up on a number of these studies now exceeding 20 years [49–52]. Today HAp is the most used non-structural ceramic in joint arthroplasty [53]. Unfortunately, it cannot be employed in load bearing devices due to its extreme brittleness and poor strength. Its usefulness is solely for the promotion of new bone growth. HAp is considered osteoconductive similar to autologous or allograft bone. When exposed to physiologic fluids, it releases ions that stimulate bone formation and bone bonding, which aids in the stabilization and fixation of implants possessing porous ingrowth surfaces. Although porous metals, such as titanium alloys, are capable of similar bone ongrowth or ingrowth even without hydroxyapatite coatings, HAp accelerates the appositional process, and is used clinically. The original (and still preferred) method of applying hydroxyapatite is by thermal spraying of synthesized powders at temperatures between 15,000 K and 30,000 K to form thin (50–150 μm) surface coatings, with roughened or porous titanium being the preferred metallic member [54,55]. Melting of the hydroxyapatite occurs within the plasma stream, and fortuitously, when the particles impact on the cooler metallic substrate, a range of disordered calcium phosphate phases are formed possessing differing biologic dissolution kinetics, which favor both short- and long-term osseointegration. These phases include predominately amorphous calcium phosphate (ACP), α- and β-tri-calcium phosphates (TCP), and hydroxyapatite (HAp). The reported relative biological solubility of these compounds is as follows: ACP ≫ α- or β-TCP ≫ HAp [55]. Their dissolution rate is not only related to crystal chemistry, but also affected by physical parameters such as the size of melted splats, the amount of porosity within the coating, the presence of thermally induced cracks, pits or other defects, and the coating's crystallinity. Reportedly, initial bone growth occurs at an enhanced rate when the coating contains a higher percentage of the amorphous phase [55]. Its dissolution increases the local concentration of calcium and phosphate ions followed by precipitation of a calcium carbonaceous phosphate with a composition similar to native bone. These precipitates attract osteoblasts inducing bone growth towards the implant. Concurrently, osteoclasts remodel native bone surrounding the implant according to applied physiologic stresses. The osteoclast cells dissolve the carbonate precipitates as new native bone grows into fissures, pits, and defects of the slower resorbing HAp during post- operative periods. Poor fixation and implant loosening may occur if the applied coating has too much ACP or TCP. High concentrations of these two phases results in rapid bone formation at the expense of longer-term osseointegration. Conversely, an insufficient amount of these compounds will fail to attract the necessary osteoblasts to initiate fixation; or the higher concentration of HAp can occlude the porosity of the underlying metallic surface thereby failing to achieve adequate apposition of the implant and native bone [56,57]. Herein lies the key concern and controversy of HAp coated implants. Resorption kinetics govern implant fixation. Thermal spraying conditions have been experimentally determined to achieve appropriate concentrations of ACP, TCP, and HAp. The HAp feedstock composition, purity, particle size, gas- stream temperature and its composition, and substrate temperature are among the important experimental parameters. Recent work has also explored the preparation and characterization of biomimetic and nano-hydroxyapatite compositions with the hope that they might also lead to improved implant fixation [58–60]. Although not indispensable in arthroplasty surgery, HAp and its associated calcium phosphates are

useful for promoting bone ingrowth and accelerating the biologic anchoring of joint prostheses to host bone. Their effectiveness for this purpose continues to be robustly demonstrated and reviewed [53,61–63,656].

2.3. Zirconia

Continuing concerns over *in vivo* fractures of Al_2O_3 femoral heads and liners in total hip arthroplasty in the 1980s led to the introduction of zirconia ceramics in 1985 [64], including partially stabilized zirconia using magnesia (Mg-PSZ) and a yttria-doped composition known as Tetragonal Zirconia Polycrystals (Y-TZP) [64–66]. These ceramics represented a new generation of implants. They were biocompatible [37] and had approximately twice the strength and toughness of Al_2O_3 [66]. They also had exceptionally low coefficients of friction and lower wear on polyethylene. They promised to provide a new level of care and safety over metallic and Al_2O_3 implants [64,67–69]. Their improved mechanical properties were achieved by taking advantage of a polymorphic phase transformation that occurs in doped zirconia known as phase transformation toughening [70]. This mechanism involves the meta-stabilization of a high-temperature tetragonal phase through the incorporation of magnesia, yttria, or other dopants. In the presence of an advancing crack, the metastable phase transforms to its stable monoclinic polymorph with an accompanying volume increase of ~4–5%. The sudden volume change exerts compressive forces on the crack tip, thereby slowing or arresting its propagation. Mg-PSZ implants entered the marketplace and an industrial standard for their composition, processing, and properties was created [71]. However, the strength of Mg-PSZ was inferior to Y-TZP, so, considerable physician interest and rapid uptake of Y-TZP ceramics occurred after its clearance by US and EU regulatory bodies. Over 600,000 Y-TZP femoral heads were implanted between 1985 and the turn of the century largely based on bench test data, with little clinical evidence as to the material's longer-term effectiveness [72,73]. There were initially few reported *in vivo* failures [69], but a change in manufacturing methods (from batch to tunnel furnace) by the leading vendor of Y-TZP in 1998 resulted in a significant increase in fractures beginning in 2000, many occurring only months after implantation [73]. Independent investigations by a number of scientific groups in cooperation with regulatory agencies highlighted the material's inherent instability [72–74]. After more than a decade of use, Y-TZP was withdrawn from the US and EU markets in 2001 and its industrial standard was subsequently abandoned [75]. Despite its improved initial strength, Y-TZP possesses one critical weakness. It may spontaneously transform to its stable monoclinic form under *in vivo* conditions. This effect has become known as low-temperature hydrothermal degradation (LTD) [76]. The transformation results in increased implant surface roughness, enhanced wear, weakening of the material, and eventual fracture [72–74,77,78]. Despite its withdrawal from EU and US markets, Y-TZP femoral heads are still available for implantation in Asia, and recent physical chemistry analyses suggest that the unconstrained transformation experienced by the original EU manufacturer may be limited and controlled through improved processing and careful assessment before clinical use [79]. Y-TZP is also extensively used and preferred as esthetic and functional dental prostheses [80], although concerns have also been raised about its longevity in this application due to low-temperature hydrothermal degradation [81]. LTD is considered the Achilles' heel of zirconia with its occurrence being highly dependent on its microstructure; therefore, the overall process must be strictly controlled and any change in one of the process steps must be carefully assessed. In other, simple terms, Y-TZP may perform better than Al_2O_3 but is less robust as far as industrial variations are concerned.

2.4. Silicon nitride

Silicon nitride (Si_3N_4) is another high-strength and tough industrial ceramic which is also considered to be a viable implant material [82–84]. In 1986, it was first utilized in a small clinical trial in Australia (30 patients) to determine its capability as an arthrodesis device in the lumbar spine [85]. This medical study happened to coincide with massive investments by the US Government in the development of this new ceramic for aerospace, automotive, and industrial applications [86–90], although no funding was ever channeled to medical devices at that time. Over two decades passed before Si_3N_4 became a commercially available biomaterial in the US and EU, partially thanks to a small grant from the US National Institutes of Health [91]. Since 2008, it has been used as a fusion cage for arthrodesis of the cervical and thoracolumbar spine [92]; and to date, approximately 25,000 Si_3N_4 spinal fusion cages have been implanted with few adverse reported events [93]. Extensive testing of silicon nitride has indicated its potential as an articulation member as well, but it has yet to be cleared by regulatory agencies for this purpose [82,94]. Two industrial standards have been adopted for its composition, processing, and properties [95,96]. They are appropriate for its use as a biomaterial, but need to be augmented with provisions that address biologic issues. Si_3N_4 has been shown to be biocompatible, possessing favorable cell interaction characteristics [83,84,97–102]. These and other studies indicate that porous or unpolished Si_3N_4 osteointegrates with adjacent bone [102–106] and exhibits bacteriostasis [106,107] . In its dense and polished form, it has been shown to produce implants with exceptionally low wear rates [108–118]. Its strength and toughness are comparable to the best values obtained for other polycrystalline ceramics [82]. Si_3N_4 derives its strength and toughness through microstructural engineering and not from phase transformation. Similar to Al_2O_3, Si_3N_4 exists as an irreversibly stable phase at room temperature; but unlike Al_2O_3, its microstructure is composed of asymmetric needle-like interlocking grains surrounded by a thin (<2 nm) refractory grain-boundary glass [119]. This unique structure provides Si_3N_4 with exceptional strength and toughness. An advancing crack must navigate a tortuous high energy path through the ceramic, and bridging grains within the crack wake restrict its continued propagation [120–122]. Si_3N_4 can not only be produced as a polycrystalline ceramic, but it can also be applied as a wear resistant coating using physical vapor (PVD) or chemical vapor deposition (CVD) methods [123–127]. Si_3N_4 is the only ceramic material being considered thus far for both bulk and metal-coated orthopedic applications. Although bulk and coated silicon nitrides are chemically similar, the coated material is amorphous or nano-crystalline and non-stoichiometric. It can be either silicon or nitrogen rich and may also contain other elements, either by design or as impurities, such as carbon, oxygen, or fluorine. Mechanically, it does not have the same strength or toughness as the polycrystalline material, but can have comparable hardness.

2.5. Ceramic coatings for bearing applications

Other ceramic coatings for medical applications predated silicon nitride. The first of these was PVD deposited titanium nitride (TiN) on titanium. It was developed and introduced into the marketplace for total joint arthroplasty beginning in the late 1980s [128] with formal clinical investigations beginning in 1990 [129–131]. At about this same time, another hard coating, diamond-like carbon (DLC), was applied to titanium implants for shoulder, ankle, and knee arthroplastic devices in Europe. However, no pre-operative *in vitro* testing of these DLC coated implants was ever conducted. Neither were there any clinical data nor regulatory oversight because the manufacturer failed to obtain the necessary clearances prior to marketing these devices. Consequently, these products fared poorly

and were quickly removed from distribution [132]. The first and only legitimate premarket approved clinical trial of DLC coated devices was initiated in 1993 [133]. Other hard ceramic coatings were subsequently introduced, including zirconium nitride (ZrN) on a cobalt chromium (CoCr) substrate [134] and titanium niobium nitride (TiNbN) also on CoCr [135,136]. These single or mixed nitride coatings are nano-crystalline and have thicknesses in the range of 1 μm to 15 μm. All have been shown to be biocompatible [123–127,136–139], and they are currently used or considered for use as hip resurfacing implants, for total hip arthroplasty, or as femoral knee components. In 1997 another new metal–ceramic composite was introduced via clinical trials [140,141]. Known by the trade name of Oxinium® [142], it is not technically a coating. It consists of a ~5 μm thick monoclinic ZrO_2 ceramic layer which is grown *in situ* on a Zr–2.5Nb alloy. However, like coatings, it combines the strength of a metal core with the wear resistance of a ceramic surface. This composite has been shown to be biocompatible [143] and is currently successfully used in both hip and knee arthroplasty [144,145]. In principle, ceramic coatings appear to be excellent solutions for three prevalent problems in articulating prostheses. First, they eliminate brittle fracture because of their high toughness metallic substrates. Second, in comparison to metal implants, they minimize wear debris due to the high hardness and abrasion resistance of the outer ceramic layer. Third, they place a barrier between the metallic implant and human bone or tissue, which lessens allergic reactions from soluble metal ions (Co, Cr, and particularly Ni) for hypersensitive patients [146]. However, there are concerns with all thin ceramic coatings or layers. Their fabrication processes can generate high surface stresses, which challenge adhesion to their respective substrates. Thermal expansion differences can exacerbate these stresses. Also, *in vivo* scratching, pitting, or even delamination of these coatings have been observed [147–149], leading to increased surface roughness and excessive wear of the coating, the underlying metal, or the counterface material [150,151].

2.6. Zirconia toughened alumina

A group of new ceramics containing mixtures of Al_2O_3 and ZrO_2 were brought to US and EU markets beginning in about 2000, almost simultaneous with the withdrawal of Y-TZP [152]. They were introduced in an attempt to overcome the hydrothermal deficiencies of Y-TZP and the relatively modest strength of Al_2O_3. At one end of the composition spectrum are zirconia-toughened alumina (ZTA) [153,154] and an alumina matrix composite (AMC) [152]. ZTA is a fully dense ceramic consisting typically of about 7–25 wt.% unstabilized ZrO_2 or Y-TZP incorporated into an Al_2O_3 matrix [155,156]. Alternative ZTA materials have also been developed using cerium oxide as the stabilization additive instead of yttria [157–159]. AMC became a special ZTA composition consisting of 24 wt.% ZrO_2 (*i.e.*, 17 vol.%) with 1.7 wt.% mixed oxides (Y_2O_3, Cr_2O_3, and SrO), the balance being Al_2O_3 (74 wt.%) [160]. Since its introduction in 2000, AMC has become the most popular orthopaedic ceramic for articulation implants used in the world today. It is commercially known as BIOLOX® *delta* [160]. An industrial standard for its composition and testing has been prepared and published [161]. At the opposite end of the spectrum, but still consisting of Al_2O_3 and ZrO_2, is alumina-toughened zirconia (ATZ) [162]. ATZ is also a completely dense ceramic composed of 80 wt.% Y-TZP and 20 wt.% Al_2O_3 [162]. As might be expected, this broad range of Al_2O_3–ZrO_2 mixtures resulted in marked differences in properties, but all are superior to both pure Al_2O_3 and Y-TZP. All have been tested and determined to be biocompatible [163,164]. They have excellent strength, toughness, and hardness [154,165,166], and are highly abrasion [167] and wear resistant [168–174]. Clinical studies using these devices have been on-going since their introduction with acceptable overall outcomes [172,175–178]. However, they all achieve their enhanced mechanical properties through transformation toughening, and may be susceptible to *in vivo* hydrothermal instability, although its effects are retarded due to the presence of the non-transforming Al_2O_3 phase.

Undoubtedly, there will be other ceramics and coatings considered for arthroplasty over the coming decades as scientists and engineers attempt to match specific material properties or characteristics to existing or new orthopaedic applications. However, in learning from past experience, they will likely be introduced gradually [179], and only after significant scientific *in vitro* and *in vivo* scrutiny.

In the following sections, a comparative review of the physical and mechanical properties of these ceramics and coatings will be provided and correlated with available *in vitro* and *in vivo* data for their specific applications. The physicochemical stability of each material will follow, along with a discussion of degradation mechanisms. A summary of important findings and future directions for research and product development will be given.

3. Properties and performance

This section is devoted to a comparative discussion of ceramic material properties, bio-stability, *in vitro*, and *in vivo* performance as they relate to specific applications. Certain properties are unavailable for some materials, particularly the coatings; and the range of applications precludes direct comparison of some performance characteristics. In addition, differences in testing methods used in assessing properties make precise comparisons problematic. Nevertheless, given in Tables 1a and 1b are representative values for the physical and mechanical properties of polycrystalline ceramics and ceramic coatings contained within this review, respectively. Two medical grade alloys (CoCr and Ti6Al4V) and polyetheretherketone (PEEK) are included in Table 1a for comparison purposes. The data provided in these tables were compiled from peer-reviewed literature cited in this review. It is important to note that these published values are not considered material specifications. ASTM and/or ISO standards have been prepared for the bulk ceramics [35,36,71,75,95,96,161] and key specifications from these standards are shown in Table 2. These specifications reasonably represent the properties that orthopaedic implants must meet when they leave their respective manufacturing plants. A perusal of this information provides an interesting contrast between reported data from technical literature and actual specifications from the standards. They indicate considerable equivalence for bioceramics used in similar applications. Standard specifications do not exist for the hard ceramic coatings or oxidized zirconium, although processing and characterization techniques have been published by ASTM and ISO organizations [180,181].

Parameters considered important for total joint arthroplasty are density, grain size, flexural and compressive strength, Weibull modulus, fracture toughness and slow crack growth (SCG), hardness and wear resistance, biocompatibility, corrosion, and low-temperature hydrothermal degradation (LTD). Additionally, for bioceramics used as arthrodesis devices or for bone fixation, such as HAp, Al_2O_3, or Si_3N_4, the ceramic's hydrophilicity, bacterial resistance, and osseointegration ability are important characteristics. Other properties such as elastic modulus, Poisson's ratio, thermal expansion, and conductivity are specific to each material and not directly comparable, although they may play important roles in performance. All are included in Tables 1a and 1b for the purpose of providing a reasonable reference source for these bioceramics and coatings.

Table 1a
Physical and mechanical properties, and performance of biomaterials.

Property or performance	Units	Alumina	Zirconia		Zirconia–alumina composites			Silicon nitride	Cobalt chromium	Ti6Al4V	PEEK	Cortical bone
Composition or designation	NA	Al_2O_3	Mg-PSZ	Ce- or Y-TZP	m-ZTA	AMC	ATZ	Si_3N_4	ASTM F799	ASTM F136	ASTM F2026	Collagen, proteins, HAp
Density	g/cc	3.98	5.65–5.77	6.00–6.05	4.25	4.37	5.51	3.22– 3.35	8.29– 8.50	4.43–4.50	1.29	1.5–2.0
Grain size	μm	<1.8 Equiaxed	50 Equiaxed	0.1–0.6 Equiaxed	0.4–0.7 Equiaxed	0.54 Equiaxed	0.4 Equiaxed	0.5 × 5.0 Equiaxed	∼62 Equiaxed	∼10 × 60 Lamellar	NA	NA
Flexural or tensile strength	MPa	400–580 Flexural	450–700 Flexural	700–1500 Flexural	700– 1248 Flexural	1250–1400 Flexural	755–1163 Flex./biaxial	800–1100 Flexural	827 Tensile	860–970 Tensile	170 Flexural	90–228 Flexural
Compressive strength	MPa	4100–5000	2000–3000	2000–2200	4000–4500	4300	∼2600	4000	600–1800	800–970	118	150–260 ∥ 70–110 ⊥
Elastic modulus	GPa	380	200–250	210–223	340–390	358	240–250	296–313	197–210	105–120	4	7.5–25.8 ∥ 5–20 ⊥
Poisson's ratio	NA	0.23	0.30	0.30–0.33	∼0.24	0.24	∼0.28	0.27	0.27–0.32	0.31–0.34	0.4	0.19– 0.48
Weibull modulus	NA	5–29	22	7–87	NA	10–15	6–17	8–53	NA	NA	NA	NA
Fracture toughness K_{IC}	MPa $m^{1/2}$	3.3–4.2	2.9–16.0	4.5–20.0	>4.1	6.4–8.5	8.0–12.0	4.4–15.0	50–100	46.3–93.3	7.6 kJ/m^2 Impact Test	1.0–5.0 ∥ 3.0–20.0 ⊥
Fatigue resistance K_{TH}/K_{IC}		0.52–0.84	0.45–0.90	0.37–0.92	NA	0.67	NA	0.50– 0.97	0.14–0.36	0.10–0.40	0.53–0.62	0.30–0.83
Biocompatibility	NA	Pass	Pass	Pass	Pass	Pass	Pass	Pass	Marginal	Pass	Marginal	Pass
Surface phase Composition	%	100% α-Al_2O_3	42–54% t-ZrO_2	65–95% t-ZrO_2	83–93% t-ZrO_2	58–90% t-ZrO_2	95–99% t-ZrO_2	100% β-Si_3N_4	NA	Mixture of α & β Ti	Amorphous & crystalline	Collagen and HAp
LTD susceptibility	NA	Stable	Marginal	Metastable (Y-TZP; marginal (Ce-TZP)	Stable	Marginal	Metastable	Stable	Stable	Stable	Stable	NA
Hardness	GPa	18.0–23.0	10.0–12.0	11.0–12.5	15.7–20.8	19	13.7–15.0	15.0	3.0–4.0	2.8–3.3	99 Rockwell M	0.68–0.78 ∥ 0.46–0.57⊥
Wear rate PE	mm^3/MC	20–58	– 1.8–5.1 NA	11–63	NA	1–20	17–32	17–25	14–201	NA	NA	NA
HXLPE		0.0–6.9		5.0–6.0		0.1–4.4	5.6–6.1	3.7–6.3	0.0–11.7			
Hard-on-hard		0.02–4.71		Catastrophic		0.00–0.45	0.02–0.06	0.18–0.98	0.18–25.00			
Thermal expansion coefficient	10^{-6}/°C	8	7–10	11	∼8	8.1	∼10	2.0–4.6	7.32	8.5–9.7	47	22.0–32.4
Thermal conductivity	W/m K	30	2	2–3	∼17	17	∼6	30–50	12.7	6.7–7.0	0.29	0.41–0.63
X-ray radiolucency	NA	Radiolucent	Opaque	Opaque	Opaque	Opaque	Opaque	Radiolucent	Opaque	Opaque	Transparent	Radiolucent
Sessile water contact angle	Degree (°)	50–72	79	82	90	90	90	40–70	55–93	76	95	NA
Bacteriostatic capabilities	⊕ = excellent; + = good;	⊘	+	+	NA	+	NA	⊕	⊗	+	x	NA
Osseointegration ability	⊘ = fair; ⊗ = poor; x = very poor	⊘	+	+	NA	+	NA	⊕	⊗	+	x	⊕

NA = not applicable or not available. MC = Million cycles.

Table 1b
Physical and mechanical properties, and performance of biomaterials.

Property or performance	Units	Titanium nitride	Diamond-like carbon	Zirconium nitride	Titanium–niobium nitride	Oxidized zirconium	Hydroxyapatite
Composition or designation	NA	TiN	DLC	ZrN	TiNbN	Ox–Zr	ASTM F1609
Density	g/cc	4.87–5.22	0.90–3.20	7.09	~5.69	5.84	2.55–3.21
Grain size	μm	30–300 nmColumnar	Amorphous 2–25 nm	10–30 nmNanocrystals	10–30 nm Nanocrystals	40 × 200 nm	0.4–100 μm splats
Adhesion or bond strength	MPa	10–60 N L_C Adhesion	35–160 NL_C Adhesion	24–60 N L_C Adhesion	83 N L_C Adhesion	35 N L_C Adhesion	39–89 Bond 25–60
Compressive strength	MPa	400–5500	NA	NA	NA	~2000	102–1000
Elastic modulus	GPa	402–550	110–900	175–395	200–600	200	3.2–122 coat vs. bulk
Poisson's ratio	NA	0.21	0.17–0.20	0.19	~0.20	0.34	0.11–0.27
Weibull modulus	NA	5–18	6–12	NA	NA	NA	2–19
Fracture toughness	MPa $m^{1/2}$	0.7–12.4	1.6–5.1	2.3–7.5	NA	2.2–2.8	0.5–1.2
Fatigue resistance K_{I0}/K_{IC}		NA	NA	NA	NA	NA	0.61
Biocompatibility	NA	Pass	Pass	Pass	Pass	Pass	Pass
Surface phase composition	%	TiN nanocrystals	Amorphous	ZrN nanocrystals	TiN, NbN nanocrystals	95% m-ZrO_2 5% t-ZrO_2	ACP, TCP, HA
LTD Susceptibility	NA	Stable	Stable	Stable	Stable	Stable	Purposely degradable
Hardness	GPa	33–56	14.5–80.0	14.0–31.0	14.0–24.5	12.0–14.0	3.0–9.0
Wear rate PE	mm^3/MC	21	28–67	NA	NA	–	NA
HXLPE		NA	2.8	3.5	NA	0.2–1.7	NA
Hard-on-hard		NA	NA	NA		NA	
Thermal expansion coefficient	10^{-6}/°C	7.4–9.2	2.3	5.9–7.2	~7.4–9.2	7–10	11.6–14.2
Thermal conductivity	W/m°K	11.9	0.2–30	20	~12–14	2–3	1.1–1.2
X-ray Radiolucency	NA	Opaque	Opaque	Opaque	Opaque	Opaque	Radiolucent
Sessile water contact angle	Degree (°)	31 - 69	55–71	89	73–75	71	34–39
Bacteriostatic capabilities	⊕ = excellent; + = good;	+	+	⊕	NA	+	+
Osseointegration ability	⊘ = fair; ⊗ = poor; x = very poor	+	+	⊕	NA	NA	⊕

NA = not applicable or not available. See text for discussion of adhesion and bond strength differences.

Table 2
ASTM or ISO specifications for biomaterials.

Property	Al_2O_3 ASTM F-603	Al_2O_3 ISO6474-1	Mg-PSZ ASTM F-2393	Y-TZP ASTM F-1873	ZTA, AMC ISO 6474-2	Si_3N_4 ASTM F-2094[a]	Si_3N_4 ISO 26602[a]	CoCr ASTM F799	Ti6Al4V ASTM F136	PEEK ASTM F2026
Chemical purity (%)	≥99.5	≥99.7	≥99.8	≥99.0	≥99.8	≥97.0	NS	NA	≥99.3	NA
Density (g/cc and %)	≥3.93 ≥98.6	≥3.94	≥5.80 ≥98.8	≥6.00 ≥98.4	≥4.31 ≥98.6	3.0–3.4 ≥99.8	3.0–3.6 NS	NA	NA	1.28–1.32
Grain size (μm)	≤4.5	≤2.5	NS	≤0.6	Al_2O_3 ≤1.5 ZrO_2≤ 0.6	NS	NS	≤64	NA	NA
Flexural strength (MPa)[a]	≥400	≥500	≥600	≥800	≥750	≥765	≥760	827 (YS)	760 (YS)	110
								1172 (TS)[b]	825 (TS)	
Weibull modulus	≥8	≥8	≥10	NR	≥8	≥12	≥12	NA	NA	NA
Fracture toughness (MPa $m^{1/2}$)	NS	≥2.5	NS	NS	≥3.5	≥6.0	≥6.0	NA	NA	50[c]
Hardness (GPa)	≥18	≥18	≥10	≥12	≥15.5	≥15	≥14.2	≥ 3.3	NA	NA
Elastic modulus (GPa)	≥380	≥380	≥180	≥200	≥320	270–330	270–330	NA	NA	3

NS = Not specified.
[a] Two flexural strength determination methods are allowed within ASTM F-2094 and ISO- 26602: For 3-point bending, the specification is ≥900 MPa versus ≥760–765 MPa for 4-point bending. ASTM and ISO specifications for the other bioceramics of Table 5 utilize 4-point bending.
[b] (YS) = yield strength; (TS) = ultimate tensile strength.
[c] Impact strength, notched izod method. (J/m).

3.1. Density

Although absolute density values (in g/cc) are not directly comparable for bioceramics due to chemical composition differences, attainment of near theoretical values (in %) provides insight with respect to each material's capability. Today, all ceramics for articulation purposes are densified using hot-isostatic pressing, and densities of greater than 98% are routinely achieved. HIPing results in substantial improvements in strength for these materials [16,182–185]. As an example, Garino et al. reported that HIPing of Al_2O_3 was implemented as part of a number of process improvements resulting in about a 3% change in mass density (*i.e.*, from 3.86 g/cc to 3.96 g/cc) and a 45% increase in flexural strength (*i.e.*, 400–550 MPa) [186]. Hot-isostatic pressing has since become a standard manufacturing practice for bulk ceramics used in structural applications [187]. The data presented in Table 1a and specifications shown in Table 2 demonstrate that all of these ceramics are essentially equivalent (within about 1.5%) with respect to their percentage of theoretical density.

Densities for ceramic coatings vary based on composition and application. Compiled values are provided in Table 1b. PVD coatings are typically dense amorphous or nano-crystalline structures [188]. Density determinations are difficult due to their thin nature, but measured values appear to approach theoretical limits in defect-free regions [189]. However, entrained imperfections, such as pits and micro-droplets, negatively impact average values. Oxidization of Zr–2.5Nb alloys (OxZr) produces a uniformly dense "blue–black" nano-crystalline scale. Nevertheless, its thickness is limited to about 5 μm because a porous "white" transitional oxide occurs beyond this point due to high compressive growth stresses [190]. HAp coatings are purposely engineered to be porous for osseous fixation. Porosity in thermally sprayed HAp coatings is governed by plasma conditions [191] and can vary from about 2% to greater than 10% [192,193]. A broad range of porosity can also be engineered into most ceramics for use as arthrodesis devices, scaffolds, or bone substitutes [21,105,194–197]. In summary, the amount of porosity within an implant is an important design parameter. Low porosity implants with concomitant small flaw populations are essential for load bearing applications whereas high porosity or mixed porosity devices are required for bone fixation.

3.2. Grain size and morphology

Grain size is an important parameter governing mechanical properties. The grain size values shown in Table 1a and the specifications of Table 2 are indicative of the control that is required in processing ceramics. Smaller grains are essential for maintaining a reasonable level of fracture strength in Al_2O_3. Minimizing grain size is the only method of improving the performance of devices made from this material [40,198]. While larger grained microstructures in Al_2O_3 resist crack propagation due to grain bridging and pull-out (which effectively increases local fracture toughness) [199,200], these large grains themselves can become inherent strength limiting flaws. Consequently, smaller grains are preferred. One approach to designing brittle ceramics for structural applications (as has been done for Al_2O_3) is to reduce the probability of failure through grain-refinement and flaw elimination, both of which increase fracture strength and improve Weibull modulus (*i.e.*, less variability in strength). Provided in Fig. 1(a) is a microstructural example of a biomedical Al_2O_3 [154].

Unlike Al_2O_3, Mg-PSZ has a unique microstructure. Its average grain size is large – 50–60 μm – and is composed of a cubic- ZrO_2 matrix embedded with metastable coherent tetragonal-ZrO_2 precipitates having diameters of ~250 nm and aspect ratios of ~5:1. The lenticular t- ZrO_2 precipitates occupy 40–50 vol.% of the c-ZrO_2 grains [70]. Because Mg-PSZ is transformation-toughened by these

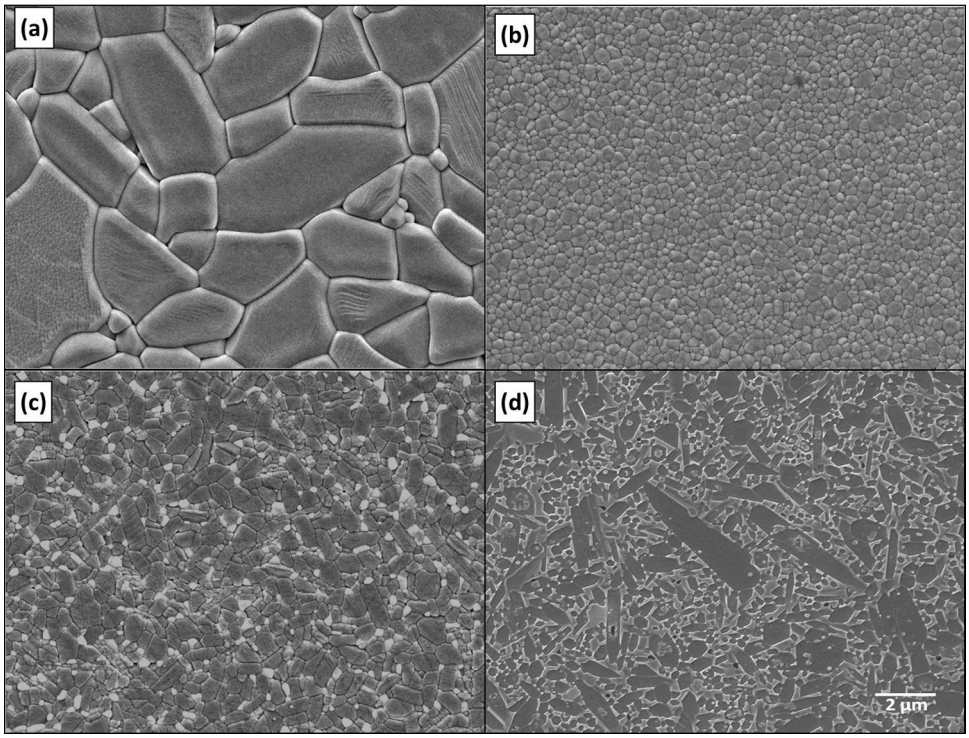

Fig. 1. Microstructures of biomedical ceramics: (a) Al_2O_3; (b) Y-TZP; (c) ZTA; and, (d) β-Si_3N_4; Courtesy Kyocera and Amedica Corporations.

nano-sized acicular t-ZrO2 precipitates, grain size control of the larger c-ZrO_2 is less important. Trials were conducted in the 1990s in an effort to decrease the grain size of Mg-PSZ by adding a small amount of yttria and/or a second phase (alumina or an aluminate) [201,202]. The purpose of these additives was to limit grain boundary mobility. However, follow-up studies were limited because Y-TZP was considered the system of choice during that period. Because of concerns with LTD in Y-TZP, there might be renewed interest in these Mg-PSZ systems, with the goal of improving their strength by careful control of their microstructure.

Grain refinement is essential for Y-TZP, ZTA, AMC, and ATZ composites, but for one additional key reason. The transformation of the t-ZrO_2 phase within these materials occurs more readily when ZrO_2 grains are beyond a critical size [203]. This size for Y-TZP under hydrothermal conditions is reportedly less than 360 nm [204]. Deville et al. confirmed that small ZrO_2 grains <500 nm are also required in ZTA ceramics [205], with the Al_2O_3 matrix influencing their critical transformation size. Typically, the t- ZrO_2 grains are located at alumina grain boundaries or at triple-point grain junctions [206]; but unique intragranular composites have been developed having submicron Al_2O_3/t-ZrO_2 grains embedded within larger Al_2O_3 grains [207]. The concentration and dispersion of the t-ZrO_2 grains within the Al_2O_3 matrix (or the converse for ATZ composites) is important for optimum strength. Adequate intermixing of the Al_2O_3 and ZrO_2 ceramic powders prior to densification is essential [208]. For ZTA composites, where Al_2O_3 is the dominant phase, keeping the ZrO_2 concentration below the theoretical percolation limit (~16 vol.%) prevents linking-up of t-ZrO_2 grains throughout the Al_2O_3 matrix [205]. Their isolation is important in inhibiting intergranular H_2O diffusion which leads to premature transformation. AMC composites have an additional tertiary phase engineered into their microstructure composed of magnetoplumbite platelet grains [209]. Their purpose is to increase the ceramic's overall resistance to fracture via crack deflection [152,156], which is plausible in principle, but their actual contribution to increased toughness, considering their small volume percentage in the composition, has not been fully verified [210]. For ATZ, where t-ZrO_2 is the matrix and Al_2O_3 is the minor phase, strength improvements are due to transformation toughening and intergranular crack deflection induced by the presence of the Al_2O_3 particulates at t- ZrO_2 grain boundaries [211,212]. Dispersion of the Al_2O_3 and ZrO_2 grains is therefore an important design element of this material. However, this ceramic is also highly susceptible to hydrothermally induced phase transformation because of the large proportion of t-ZrO_2 grains, although its kinetics are reportedly retarded when compared to Y-TZP ceramics [162]. Representative microstructures of Y-TZP [213] and ZTA [154] are shown in Fig. 1(b) and (c), respectively.

Grain size control is also important for Si_3N_4, yet it is not as critical as it is for transformation-toughened materials. Because β-Si_3N_4 grains are acicular, it has been shown that bimodal structures [214] or large aspect ratio grains [120–122] are beneficial in improving fracture toughness through a number of mechanisms, including crack deflection, crack bridging, grain pull-out, and compressive stresses [122]. The acicular grain structure of Si_3N_4 is unique among bioceramics. Elongated grains are generated during densification via a dissolution re-precipitation process that irreversibly converts equiaxed α-Si_3N_4 particles to their acicular β-Si_3N_4 counterparts. The β-Si_3N_4 grains impart high toughness and strength comparable to transformation-toughened ceramics without the inclusion of a metastable phase. Consequently, Si_3N_4 is not susceptible to hydrothermal degradation. A representative microstructure of a biomedical Si_3N_4 ceramic is provided in Fig. 1(d).

A summary of grain sizes for the various ceramic coatings is provided in Table 1b. PVD ceramic coatings are either amorphous or nano-crystalline. Their stoichiometry can vary depending on chemistry and deposition conditions [215]. For instance, DLC coatings are amorphous but can differ in their atomic bonding structure. Co-deposition of carbon with hydrogen results in softer sp^2 graphitic type bonds, whereas pure carbon deposition can produce hard sp^3 bonding with corresponding hardness values ranging from about 14 GPa to 80 GPa [148,216]. Other PVD coatings such as TiN,

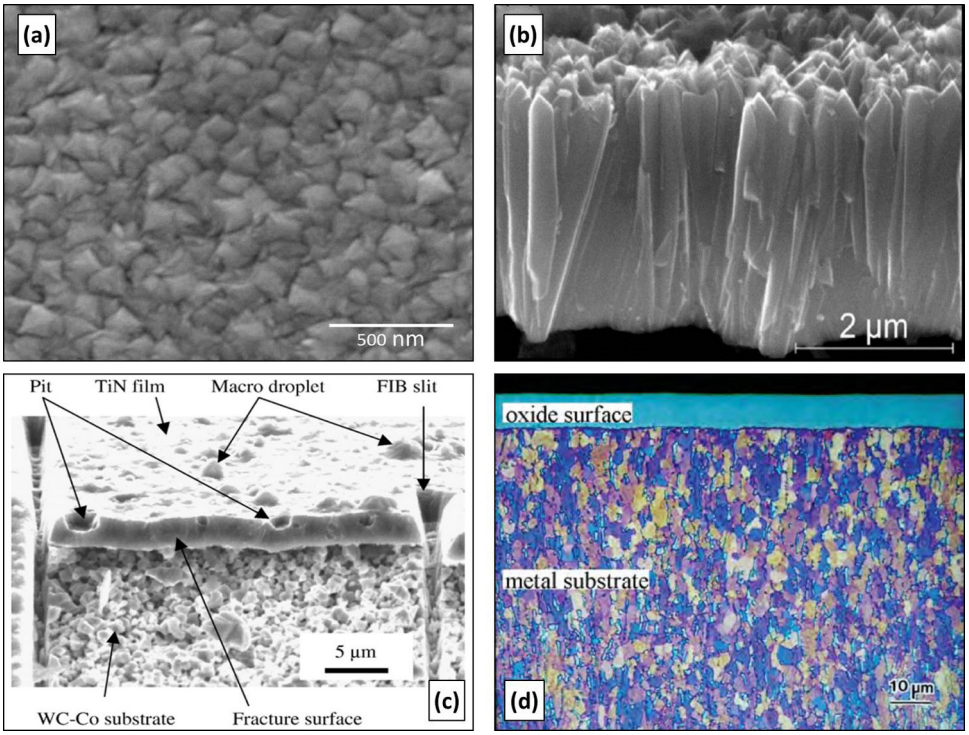

Fig. 2. Microstructures of ceramic coatings on metallic substrates: (a) TiN coating at 1.26 μm thickness [226]; (b) cross-section of TiN coating [227]; (c) fracture surface of TiN coating showing the presence of pit and droplet defects [228] ; and, (d) cross-section of Ox–Zr *in situ* grown layer [180]. Reprinted with permission.

ZrN, and TiNbN possess nano-crystalline columnar microstructures [129,208,209]. Their acicular size can be 30 × 300 nm, with the thickness of the grains increasing proportionately in the crystallite growth direction. It is also common practice within industry to deposit multiple transitional layers to increase substrate adhesion [217–219]. For example, in coating a CoCr alloy with ZrN, one manufacturer includes a bond layer and up to five interlayers, alternating between CrN and CrCN, with the final surface layer being ZrN [134,220]. The initial layer, which is generally a compositional variant of the substrate, is designed to achieve good chemical bonding while subsequent layers modulate a transition in elastic properties. These layers reduce deposition and thermally induced compressive residual stresses, which can be significant—up to 11 GPa [221]. Delamination of the coating would readily occur in their absence [222]. The composition of these layers is experimentally determined, with the thickness of the total deposition typically being less than about 15 μm. Most PVD coatings also contain undesirable micro-droplets as a result of the deposition process. These are larger particles ablated from the PVD target and accelerated toward the substrate within the plasma. They result in degradation of the smoothness, uniformity and thickness of the deposited layer, and can be a source of mechanical or corrosive failure [223,224]. Elimination of 100% of these defects is statistically improbable, and special filters have been added to PVD equipment to minimize their occurrence [225] . Examples of the surface texture and cross-section of two different TiN coatings are shown in Fig. 2(a) and (b), respectively [226,227], and a graphic example of coating defects is shown in Fig. 2(c) from the work of Kamiya et al. [228] .

A detailed examination of the grain morphology of OxZr was performed by Hobbs et al. [190] This *in situ* grown layer predominately consists of nano- crystalline columnar monoclinic ZrO_2 grains that are about 20–70 nm wide × 200–300 nm long, arranged in an anisotropic brickwork pattern, with their long axis orthogonal to the surface of the Zr–2.5Nb substrate. Fortuitously, this aligned grain structure resists crack propagation parallel to the alloy's surface, thus reducing the layer's chances for delamination. Also, their large aspect ratio and parallel alignment advantageously resist pull-out from the polished articulation surface. Adhesion of the oxidized layer to the substrate is facilitated by Nb stringers which extend from the metal into the oxide and serve as anchors. Compressive oxidation surface stresses, reportedly ~670 MPa, further assure coherency of the monoclinic ZrO_2 layer [190]. A typical microstructure of OxZr at the Zr–2.5Nb alloy interface is presented in Fig. 2 (d) [180].

The grain structure of hydroxyapatite coatings is lamellar due to the nature of the deposition process. Plasma spraying results in partial or full melting of the hydroxyapatite particles. Demnati et al. suggest that the compositional structure of the particles is composed of concentric layers of different apatite compounds as shown in Fig. 3 [63]. The outermost layer is CaO and a melt, followed by successive inner layers of tri- and tetra-calcium phosphate (TCP, TTCP) and orthohydroxyapatite (OHAp). At the core of the particle is solid hydroxyapatite (HAp). Upon impaction, partially melted particles solidify as multiphase mixtures in small-sized deformed splats at the substrate's surface. The size of these splats is proportional to the original HAp particles and can range up to about 100 μm. Successive particles impacting on their predecessors form the lamellar structure [229]. The initial lamellae are different from their successors since the first layer is deposited on the high thermal conductivity metallic surface, whereas subsequent layers adhere to their thermally insulating predecessors. The apatite composition of the coating changes with successive deposition passes as indicated in Fig. 3.

Differential cooling and reheating is responsible for migration and segregation of the apatite phases within the coating. The amorphous phase (ACP) dominates the composition in the as-sprayed condition; but controlled crystallization of ACP can be accomplished by post deposition thermal treatments [230]. Porosity is generated within the coating during cooling due to entrapped air, and cracks form due to differential shrinkage. Microstructures for a thermally sprayed HAp coating are shown in Fig. 4(a) and (b) [229]. Newer HAp coating compositions incorporate ZrO_2 or

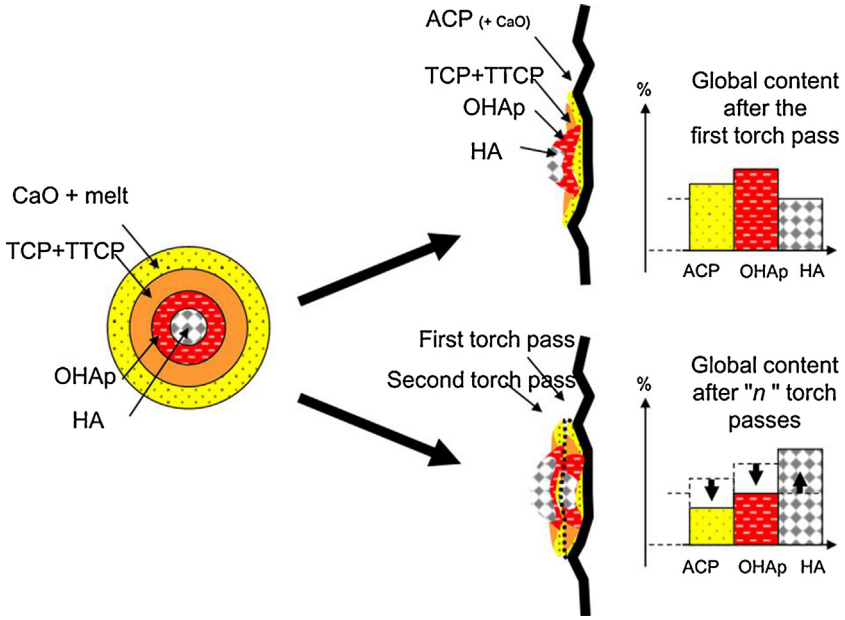

Fig. 3. Sequence of events during deposition of a semi-molten HAp particle impinging on a roughened surface [63]. Reprinted with permission.

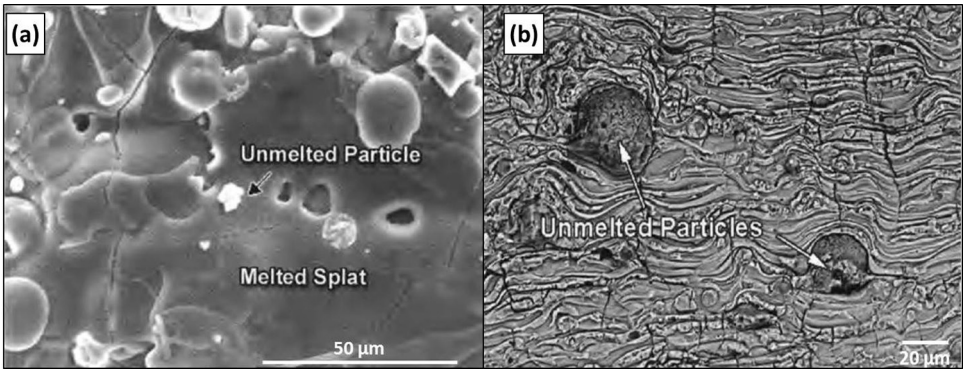

Fig. 4. Flame-sprayed HAp coating: (a) surface grain structure; (b) cross-section of grain structure [229]. Reprinted with permission.

Ti6Al4 V as additives to improve substrate bonding and increase coating toughness [231]. More recently, HAp has also been coated onto, or incorporated into polyetheretherketone (PEEK) to improve osseointegration of spinal fusion cages. In the former case, HAp coatings are applied using PVD methods [232,233]. In the latter instance, HAp particles are compounded into PEEK prior to thermal forming and machining of the implant [234,235,236].

In summary, microstructural engineering has been essential in enabling and improving biologic functions of ceramics and ceramic coatings. Reduction of grain size is necessary for increased strength and toughness in Al_2O_3. Its control is also critical for phase transformation toughening at the crack tip under applied stresses and the prevention of premature transformation under hydrothermal conditions in Y-TZP, ZTA, AMC, and ATZ compositions. Conversely, growth of acicular β- Si_3N_4 grains to an appropriate aspect ratio results in increased strength and toughness without the necessity of a metastable transformable phase. Microstructures for PVD coatings are amorphous or nano- crystalline, and vary in size based on chemistry and deposition conditions, but micro-droplet defects and high residual deposition stresses are common. Improved substrate adhesion via incorporation of multiple interlayers is employed to reduce stress and modulate differential elastic properties. OxZr microstructures are also nano- crystalline with excellent substrate adhesion and anisotropic grain orientation that resists delamination and grain pull-out. Plasma sprayed HAp (or HAp mixtures with toughening additives) coupled with post-deposition heat treatments provide microstructures possessing adequate bond strength and fortuitous mixtures of apatite phases, porosity, and other defects for effective osseointegration. Finally, HAp has been incorporated into PEEK devices, either as a PVD coating, or as particles compounded with the polymer.

3.3. Strength

Strength is the ability of a material to resist deformation or fracture. The common method for measuring bulk strength of ceramics is flexural testing, which involves symmetrical bending of carefully prepared parallelepiped specimens in accordance with international standards [237,238]. Shown in Table 1a are compiled flexural strengths for ceramics, which range from 400 MPa for Al_2O_3 to 1500 MPa for Ce- or Y-TZP. While this is indeed a broad range, differences in reported strengths of up to 90% have also been observed for some individual ceramics, particularly Mg-PSZ, Ce-, and Y-TZP. This spread in data is not only due to variations in material and processing, but also a result of differences in testing methods. Three specimen geometries and the use of either 3- or 4-point bending are allowed within the standards. Due to the stochastic nature of brittle fracture, maximum strengths are always

observed when using the smallest specimens in 3-point bending. Consequently, some of the highest reported strengths in Table 1a were obtained in this manner. Using Si_3N_4 as a model material, Katayama et al. found up to a ~60% difference in strength between 3- and 4-point flexural testing, when using the smallest and largest allowable specimens, respectively [239]. However, they and Quinn et al. [240] pointed out that reconciliation of differing data can be accomplished through a simple relationship, provided an adequate number of specimens have been tested and a meaningful Weibull modulus determined. Nevertheless, this reconciliation might be more difficult in highly transformable ceramics, such as Ce-TZP, where the maximum failure stress relates to the transformation itself rather than to pre-existing defects.

Al_2O_3 has a modest flexural strength of about 580 MPa, (*cf.*, Table 1a) [40]. The ASTM and ISO specifications for this material are listed as ≥400 MPa and ≥500 MPa, respectively (*cf.*, Table 2). Al_2O_3's lower strength is the primary reason it has lost favor in recent years for use as femoral heads and liners, having been replaced by the higher strength and toughness ZTA and AMC ceramics. Nevertheless, *in vivo* fractures of Al_2O_3 components are now extremely rare. Reported failures declined from about 13.4% for implants produced prior to 1990 to 0.021% for parts produced between 2000 and 2013 [40,241]. This reduction was due to the aforementioned process improvements; and suggests that even a modest strength material can provide excellent *in vivo* reliability.

With the advent of Mg-PSZ and Y-TZP, flexural strengths improved markedly—from 700 up to 1500 MPa, respectively (*cf.*, Table 1a) [65,70,187]. However, their ASTM specifications were only set at 600 and 800 MPa, respectively (*cf.*, Table 2). Y-TZP might have been one of the best materials for articulation, were it not for its susceptibility to LTD. An incompletely validated process change by the leading manufacturer of Y-TZP in the late 1990s led to a dramatic increase of *in vivo* fractures, from 0.002% prior to the process change to 8% afterwards [73], resulting in their recall from US and EU markets in 2001 [242].

The introduction of ZTA and AMC composites was a significant step forward in joint arthroplasty due to a combination of improved flexural strength and reduced sensitivity to hydrothermal degradation. ZTA strengths as high as 1248 MPa have been observed, and flexural strengths of up to 1400 MPa have been reported for AMC on a series of ~40 production lots (*cf.*, Table 1a) [154,243]. *In vivo* fracture rates for AMC are extremely low, at 0.001% [40]. It is now the preferred ceramic worldwide for hip joint replacements, although its LTD resistance remains an area of long-term research [79,172,244–248]. In spite of their high reported values, the minimum flexural strength for ZTA and AMC ceramics per the ISO standard was set at ≥750 MPa (*cf.*, Table 2).

Only limited strength data are available for ATZ composites, with values ranging between 755 and 1163 MPa (*cf.*, Table 1a) [249,250]. The lower average value was determined from 4-point bending of standard test bars, whereas the higher strength was obtained by biaxial flexural testing [251]. One manufacturer lists their ATZ's biaxial strength at 2000 MPa; but this extraordinary value is not found in the technical literature [252]. ATZ orthopaedic devices clearly show a certain degree of LTD since their major phase is Y-TZP [81], although the transformation kinetics appear to be slower than Y-TZP and the impact less dramatic.

Si_3N_4 is the latest entrant in load-bearing medical applications. It is a non-oxide ceramic with flexural strengths comparable to the oxide materials, typically between 800 and 1100 MPa (*cf.*, Table 1a) [82], with ASTM or ISO specifications of ≥760 MPa (*cf.*, Table 2). It has an advantage over ZTA and AMC ceramics in that its high strength is not reliant on the presence of a metastable transformable phase. It is therefore immune to LTD. Its acicular microstructure is responsible for its high flexural strength. An advancing crack must follow a tortuous and chaotic high-energy path in its propagation. Grain bridging and pull-out in the crack wake serve to reduce tensile stresses at the crack-tip resulting in increasing resistance to crack propagation during crack extension, which is known as *R*-curve behavior [253].

Strength testing of PVD ceramic coatings is problematic due to their thin nature, small specimen sizes, substrate adherence, and existence of residual internal stresses. As reviewed by Borrero-Lopez et al., a number of techniques have been explored, including tensile, flexure, nano-indentation, and scratch methods [254]. They reported characteristic strengths for TiN and DLC coatings ranging from 1.25 GPa to 7.6 GPa. Jaeger et al. developed a novel flexural technique using pre-cracked metallic substrates and measured strengths for TiN coatings from 183 to 491 MPa. They concluded that their results were reasonable based on comparable data for HIPed TiN. Separately, Wiklund et al. used four-point bending inside an SEM to evaluate fracture resistance of TiN thin films using relatively large specimens (*i.e.*, 60 mm^2), and measured flexural strengths of between 600 MPa and 1.0 GPa [255]. Later, Kamiya et al. prepared free-standing TiN films and performed flexural tests with strengths varying from 2.60 to 3.87 GPa. However, the area of their specimens was only 1 μm^2. They rationalized that their higher strengths were not inconsistent with Wiklund's findings after accounting for surface area differences [228]. Finally, for DLC films, Espinosa et al. used nano-indentation to measure fracture strength and obtained values of 4.7–5.2 GPa on samples with surface areas ranging from 500 μm^2 to 4000 μm^2 [256].

This broad and inconsistent range of observed strengths highlights the difficulty in obtaining quality data for coatings. Consequently, scratch adhesion testing was developed as a practical engineering method for assessing coating viability [257]. This technique involves dragging a diamond stylus across the coating's surface under a linearly increasing load. Typically, two critical loads (L_{C1} and L_{C2}) are determined by examining the scratch track for brittle damage events such as cracking, delamination, chipping, spallation, or buckling. L_{C1} is recorded at the first sign of cohesive failure, with L_{C2} noted at complete coating failure. One or both of these values are often reported in the literature, with L_{C2} typically designated as the coating's scratch adhesion strength. It is important to note that this test does not provide intrinsic scientific information on adhesion. Rather, it yields valuable comparative engineering data. As pointed out in the standard, test outcomes are dependent upon a number of factors including stylus properties, geometry, loading and displacement rates [257].With this background information, shown in Table 1b is the range of scratch adhesion values reported in the literature for various hard ceramic coatings. Values from 10 N to 160 N were observed. Differences are due to deposition chemistry and methods, coating thicknesses, and substrate materials.

Hardness of the substrate plays a major role in determining scratch adhesion. As demonstrated by Roy et al., hard substrates perform better than soft ones. Their study correlated scratch adhesion data for DLC coatings applied to Mg-PSZ and CoCr substrates, with hardness values of 10–12 GPa and 3–4 GPa, respectively. Also included was an OxZr coating with a Zr–2.5Nb substrate hardness of 2.5 GPa. L_{C2} values of 46.8 N were obtained when the DLC was applied to Mg-PSZ versus 35.2 N on CoCr, which was remarkably close to the OxZr result of 34.8 N [258]. A similar conclusion was reached by Utsumi et al. after applying an interlayer of hard tungsten carbide between an aluminum substrate and a thin DLC coating. Scratch adhesion values were increased from about 12 N to 80 N [259]. These results are not surprising given that a hard brittle ceramic coating on a soft metallic substrate is analogous to applying a "hard candy coating over soft chocolate." Under an applied load, slight elastic deformation will readily fracture the thin brittle coating. Even though scratch adhesion does not determine the intrinsic strength of thin films, it is an important engineering measurement

in predicting *in vivo* viability. As will be discussed in more detail later in this review, one of the failure modes for coated orthopaedic devices is poor adhesion. Adhesion can be significantly improved by closely matching elastic properties between the coating and substrate, and by ensuring strong chemical and mechanical interfacial bonding.

Strength testing of HAp coatings is also problematic due to their thin nature and inherently defective structure. However, flexural tests have been obtained for bulk HAp densified using conventional sintering, spark-plasma sintering, and hot-isostatic pressing with reported values ranging from 113 MPa to 189 MPa [260–262]. Strengths were increased up to 220 MPa by reactive sintering of HAp and fluorapatite admixed with up to 40 vol.% ZrO_2 [263], and values of ~250 MPa were obtained when using 40 vol.% Al_2O_3 [264]. Even higher strengths of about 300 MPa were obtained when combining HAp with 30 vol.% Al_2O_3 and 15 vol.% ZrO_2 [265]. While these compositional studies on bulk HAp are instructive, they are not directly transferrable to coatings, and strength testing of coatings is essentially impossible. Scratch adhesion can be employed, but the more practical approach for evaluating HAp coatings is to utilize "pull-off" testing in accordance with international standards [266,267]. Specimen preparation and testing is straightforward. After applying the HAp coating to one end of a 25.4 mm diameter metallic rod, an identical rod is bonded to the coating using adhesive glue. The joined test specimen is then subjected to tensile loading, and the "pull-off" load recorded. The test yields valuable engineering data about the bond strength of the coating; but, similar to scratch adhesion, it does not provide scientific data on the strength of the coating itself. The standards require that the "pull-off" adhesion strength be greater than 15 MPa, which is one-fourth to one-tenth of the reported flexural strengths for dense HAp. Different deposition practices have been explored to improve "pull-off" strengths, including plasma, induction, vacuum–aerosol and high velocity oxy-fuel combustion spraying, hot-isostatic pressing, dip coating, electrophoretic deposition, sol–gel adhesion, pulsed-laser, ion-beam, or co-spraying HAp with a toughening agent such as Al_2O_3, ZrO_2, or a titanium alloy [268–272]. However, none of these processes produce "pull-off" strengths approaching flexural data for bulk HAp, with values ranging between about 10 MPa and 80 MPa [54,268]. The highest reported "pull-off" strengths of 60–80 MPa were produced using either a high power laminar jet coating method or vacuum deposition [268,272]. Shown in Fig. 5 is a range of "pull- off" adhesion strengths obtained using various deposition techniques [268]. It is easy to understand why both bulk HAp and HAp coatings cannot be used as structural members in orthopaedic devices given these observed low flexural and "pull-off" strengths.

This section on strength was initiated with a discussion of observed fracture rates for ceramics in THA. Even though their occurrence is small, they are serious events, requiring immediate revision surgery, debridement of damaged tissue, and replacement of THA components. Nevertheless, it is now evident that failure rates for metals have eclipsed those of ceramics. National registries and follow-up studies indicate that the hip systems with metal-on-metal (MoM) articulation have higher revision rates than any current ceramic based devices [273–275]. Fig. 6 shows survivability statistics for a combination of cemented and uncemented THAs from the UK national joint registry [273]. The revision rate for MoM articulation is over four times that of ceramic containing devices at ten-years postoperatively. The pathology of these MoM failures is not catastrophic fracture, but rather, excessive component wear, which symptomatically presents itself as groin pain, component loosening, metallosis, formation of pseudotumors, and localized tissue necrosis, with elevated serum levels of Co and Cr ions. Patient morbidity and the requirement for revision surgery to replace worn metal components are no less serious, and in many instances more severe than for ceramic fractures. In retrospect, the harm and suffering endured by patients with MoM devices might have been substantially eliminated by using ceramic-based THA systems. Keep in mind that the strength of ceramics is even higher than most metals. The issue is their low strain to failure as a consequence of high elastic modulus and lack of plasticity. Material strength is therefore only one of many factors that should be considered in the selection of appropriate orthopaedic implants.

3.4. Weibull modulus

A biomaterial's Weibull modulus provides a statistical measure of its strength variability. The range of observed strengths for a brittle material is related to the number and size distribution of its inherent flaws. As reviewed by Quinn et al., [240] the two parameter Weibull distribution function is commonly used to characterize experimentally determined strengths. The probability of a failure, P_f, under an applied stress, σ, is given by the following expression:

$$P_f = 1 - \exp\left(-\int_v \left(\sigma/\sigma_0\right)^m dV\right) \quad (1)$$

where σ_0 is the Weibull scale parameter or characteristic strength, which is a measure of the centrality of the distribution and represents a failure probability of 63%. The Weibull modulus, m, is an indicator of the dispersion in strength values. A material with a high modulus has a narrower strength distribution and improved reliability. V is the volume of the specimen or component. The two parameters, σ_0 and m, are determined from strength testing followed by graphical interpretation of the results in accordance with an international standard [276].

A wide range of Weibull moduli is reported for bioceramics (*cf.*, Table 1a). Values between about 7 and 18 are nominally observed, but measurements from 5 to 87 have been reported. Most ceramics fall within the nominal range, and repetitive measurements on serially produced batches and round-robin studies confirm this fact [239,277,278] . A low value of 5 was reported for Al_2O_3 [171], but this appears inconsistent when compared with the aforementioned repetitive studies. Extreme values of 53 and 87 were found for Si_3N_4 and ZTA, respectively, but these are not routinely observed for standard production batches [279,280]. Note that the ASTM and ISO specifications for Al_2O_3, Mg-PSZ, Y-TZP, ZTA, and AMC have been set at ≥8–10 (*cf.*, Table 2). Conversely, for Si_3N_4, its Weibull modulus was set at ≥12, (*cf.*, Table 2). Si_3N_4's elongated grain structure can influence its Weibull modulus. Increases in size and aspect ratio of grains result in higher fracture toughness and strength due to *R*-curve behavior [281–283]. Without acicular growth, the mechanical properties of equiaxed Si_3N_4 are similar to oxide ceramics [284,285]. Also, Weibull moduli concomitantly increase for larger high aspect ratio grains because they become strength limiting flaws [283].

There is a paucity of Weibull strength data for ceramic coatings due to the difficulty in preparing specimens and conducting tests (*cf.*, Table 1b). This is particularly true for PVD thin films. For instance, Borreo-Lopez et al. assessed a number of hard ceramic coatings, including DLC and TiN and found Weibull moduli of 6–12 and 10–18, respectively [254,286]. Their results are consistent with Kamiya et al., who conducted flexural fracture tests on TiN films and found their moduli varied between 5 and 12 [228]. No Weibull data were found in the literature for ZrN, TiNbN, or OxZr thin films. Limited Weibull statistics have been compiled for HAp using biaxial flexural strength (BFS) and nano-indentation hardness measurements. Weibull moduli for strontium doped HAp fell within the range of 4–19 from BFS tests [287]. Using nano-indentation, Yang et al. found Weibull moduli ranging from 3 to 4 [288], and Dey et al. measured values between 2 and 9 [289]. Overall, the range of

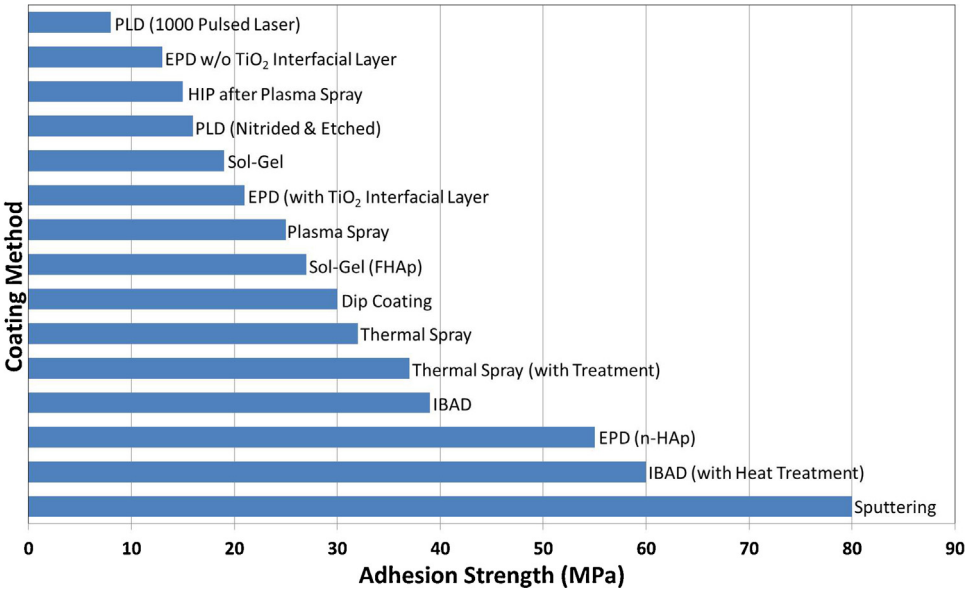

Fig. 5. HAp adhesion strengths for different coating methods. Adapted from Mohseni et al. [268] Used with permission.

results for coatings is not markedly different than those observed for bulk ceramics.

Consistently attaining both high characteristic strengths and Weibull moduli on sequential production ceramic batches is a significant challenge for process engineers. Strength-limiting defects can occur at any manufacturing step, but are most likely to be entrained during powder processing (including spray- drying). Coarse particles (or granules), large or hard agglomerates, and foreign contamination are common flaws. Inadequate particle packing after compaction further exacerbates their negative contribution, leading to formation of pores or voids during sintering [290]. Hot-isostatic pressing was largely implemented to minimize or eliminate void-related defects [187]. Surface cracks and pull-outs can be generated during post-densification grinding operations [291–293].

Furthermore, specimens used in assessing mechanical properties have different processing than components. Therefore, their characteristic strengths and Weibull moduli may not be representative of actual implants. This was the case for the recalled Y-TZP femoral heads in 2001. The defects resulting in their failure were on uninspected ID surfaces [73]. For coatings, inappropriate deposition conditions can generate droplets, or produce voids, inclusions,

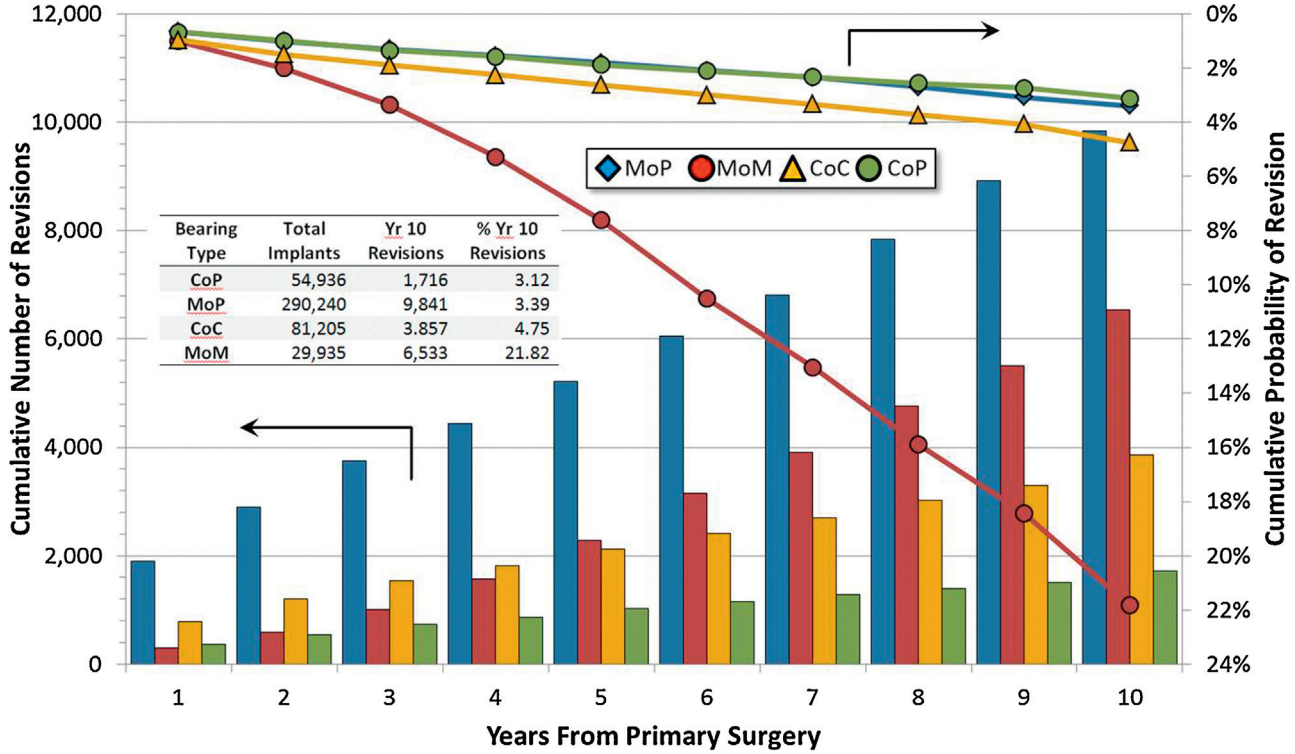

Fig. 6. Cumulative number and percentage of revisions for cemented and uncemented hips with different bearing surfaces (MoP = metal-on-polyethylene, MoM = metal-on-metal, CoC = ceramic-on-ceramic, and CoP = ceramic-on-polyethylene) [273].

and pits, all of which reduce reliability. Low characteristic strengths and Weibull moduli are signals to process engineers that special cause variation has occurred, requiring investigation and corrective action.

Alternatively, an increase in characteristic strength and Weibull modulus can be accomplished by truncating the flaw population through the use of proof-testing [198,294,295]. Proof-testing is an inspection technique that subjects finished components to a stress in excess of physiologic loads. Proof-testing eliminates *a priori* any component that has unacceptable strength, and therefore provides a threshold stress, below which no failure is likely to occur. Today, ceramic THA components and spinal fusion cages are subjected to proof-testing. Proof-test levels are based on finite element analyses, or *in vitro* and *in vivo* studies, and regulatory requirements. Because of this fact, the measurement of a Weibull modulus, while important for process investigation and control, has less meaning and is less relevant as a design parameter. Consequently, as shown in Tables 1a and 1b, the reliability of ceramics and coatings, as expressed by their respective Weibull moduli, is essentially equivalent.

3.5. Fracture toughness

Fracture toughness is a fundamental property governing strength. It describes the material's intrinsic resistance to crack propagation. While it is applicable for all materials, it is critically important for ceramics. The strength of a ceramic is related to its fracture toughness by the Griffith equation [296]:

$$\sigma_R = \frac{K_{IC}}{Y\sqrt{\pi a}} \quad (2)$$

where σ_R = fracture strength; K_{IC} = fracture toughness, or critical stress intensity for fast fracture; Y = a geometrical factor related to the crack; and, a = crack length. Fast fracture occurs when the stress intensity at the crack tip exceeds the material's innate fracture toughness, K_{IC}. From the Griffith equation, there are two routes for improvement of a ceramic's fracture strength. One method is to control processing of the material in order to reduce pre- existing defects. This approach was discussed in the prior section on Weibull modulus. The second method is to engineer the microstructure to increase its K_{IC}.

A myriad of procedures for determining fracture toughness of ceramics have been developed. Common methods include chevron-notch (CVN), indentation fracture (IF), indentation-strength (IS), single-edge notched beam (SENB), single-edge v-notched beam (SEVNB), single-edge pre-cracked beam (SEPB), surface- crack in flexural (SCF), and Vickers indentation (VIF), with newer techniques being developed periodically – the details of which are beyond the scope of this review. The reader is referred to critical commentary by a number of noted fracture mechanics authorities for in-depth discussions of these various methods [297–301], including their applicability to biomaterials [302]. Round-robin testing was conducted in the 1990s to evaluate, reconcile, and standardize fracture toughness procedures [303–306]. Shown in Fig. 7 are results for five different ceramic materials – sintered silicon carbide (Si–SiC), alumina (Al_2O_3), Y-TZP, hot-pressed silicon nitride (HPSN), and magnesia partially stabilized zirconia (Mg-PSZ), tested in ten laboratories using five methods – CVN, IF, IS, SEPB, and SENB [304]. Note that differences between techniques can range up to 95% for some materials. Conclusions from this, and the other cited studies, highlighted inadequacies with indentation methods (IF, IS and VIF), and preferences for CVN, SEPB, and SENB techniques which were judged to produce the most consistent results. These three techniques were eventually incorporated into an ASTM standard with recommendations to utilize at least two methods for assessing toughness of unfamiliar or new materials [306].

A number of strategies have been devised to enhance toughness in ceramics. For single phase materials with equiaxed structures, grain size control and grain boundary engineering are performed, with sub-critical-micro-cracking, crack-bridging, and branching yielding toughness improvements [307,308]. Transformation toughening is used in Mg-PSZ, Y- and Ce-TZP, ZTA, AMC, and ATZ; whereas *in situ* growth of elongated grain structures in Si_3N_4 increases its K_{IC}. Composites incorporating metal or ceramic dispersoids, platelets, whiskers, fibers, or laminates also lead to increased toughness by crack deflection and branching [307] . Fracture toughness values for the ceramics are listed in Table 1a. Al_2O_3 has a fracture toughness between 3.3 and 4.2 MPa $m^{1/2}$, which is the lowest among the structural ceramics used in joint arthroplasty [309,310]. It also has the lowest ISO specification at 2.5 MPa $m^{1/2}$ (*cf.*, Table 2). Its toughness is related to its microstructure, which consists of equiaxed grains of less than about 2 μm. Strength improvements in Al_2O_3 have not been due to marked increases in fracture toughness [206]. Rather, they have been achieved by controlling processing defects and decreasing grain size. As reviewed by Pezzotti et al., thermal expansion anisotropy within the corundum crystal structure between the *c*-axis and *a*- or *m*-axes leads to weak grain interfaces in the densified ceramic [311]. These interfaces become defect origins under applied tensile loads, with crack propagation typically occurring along grain boundaries. Consequently, larger grains (usually referred to as "abnormally grown" ones) not only originate fractures, but also allow a crack to easily propagate along very weak or even already broken grain boundaries. With a smaller grained material, this detrimental phenomenon is less effective; but the crack possesses a less tortuous path through the matrix. However, it is principally a difficulty in engineering the strength of grain boundaries while concurrently controlling the grain morphology that limits the toughness of Al_2O_3. On the other hand, Mg-PSZ, Ce- and Y-TZP, ZTA, AMC, and ATZ ceramics also have equiaxed grains, but the polymorphic expansion of the ZrO_2 crystal lattice during the $t \rightarrow m$ transformation shields the crack-tip from excessive tensile forces, thereby slowing or arresting its progression. Because of this, K_{IC} values for these ceramics are higher than for Al_2O_3, ranging from 4.1 up to 20.0 MPa $m^{1/2}$ [153,312] . The ASTM standards are silent with respect to a fracture toughness specification for Mg-PSZ and Ce- or Y- TZP, whereas the ISO standard for ZTA and AMC materials was set at 3.5 MPa $m^{1/2}$. Si_3N_4 has the highest ASTM or ISO specification for fracture toughness, at ≥6 MPa $m^{1/2}$ (*cf.*, Table 2), with reported K_{IC} values between 4.4 and 15.0 MPa $m^{1/2}$ [304,313]. This range is not only due to testing differences, but also from its diverse microstructures, which, depending on composition and processing, can be engineered to have smaller more equiaxed or larger high aspect ratio grains. Increased toughness from the latter type of microstructure is due to its interlocking nature. Crack tortuosity and bridging grains in the crack wake reduce critical stress intensities at crack tips by absorbing significant tensile energy (up to 1.5 GPa), which enhances *R*-curve behavior [308,313]. Indeed, Si_3N_4 has the strongest *R*-curve of any ceramic, with K_{IC} values rising from 4 to 15 MPa $m^{1/2}$ over crack extensions of ~800 μm [313]. *R*-curve trends for Al_2O_3, Y-TZP, ZTA, and two Si_3N_4 materials are given in Fig. 8 [311].

Acquisition of fracture toughness data for ceramic coatings suffers from the same difficulties encountered in assessing their strength. Measuring K_{IC} values is challenging given their thinness and bonding to softer metallic substrates. Techniques including bending, buckling, scratching, and indentation have been used, but as of yet there are no standards nor consensual methods [314,315]. Scratch adhesion and Vickers indentation are most practiced because of their operational simplicity. Empirical formulas are employed for scratch adhesion, which arguably are more a measure of load carrying capability than intrinsic toughness. Indentation

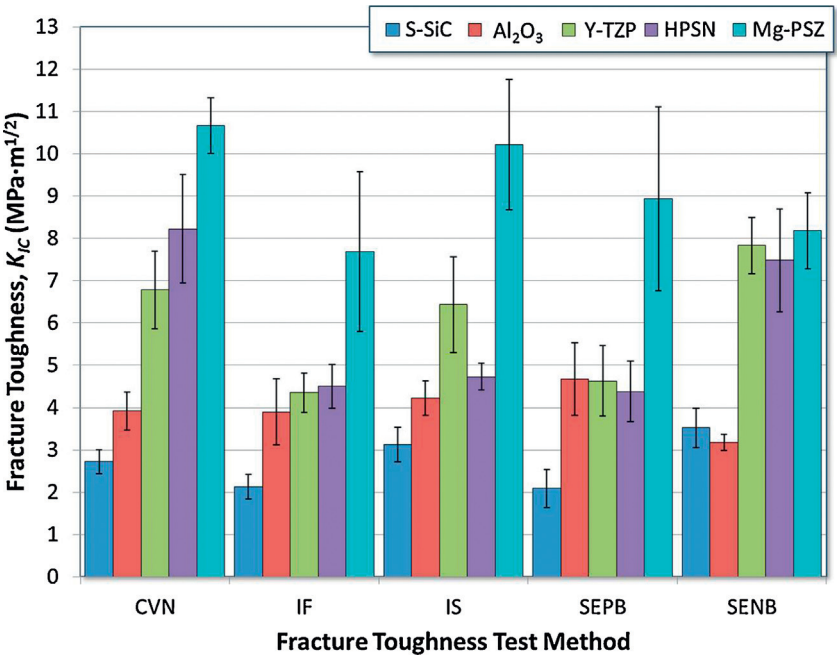

Fig. 7. Results from round robin evaluation of different methods of assessing fracture toughness [304].

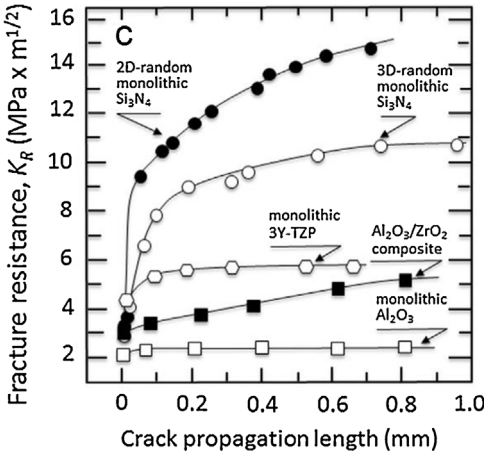

Fig. 8. Comparative *R*-curve measurements of bioceramics [311]. Reprinted with permission.

methods which use the equations and measurement methods for ceramics suffer from the same inconsistencies [316]. Due to their thinness, nano-indentation is often employed to avoid substrate interactions, with concomitant difficulties arising in the formation and measurement of acceptable crack lengths. Compounding these problems are issues associated with intrinsic coating defects and residual stress which also alter apparent K_{IC} values [315].

Increased fracture toughness is deemed to be important for coatings, particularly in tribology applications. As reviewed by Zhang et al., research continues to be conducted on improving toughness of these brittle films [222]. Not surprisingly, the envisioned techniques are similar to "tried and true" practices used for ceramics, including cohesive strengthening of grain boundaries and its juxtaposition of providing for grain boundary sliding, phase transformation, utilization of multiple layers, fiber reinforcement (*i.e.*, carbon nanotubes), compressive stress toughening, and incorporation of a ductile phase. The most practiced and therefore the most reported method for improving toughness is incorporation of multiple interlayers. Sequential layering of coatings with varying hardness and metallic content was originally developed for the express purpose of increasing adhesion. However, it was soon realized that composite layered structures provide beneficial improvements in fracture toughness as well [222,317–319]. Provided in Table 1b are reported fracture toughness data for hard ceramic coatings, which range from 0.7 to 12.4 MPa m$^{1/2}$ for TiN coatings [320,321]; and from 1.6 to 5.1 MPa m$^{1/2}$ for DLC [316,322]; with ZrN between 2.3 and 7.5 MPa m$^{1/2}$ [323,324]. TiN is perhaps the most studied, and therefore it is not surprising that its observed K_{IC} range is broader than for any of the other PVD coatings. However, as pointed out by Zhang et al. [321] and by Mofidi et al. [325], toughness values for TiN films vary considerably based on film thickness and interlayers. There are no reported data for TiNbN, but its K_{IC} range will likely be similar to TiN. An investigation of the fracture toughness of OxZr layers was performed by Leto et al. using cathodoluminescence spectroscopy, resulting in K_{IC} values of between 2.2 and 2.8 MPa m$^{1/2}$ [326]. Their results are similar to values observed for bulk monoclinic zirconia [327].

To summarize, K_{IC} values for various biomaterials as a function of their elastic moduli are shown in the Ashby diagram of Fig. 9 [328]. This chart compares ceramics, metals, and polymers and contrasts them to cortical and cancellous bone. The chart highlights interesting engineering trade-offs in the selection of implant materials. Metals are an order of magnitude greater in toughness and elastic moduli than cortical bone. The structural bioceramics and ceramic coatings also have high moduli; but, with the exception of HAp, their toughness values are essentially equivalent to bone. Neither class of materials has a combination of elastic or fracture properties that closely match cortical bone. However, only engineered polymers have a combination of toughness and elastic moduli that approximate native bone; and yet these plastics are not exclusively used as structural replacements because of their low yield or fracture strengths. Consequently, joint arthroplasty systems have evolved to typically include a combination of two or more materials—polymers, ceramics, and metals.

To understand this evolution requires a brief review of the chemistry, structure, and properties of bone. Approximately 70 wt.% of bone is composed of a variant of HAp-nanocrystals, which are slightly deficient in calcium with added carbonate [55].

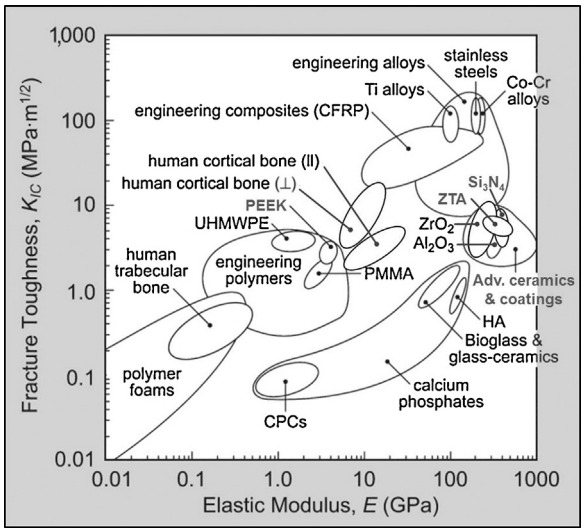

Fig. 9. An Ashby diagram showing the elastic modulus and fracture toughness of bone tissue compared to biomaterials commonly used as orthopaedic implants. The mechanical properties of cortical bone are shown for loading parallel (∥) and perpendicular (⊥) to the longitudinal anatomic axis. Adapted from Roeder et al. [328] Used with permission.

However, as previously noted, HAp is too brittle for use as a structural member alone. Consequently, the remaining 30% of bone is composed of collagen that is bound and supported by an arrangement of apatite nanocrystals, forming mineralized fibrils that are organized into lamellar structures. The basic metabolic unit is an osteon, which consists of vascular canals that are surrounded by the lamellae in concentric rings. Bone composition is essentially constant despite the fact that its properties vary based on location—from its dense and strong exterior cortical surface to its porous and flexible cancellous core.

Due to this architecture, its mechanical properties are generally reported as a function of density [329]. For cortical bone, alignment of the osteons with the bone's long axis bestows unique and beneficial anisotropy. Strength and elastic modulus are higher parallel to the axis [330–336]; whereas, hardness and fracture toughness are greater in the orthogonal direction [337] (*cf.*, Table 1a). It is stiff and strong in its longitudinal direction and yet tough and flexible in its transverse direction. Although soft when compared to *non-living* engineered materials, cortical bone of the femur is hardest along the diaphysis and the distal radius next to the articulation surface [338]. It exhibits remarkable *R*-curve behavior in its transverse direction, with toughness values increasing from approximately 5–20 MPa m$^{1/2}$ under crack extensions of up to 400 μm [337]. It can withstand reasonable loads and deformation with no residual damage, and yet, absorb considerable energy through micro-cracking, crack deflection, fiber pullout, or crack bridging to prevent complete failure when stress levels are excessive [335]. Because it is *living tissue*, bone remodeling is a natural response to applied stress, allowing it to reshape and repair itself. Nature has indeed engineered bone to be an extraordinary responsive composite consisting of a *native* bioceramic (hydroxyapatite) and a *native* polymer (collagen fibrils). It uniquely combines appropriate mechanical attributes from each material into a *living* composite. It is therefore not surprising that modern arthroplasty designs typically consist of combinations of two or more engineered materials. Yet, because biomaterials are *non-living*, they lack the ability to self-repair or remodel, and therefore a level of additional safety is needed in their properties, particularly fracture toughness and strength, both of which must exceed native bone to ensure adequate performance and prevent premature failure.

3.6. Slow crack growth and fatigue resistance

It is well known that ceramics and glasses are susceptible to delayed failure at stress intensities below K_{IC} under fixed or dynamic loads. This failure phenomenon is often referred to as slow crack growth (SCG) or sub-critical crack growth. Slow crack propagation occurs through linking- up of inherent microstructural defects under static or cyclic stress. The reader is referred to the work of Ritchie et al. for a comprehensive review of the mechanics and mechanisms for fatigue in ceramics, with contrasts to similar processes in metals and composites [339–341] . In brief, there are two operative mechanisms in ceramics, designated as *intrinsic* and *extrinsic*, that either advance or retard crack propagation, respectively. Growth is promoted ahead of the crack tip by *intrinsic* factors such as processing defects (pores, cracks, inclusions, etc.) or due to weak grain boundaries, and is retarded in the wake of the crack by *extrinsic* factors that increase toughness (*i.e.*, transformation- or microcrack-toughening, crack deflection, the presence of bridging grains, and frictional interfaces, etc.). As discussed in the prior section, K_{IC} is a basic material property, which determines a lower limit for instantaneous rupture. While SCG can be operative beneath this critical stress intensity, there also exists a stress intensity threshold below which no sub-critical crack growth occurs. This value is designated as K_{TH}. It is also a major basic material property and indicates the level of stress intensity that a material can withstand without SCG initiation (*i.e.*, thus without delayed failure). Measurements of K_{TH} have traditionally been computed from cyclic stress rupture data, where the rate of crack propagation in a specimen is monitored as a function of load in accordance with the Paris equation [342]:

$$\frac{da}{dN} = A(\Delta K)^m \tag{3}$$

where A and m are scaling factors specific to the material and test conditions, and da/dN is the crack growth rate, ΔK is the stress intensity range (K_{max}–K_{min}), and K_{max} and K_{min} are the maximum and minimum stress intensities applied during cyclic loading, respectively. In his review, Ritchie et al. further taught that K_{TH} was more sensitive to the maximum stress intensity, K_{max}, than to ΔK, and incorporated this into a modification of the Paris equation [339]:

$$\frac{da}{dN} = C'(K_{max})^n(\Delta K)^p \tag{4}$$

where C' is a constant for the material and testing conditions, and $(n+p)=m$. For brittle materials, n is much larger than p, and therefore has a greater influence on K_{max}. The SCG characteristics for a given ceramic can then be represented on a V–K_I diagram where the velocity of the crack, V or da/dN (on the y-axis), can be plotted against the applied stress intensity, K_I (on the x-axis). Traditionally, the lowest observed K_I value has been interpreted as the threshold stress intensity, K_{TH}. While specific values of K_{TH} are often reported, a ratio (K_{TH}/K_{IC}) is usually also computed to normalize operative ranges for SCG. Doing so allows comparisons between different materials and testing methods. Using this methodology, available or computed ratios for K_{TH}/K_{IC} based on graphical interpretations of V–K_I diagrams are provided in Tables 1a and 1b for ceramics and coatings.

For the materials of Table 1a, it can be observed that K_{TH}/K_{IC} values lie between 0.37 and 0.97. This range is due to several factors. Results obviously vary by material, but can also differ due to test conditions and applied stress ratios. Furthermore, the data shown in the Table are inclusive of various environmental conditions – particularly the presence of moisture [211,212,343–355]. Stress corrosion cracking is a common problem for all polycrystalline ceramics due in part to the presence of grain boundary impurities.

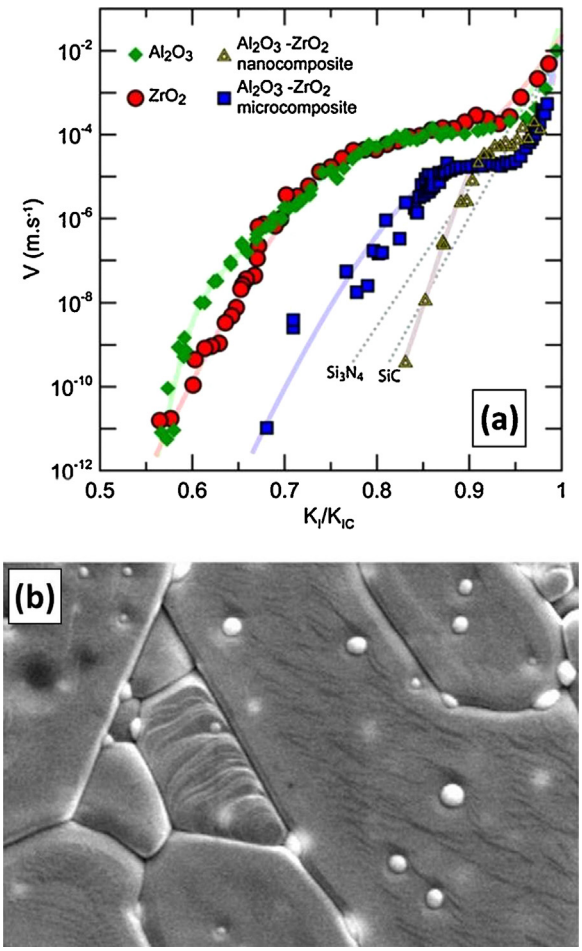

Fig. 10. (a) V–K_I/K_{IC} of biomedical grade alumina, yttria stabilized zirconia, conventional zirconia-toughened alumina 'micro'-composite, and nano-structured alumina–zirconia composite. Schematic V–K_I/K_{IC} of covalent ceramics (SiC and Si_3N_4) are given for comparison [310]; and (b) Microstructure of an Al_2O_3–ZrO_2 composite showing a nano-ZrO_2 grain imbedded in a larger Al_2O_3 grain. (a) Reprinted with permission; (b) courtesy INSA Lyon.

Ceramics with fewer impurities are less sensitive [212,345], and grain boundaries that have high nitrogen content show increased resistance to SCG [349,350]. Compositional and microstructural engineering of these advanced ceramics is on-going by many organizations in an effort to reduce their sensitivity to fatigue. For example, shown in Fig. 10(a) is a V–K_I diagram demonstrating ~50% improvement in K_{TH}/K_{IC} between a biomedical alumina and two ZTA composites, one of which has a highly refined microstructure [310] . Projected values for SiC and Si_3N_4 are also shown for reference purposes. This figure highlights intrinsic differences between oxide and non-oxide ceramics. Traditional oxide ceramics, such as Al_2O_3 and ZrO_2, have higher propensities for SCG than do non-oxides (*i.e.*, SiC and Si_3N_4) because of differences in atomic bonding. Ionic bonds in oxide ceramics are particularly sensitive to attack by moisture at crack-tips (driven by a strong decrease in surface free energy), whereas covalent ceramics are more resistant to bond breakage [356]. Selection of covalent ceramics is therefore preferred for demanding structural applications. However, it is remarkable that the nano-Al_2O_3–ZrO_2 composite shown in Fig. 10(a) has SCG behavior similar to that of covalent ceramics [355]. Furthermore, this accomplishment is indicative of the importance of microstructural engineering and of its impact on mechanical properties. Shown in Fig. 10(b) is a representative microstructure of these types of Al_2O_3–ZrO_2 nano-composites. For reference purposes, fatigue testing has been conducted for most of the biomaterials of Table 1a, and the reader is referred to selected publications for Al_2O_3 [357–362], Mg-PSZ [363–365], Ce-TZP [366,367], Y-TZP [346,368–370], Ce- and Y-ZTA [212,348,355,371,372], ATZ [211], Si_3N_4 [344,354,373,374], CoCr [375], Ti6Al4V [376,377], PEEK [378–380], and cortical bone [381–383].

Note from Table 1b that there is a conspicuous absence of K_{TH}/K_{IC} results for coatings. Inherent fatigue data for coatings are difficult to obtain because of their thin nature. Indeed, excluding hydroxyapatite [384,385], fatigue results for coatings are more associated with the substrate, or the interface between the coating and the substrate, than the coating itself; and even here, there is a scarcity of reported values. The coating obviously imparts fatigue resistance to the substrate because of its combination of inertness, higher hardness, compressive stress, and adhesion [384,385]. However, if the coating delaminates *in vivo*, it can have a dramatic opposite effect, leading to poorer fatigue of the underlying metal [133]. Comprehensive reviews on coating/substrate fatigue, and corrosive fatigue of implantable metals have been provided by Sadananda et al. [386] and Antunes et al. [387].

Nowadays, a new method of assessing K_{TH} has been proposed that goes beyond the traditional graphical interpretations of V–K_I diagrams. It uniquely incorporates and demonstrates the importance of R-curves in determining fatigue resistance. First elucidated by Kruzic et al. [388] using Al_2O_3 and Si_3N_4 as model systems, and later expanded and verified by Gallops et al. [389], Hartelt et al. [390], and Greene et al. [391,392], it deconvolutes K_{TH} into two terms:

$$K_{TH} = K_{I0} + K_R \quad (5)$$

where, K_{I0} is the *intrinsic* toughness of the material without R-curve effects, and K_R is R-curve toughness, due (in the model cases) to bridging grains in the crack wake. To determine K_{TH}, the R-curve toughness is first obtained in the usual manner, followed by a determination of crack dimensions at each point along the R-curve by either direct measurement or indirectly imputed using substitutional modifications to the Griffith and Paris equations. (The derivation can be found in the foregoing references.) Using this methodology, Kruzic et al. found K_{I0} values of 1.3 MPa $m^{1/2}$ and 1.4 MPa $m^{1/2}$ for Al_2O_3 and Si_3N_4, respectively [388]. Remarkably, their results demonstrate little difference in *intrinsic* toughness between materials that have strongly different *R-curve* behavior. Then, using the K_{I0} and K_R values, they derived practical fatigue diagrams for these model materials. The diagram for Si_3N_4 is reproduced in Fig. 11 [388].

Depicted are areas of stress intensity versus crack size where: (1) no SCG is operative under either static or cyclic loading (*i.e.*, below K_{TH}); (2) mixed mode behavior is present, with unstable crack growth under cyclic, but not static loading (*i.e.*, above K_{TH}, but below K_{IC}); and, (3) unstable behavior occurs with either static or cyclic loading (*i.e.*, fast fracture, or above K_{IC}). Later, Greene et al. extended the method to a series of silicon nitrides and reported K_{I0} ranging between 2.0 and 2.3 MPa $m^{1/2}$ and K_{TH} falling between 2.6 and 4.1 MPa $m^{1/2}$ [391]. The corresponding K_{TH}/K_{IC} ratios ranged from 0.47 to 0.59. In accordance with predictions, they demonstrated 100% survivability of a limited number of test specimens subjected to cyclic fatigue below K_{TH} for a range of crack sizes from about 60 to 230 μm. The unique feature of this methodology is the combination of R- curves with fatigue data. Their research provides an important summary to this section of the review, with pertinent instructions for practicing biomedical engineers. When designing an implant system which incorporates a bioceramic, predictive service stresses need to be kept below K_{TH} for the reasonable range of inherent flaws present within the ceramic; *and*, perhaps, more importantly, selection of a bioceramic with high *intrinsic* (K_{I0}) and strong R-curve toughness (K_R) is preferred. A pronounced R-curve

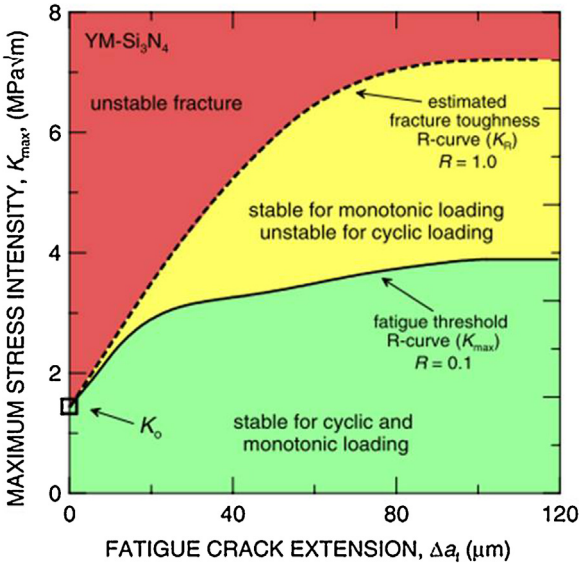

Fig. 11. Fatigue map for YM-Si_3N_4, illustrating regimes of stable behavior for both monotonic and cyclic loading conditions [388]. (YM = Yttria–Magnesia doped). Reprinted with permission.

provides additional safety because short cracks will arrest after a small amount of sub-critical extension rather than progress to failure.

3.7. Biocompatibility

Biocompatibility is an obvious essential requirement for an implantable material. A comprehensive ISO standard has been established for assessing biocompatibility which includes both *in vitro* and *in vivo* tests for cytotoxicity, genotoxicity, carcinogenicity, reproductive toxicity, irritation, delayed hypersensitivity, and systemic toxicity. Testing in accordance with this standard is a prerequisite for legally marketed orthopaedic devices in the US and EU [393]. In general, all of the materials shown in Tables 1a and 1b comply with this requirement. However, passing the standard does not guarantee an absence of adverse reactions or potential systemic problems *in vivo*. A key example is ASTM F799CoCr. While it is employed in multiple implantable applications, its use as both femoral heads and acetabular liners in THA has resulted in considerable morbidity due to tissue incompatibility. CoCr is considered bioinert per the ISO standard principally due to its apparent low solubility. However, the testing protocol does not replicate an evaluation of submicron wear particles which have enhanced dissolution rates. Clinical evidence of the induced harm of these small particles is rapidly growing with numerous adverse events being reported annually. Patients with these devices are advised to have their blood serum levels frequently checked for high concentrations of cobalt, chromium, and nickel which can lead to neurologic, cardiac, endocrine, or ocular impairment [394]. Local formation of pseudo-tumors and tissue necrosis are commonly observed [395,396], and isolated cases of metallosis induced fatalities have been reported [397]. Even for an Al_2O_3 ceramic, which is considered to be completely bioinert, the presence of small wear particles can still produce an inflammatory response. This was aptly demonstrated from *in vitro* and *ex vivo* studies by Yagil-Kelmer et al. [398]. They tested the effect of a range of clinically relevant wear particles from 0.5 μm to 1.5 μm on the viability and cytokine expression from human monocyte cells at a particle to cell concentration ratio of 100:1. While no cell lysis was observed, they found that the smallest particles consistently provoked increased generation of cytokines, suggesting that the smaller particles are bio- incompatible. Another pertinent example is the use of PEEK polymers. Again, these compounds are assessed as being biocompatible, and their performance as arthrodesis devices is acceptable. However, even one manufacturer readily acknowledges that PEEK's osseointegration capabilities are inadequate, resulting in sparse bone on-growth and fibrous tissue formation [235]. These observations have prompted development of Ti- or HAp-coated PEEK or HAp/PEEK composites which effectively employ the added material to solve bone apposition problems [399].

One must remember that the human immunological system is attuned to treating any foreign body as a potential hazard, and prioritizes its defensive actions as: (1) dissolution – if possible, (2) encapsulation – if necessary, and, (3) integration – if appropriate. The physicochemical and physiologic reactions that take place at the implant's surface are complex involving interactions with both inorganic and microbial chemical moieties. Small changes in chemistry at the implant's surface can determine the difference between a device being bio-friendly and one that is rejected. Integration with living tissue is innately difficult for foreign bodies due to a lack of critical biologic functions, such as vascularization, self-reparation, and modification in response to external stimuli [400]. Mechanical loading, friction, and wear all play important roles in determining an implant's biocompatibility and biologic integration. While the goal of any implant is to maintain its function for the life of the patient, all have practical limitations. For articulation devices, present-day failures are due to aseptic loosening, infection, wear-debris induced osteolysis, dislocation, or fracture, with the rate of early failures remaining alarmingly high [275]. Remarkably, these same failure modes were recognized by Sir John Charnley for hip arthroplasty in his pioneering procedures [12]. This is perhaps not as surprising as it may seem, given that some popular implant materials of today are essentially the same as those used by arthroplasty pioneers. The body's rejection of an implant typically leads to fibrous tissue encapsulation [401]. The etiology of this type of failure can be due to poor surgical placement or inadequate initial fixation, or it may be associated with the biomaterial's lack of *mid-* to *long-term* functional biocompatibility [402] . It is therefore important to have *in vitro* and *in vivo* tests that go beyond the general ISO standard. Biocompatibility evidence is basic, but it must also be modified to support the implant's design functions. For instance, biocompatibility of articulation devices needs to include an assessment of the toxicity of fine wear particles; and arthrodesis devices need to be checked for fibrous tissue formation and pseudarthrosis. With this being said, ceramics and ceramic coatings do have biocompatibility advantages over their metal and plastic counterparts. As an example, direct *in vivo* comparisons of Al_2O_3, ZrO_2, Ti6Al4V, and high density polyethylene (HDP) particles implanted adjacent to murine calvarial bone were performed by Warashina et al. [403]. While all four materials are biocompatible in accordance with the ISO standard, the particles of HDP and Ti6Al4V induced two- to three-times higher osteolytic lesions with significantly greater levels of proinflamatory cytokines than the ceramic materials. Nevertheless, as previously discussed, this does not suggest that bioceramics are wholly bioinert. Indeed, as reviewed by Pezzotti, there are probably no truly bioinert substances [79], with physicochemical changes occurring on all materials in contact with human tissue. However, the biologic reactivity of ceramics is indeed lower, and as described in subsequent sections, this feature can be beneficial.

3.8. Phase composition

In this section, a comparison of phase compositions for ceramics and coatings is provided. This discussion is restricted to analyses of "new" and "retrieved" components. Subsequent sections of the review will discuss effects of hydrothermal and corrosive conditions on phase stability.

Shown in Table 1a are surface phase compositions for ceramics. Two materials, α-Al_2O_3 and β-Si_3N_4 are stable, essentially single phase materials, whereas all transformation-toughened ceramics are at least biphasic and purposely metastable. For Al_2O_3, submicron equiaxed powders are received in their α-phase form. A small amount of MgO is added to the Al_2O_3 powder to inhibit exaggerated grain growth during densification. The α-crystal structure is maintained during sintering, and resulting products consist of 100% α-Al_2O_3; but the presence of MgO, along with raw material impurities generates a residual thin glass phase at grain boundaries [404]. Preparation of dense Si_3N_4 involves an irreversible phase transformation. Similar to Al_2O_3, submicron equiaxed Si_3N_4 powders are received in their α- phase form. With addition of sintering aids, α-Si_3N_4 is 100% converted to its β- polymorph during densification. The α-phase has higher free energy (~30 kJ/mol at 25 °C), which makes the reverse β to α transformation impossible [405]. A thin residual glass or crystallized phase exists at Si_3N_4 grain boundaries. Its presence is dependent on the type and amount of sintering aids and powder impurities [406]. As discussed in subsequent sections, the physiologic environment has minimal or no impact on the phase stability of either α- Al_2O_3 or β-Si_3N_4. The phase composition of ZrO_2-based ceramics, including Mg-PSZ, Ce- and Y-TZP, ZTA, AMC, and ATZ is composed of tetragonal-, monoclinic- and cubic-ZrO_2, and α-Al_2O_3 for composites. Processing of these materials begins with co-precipitation or intricate mixing of submicron m-ZrO_2 powders with aliovalent cation dopants (MgO, CeO_2, or Y_2O_3) to form Mg-PSZ, and Ce- or Y-TZP. Separately, admixing submicron α- Al_2O_3 powder in appropriate proportions with TZP powders is performed to obtain ZTA, AMC, or ATZ composites. Other minor additives, such as Cr_2O_3, SrO, TiO_2, and SiO_2 are often included, and these compositions are then densified at temperatures above the m- to t- ZrO_2 phase transition (950–1170 °C). Metastable t-ZrO_2 is predominantly retained upon cooling due to dopant-stabilization and the dense constraining matrix. The data of Table 1a indicate that the surface phase composition of these ceramics varies from 42% to 99% t-ZrO_2, excluding α-alumina for the composites. Mg-PSZ's phase composition after initial firing is approximately 55% c-ZrO_2 with the balance being t-ZrO_2 [70]. The phase composition of as-fired Ce- and Y-TZP is predominately t-ZrO_2 (65–95%), the remainder being m-ZrO_2 and a residual amount of c- ZrO_2 [70].

Excluding α-Al_2O_3, the phase composition of ZTA, AMC, and ATZ ranges from 58% to 99% t-ZrO_2, the balance being mostly m-ZrO_2 [162,247]. Minor addition of SrO results in a tertiary magnetoplumbite phase, $SrAl_{12}O_{19}$, which forms platelet-type grains. Also, as with the other ceramics, impurities segregate at grain-boundaries forming an intergranular glass phase. For AMC, Affatato et al. documented an evolution in the phase chemistry for new, unworn femoral heads over a ten-year period and found chronological reductions in m-ZrO_2 from about ~40% to ~12%, indicating progressive improvements in composition and processing by the manufacturer. Their results are graphically presented in Fig. 12 [247]. Shown also are phase compositions for retrieved, worn femoral heads during the same period. In all cases, increased m- ZrO_2 was observed on worn components. Their results, along with similar findings cited elsewhere within this review, demonstrate the impact physiologic conditions have on the phase evolution of ZrO_2-based bioceramics. The metastability of these ZrO_2-containing materials presents both benefits and risks. Therefore, careful compositional control of the monoclinic content is necessary for enhanced toughness and strength in combination with sufficient hydrothermal resistance, which is seen as a "feature of safety" [160].

Surface phase compositions for PVD ceramic coatings, OxZr, and HAp are provided in Table 1b. The PVD coatings (DLC, TiN, ZrN, and TiNbN) exist as stable amorphous or cubic columnar phases that are epitaxially grown on their respective metallic surfaces

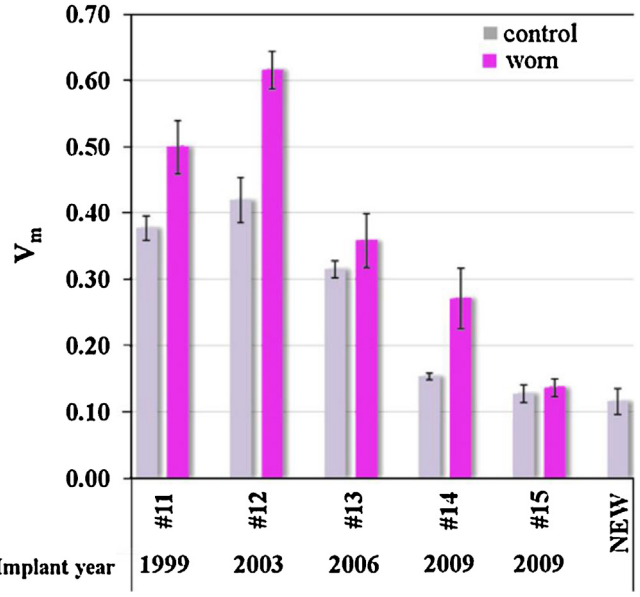

Fig. 12. Average monoclinic volume fraction (V_m) data as obtained from micro-Raman spectra recorded on the unworn (control) and worn areas of analyzed BIOLOX® *delta* femoral heads [247]. Reprinted with permission.

[217,321,407,408]. Even though they are under significant compressive stress because of their growth processes (up to 3.5 GPa), none undergo phase transformation during use [409]. Similarly, OxZr exists predominately as m- ZrO_2 because its oxidation temperature is below the $t \rightarrow m$ transition. However, a small amount of t-ZrO_2 (<5 vol.%) is observed in the microstructure, but does not appear to contribute to any instability [190]. OxZr is also under considerable compressive stress (~670 MPa) due to its growth, and this may contribute to its stability [190]. Finally, as described previously, HAp coatings are multiphase mixtures of CaO, amorphous and crystalline calcium phosphates, and a disordered range of hydroxyapatites that are intentionally designed for dissolution and resorption.

3.9. Corrosion and hydrothermal stability

Corrosive dissolution and hydrothermal degradation of a biomaterial may impact its *in vivo* performance and longevity. On the one hand, debris or dissolved ions can contaminate surrounding tissues leading to formation of pseudotumors or tissue necrosis (*e.g.*, CoCr hard-on-hard bearings), but, on the other hand, controlled dissolution is desirable for other materials (*i.e.*, calcium–phosphates and HAp). Similarly, partial resorption may be preferred for certain hard coatings such as Si_3N_4 [124] but unacceptable for others (*e.g.*, DLC, TiNbN, or OxZr). Consequently, an understanding of each material's corrosive and hydrothermal characteristics is important addenda to basic physical and mechanical properties. In this section, we elucidate on the susceptibility of these bioceramics to chemical corrosion and discuss their hydrothermal stability.

3.9.1. Chemical corrosion

Ceramics are more stable in corrosive environments because they are the oxide or nitride counterparts to metals. While corrosion in metals can be due to electrochemical or galvanic oxidation (*i.e.*, dissolution into soluble ions), ceramics degrade by corrosive attack at grain boundaries. Tribochemical wear can accelerate these processes. Active bioceramics like HAp and TCP degrade *in vivo* by a combination of physicochemical processes and osteoclastic resorption. Most corrosion studies on ceramics have been conducted for industrial applications in severe chemical environments, whereas

Table 3
Qualitative corrosion resistance of biomaterials.

Material	Weak acids	Weak bases	Strong acids	Strong bases	Molten salts	Organic solvents	Saline or SBF
Al_2O_3	⊕	⊕	⊘	⊘	⊘	⊕	⊕
ZrO_2	⊘	⊘	⊗	⊗	⊗	⊕	+
Si_3N_4	+	+	⊘	⊘	⊗	⊕	⊕
TiN	+	+	⊘	⊘	⊗	⊕	⊕
ZrN	+	+	⊘	⊘	⊗	⊕	⊕
440C SS	⊗	⊗	x	x	x	+	+

⊕ = excellent; + = good; ⊘ = fair; ⊗ = poor; x = very poor; SBF = simulated body fluids.

corrosion in the presence of various body fluids or simulated solutions is less-well characterized. This section reviews the corrosive behavior of these bioceramics in both types of environments. A qualitative assessment of the corrosive behavior of ceramics and selected coatings in acids, bases, organic solvents, molten salts, and saline or simulated body fluids is provided in Table 3. A common medical grade stainless steel (440 °C) is also included for comparative purposes.

For ceramics, α-Al_2O_3 shows excellent corrosion resistance under hydrothermal conditions at neutral pH, in saline solution [410], or in the presence of weak acids or bases [411,412]. It is stable in static saline and body fluids at room temperature [413]. Strong acidic or alkaline solutions [411,412,414,415], high-temperatures, and/or pressures are generally required to initiate significant corrosion [416–418]. Al_2O_3 also exhibits moderate corrosion resistance in the presence of high-temperature molten salts [418]. In all cases, corrosive attack occurs at grain boundaries where impurities such as SiO_2, Na_2O, CaO, and MgO segregate [412], with higher purity compositions showing improved corrosion behavior. Also, minor beneficial corrosion improvements for Al_2O_3 were obtained using nitrogen ion implantation by formation of aluminum nitride at the ceramic's surface [413,419] .

The corrosion characteristics of ZrO_2-based ceramics (*i.e.*, Mg-PSZ, Ce- Y-TZP, ZTA, AMC, and ATZ) are more complex due to variations in chemistry, phase composition, and processing. For instance, Mg-PSZ is severely attacked in dilute acids, whereas Ce-TZP shows improved corrosion resistance, with attack occurring at grain boundaries [420]. Some ZrO_2-based ceramics contain sintering additives such as TiO_2, MgO, SiO_2, or CaO, which partially segregate to grain boundaries [158,421]. Similar to Al_2O_3, these impurities provide a corrosion path from the surface to the bulk [420,422]. Intergranular microcracking associated with the $t \rightarrow m$ transformation permits corrosive solution penetration into the material, eventually leading to disintegration. In fact, hydrothermal phase instability of doped-ZrO_2 is the dominant corrosive mechanism, which is operative at all temperatures and pressures above ambient [73,422].

Si_3N_4 is resistant to attack by common organic solvents and weak acids or bases at room temperature [423,424]. Its corrosion behavior is dependent upon the amount and composition of sintering additives, processing conditions, and the type and concentration of the corrosive media [410,425]. Corrosion is more pronounced in highly acidic or caustic solutions [415,426–432] , or in combination with high-temperatures (>300 °C) and pressures (>8 MPa), [433] or in molten salts [434,435]. In one study, sintered Si_3N_4 was more susceptible to attack by HCl than hot-isostatically pressed Si_3N_4, but the opposite effect was found for HF [426]. In two comparable studies, Glauskova et al. found very nearly identical corrosion rates for Al_2O_3 and Si_3N_4 using distilled water at temperatures up to 290 °C [410]; and in a third study, Lin et al. found corrosion of Si_3N_4 in NaCl and $CaCl_2$ solutions to be negligible at room temperature [423] . Similar to other ceramics, corrosive attack occurs preferentially at grain boundaries. In some instances, crystallization of the intergranular glass improves its resistance to corrosive attack [429–433]. In a recent review, compositional tailoring of Si_3N_4's grain boundaries was advocated by Hermann as the best approach to improving its overall corrosion resistance [436].

Corrosion studies on PVD ceramic coatings typically show favorable results for all organic solvents, most acids, bases, and in hydrothermal conditions [437–444]. Because the coatings possess amorphous or columnar grain structures and are deposited epitaxially from high purity targets, they are devoid of impurities, which favors improved corrosive behavior. Nevertheless, imperfections generated during the deposition process, such as micro-droplets, pinholes, or other point defects become corrosion initiation sites, resulting in wear or delamination of the coating, leading to attack of the underlying metal [445]. As an example, Bolton and Hu studied the corrosive behavior of three biomedical PVD coatings (CrN, TiN, and DLC) on surgical grade CoCr in saline at room- temperature [224]. They found improved corrosion resistance for coated samples, but noted that pit defects continued to expose the substrate to corrosion. They also observed that coating thickness via multiple layers was an effective countermeasure to reduce pit defects. As discussed earlier in this review, the use of multiple interlayers is a method of covering-up defects that may randomly appear in any one layer. A review of corrosion mechanisms and preventive strategies for ceramic coatings has been provided by Antunes et al. [147].

There is a lack of published information on corrosion of *in situ* grown OxZr. Available data suggest that this ceramic layer is largely free of the defects observed in PVD coatings [180]. The process of forming the layer through oxidation of the base Zr–2.5Nb metal is diffusion controlled, which is self-regulating with respect to thickness. Provided the base metal is free of impurities and surface contamination, and is homogeneous in composition, the oxidized coating will mimic the chemistry and uniformity of the substrate [190]. Corrosion studies have been conducted on a range of Zr–Nb base metal compositions by Zhou et al. [446] and Branzoi et al. [447] with similar findings—increased niobium content improves the corrosion of the metal alloy. It is plausible that the characteristics of the metal may translate to the oxidized layer given that its cation composition is identical, and its microstructure is composed of lath-type m-ZrO_2 interwoven with adherent NbO_2 or Nb_2O_5 stringers [190]. It is therefore reasonable to expect that OxZr will have corrosion characteristics similar to other non-transformable ceramics for all organic and aqueous solvents, saline, and bodily fluids.

In contrast to the hard ceramic coatings which are corrosion resistant, HAp coatings are intended to degrade. In fact, the most important function of HAp is its controlled dissolution and resorption concurrent with appositional bone formation. As described earlier in this review, thermal sprayed HAp fortuitously contains a multiphase mixture of an amorphous phase, α- and β-tri-calcium phosphates, and several apatite phases, all of which have varying solubility, with the lower order phases being the most soluble. Initial attraction of osteoblasts is generated early in the post-operative period by dissolution of the amorphous phase, whereas long-term boney apposition is governed by HAp. As reviewed by Sun et al. [55], there are six potential degradation mechanisms for HAp coatings: (1) normal dissolution in homeostatic pH; (2) dissolution by

osteoclasts as part of normal bone remodeling; (3) fixation failure resulting in coating delamination; (4) micro-motion abrasion; (5) lamellae cracking due to residual deposition stresses; and (6) preferential attack and dissolution of the amorphous phase. The first two mechanisms comprise the intended function of HAp, whereas the remaining four generate unwanted coating debris. Resorption of the debris can be accomplished by macrophages if they are sufficiently small in size; but beyond about 30 μm, they are reported to be an irritant [55] . Herein lies the key dilemma for HAp coatings: Regulating degradation is essential for adequate fixation, and this is directly related to the process of applying the coating itself. Work performed by a number of researchers suggests that treatments subsequent to deposition or alternative application methods may have advantages in coating chemistry and quality. As examples, Singh et al. demonstrated that post-deposition thermal treatments between 700 °C and 800 °C completely removed undesirable phases [448]. Chen et al. [230] showed a similar result at 600 °C with an associated reduction in deposition defects, and Kwok et al. [449] used electrophoretic deposition and vacuum sintering to improve HAp's dissolution behavior. Further research will undoubtedly lead to the adoption of compositions and methods that balance HAp adhesion with short- and long-term resorption.

3.9.2. Hydrothermal stability

It is critical that the hydrothermal stability of any biomaterial used in joint arthroplasty be investigated and validated. As described earlier, the chemical environment of the human body is such that no material can truly be considered bioinert, even though they may be classified as biocompatible. In this section, studies on the hydrothermal stability of the various ceramics and coatings will be reviewed.

Any discussion of the hydrothermal stability of ceramics should begin with a review of the stability of ZrO_2. Its susceptibility to LTD brought to the forefront the need to assess all bioceramics for *in vivo* deterioration. Unfortunately, introduction of Y-TZP in the mid-1980s occurred without adequate testing and standards. An initial *in vitro* study suggested that the material had sufficient stability for long- term *in vivo* use [68], but early failures persisted [74,450]. From 1997 to 1999, two technical reports were published on the material's hydrothermal stability [451,452]. Static testing in water or an autoclave at temperatures from 60 °C to 130 °C were performed to examine transformation kinetics and polyethylene wear in a hip simulator. Hydrothermal degradation was operative under all experimental conditions; but the calculated activation energy for the transformation extrapolated to biologic temperature (37 °C) suggested that the ceramic's deterioration was kinetically limited, and "25–35 years" would elapse prior to m-ZrO_2 contents reaching 30% and 40%. At this rate, the researchers concluded that the performance of ceramic-polyethylene wear couples should be unaffected for the lifetime of most patients. Yet, retrievals as well as *in vitro* studies showed considerable changes in surface finish in some particular heads [77,453]. The apparent contradiction in performance between *in vitro* and *in vivo* Y-TZP femoral heads was likely due to higher *in vivo* stresses which were not addressed nor replicated in the laboratory studies and to variations in the processes from one producer to another, and even from batch to batch. Surface stresses particularly generated during joint laxity (*i.e.*, micro-separation) have been shown to significantly increase wear in THA joints [454,455]. Also, as described previously, a significant number of *in vivo* fractures from several batches of femoral heads – traced to a processing change – resulted in the September 2001 recall of this material [242]. Although controversial, the LTD mechanism has been described by Sato et al. [456], Guo et al. [457], and later by Chevalier et al. [73]. Addition of trivalent Y^{3+} ions introduces oxygen vacancies in the zirconia sublattice and induces metastability of the t- ZrO_2 phase. In Kröger-Vink nomenclature, the reaction is as follows:

$$Y_2O_3 \xrightarrow{2ZrO_2} 2Y'_{Zr} + 3O_O^x + V_O^{\bullet\bullet} \quad (6)$$

where, Y^{3+} ions substitute for Zr^{4+} with a net negative charge of −1 (*i.e.*, Y'_{Zr}) and $V_O^{\bullet\bullet}$ represents double positive oxygen vacancies in order to maintain charge neutrality. As long as hydroxyl ions are not present in the environment, metastability of the tetragonal phase is assured due to a reduction in the Zr^{4+} coordination number from 8 to approximately 7. However, in the presence of moisture, disassociation of water dipoles into hydroxyl ions $(OH)^-$ and protonic defects $(OH)_O^{\bullet}$ provides a mechanism for annihilation of vacancies, filling them with either the protonic defects or with oxygen ions and interstitial hydrogen. This destabilizes the tetragonal structure and initiates the polymorphic phase transformation at the surface. As described by Keuper et al. and demonstrated in Fig. 13, the process is autocatalytic, having linear kinetics controlled by the reaction of water with Y-TZP grains. Transformation-induced microcracks at grain-boundaries create diffusion paths which cascade the degradation reaction to subsurface grains, where the process is repeated [458].

Understanding the seriousness of this issue, it is remarkable that little attention was initially given to LTD of ZTA, while the basic mechanism is intrinsically the same. The first reported study was by Insley et al. in 2002 [169]. They examined two ZTAs designated CZTA and NZTA. The composition of CZTA was 74% Al_2O_3, 24% ZrO_2 and 1% of other mixed oxides, while NZTA was a 75%/25% mixture of Al_2O_3 and m-ZrO_2. X-ray diffraction analysis of the dense bodies showed only t-ZrO_2 at the surface of the NZTA, but up to 35% m- ZrO_2 in CZTA. Ageing of both compositions was conducted in an autoclave for up to 5 h at 134 °C. Samples were also placed in Ringer's solution at 37 °C for up to 12 months. Remarkably, they reported no increase in monoclinic content and no observable degradation for either composition. Later, Deville et al. published two studies on the low-temperature ageing of ZTA [205,459]. Their first paper examined a range of Al_2O_3–ZrO_2 compositions from 2.5 wt.% ZrO_2 in Al_2O_3 to pure 3Y-TZP. Ageing experiments were carried out in an autoclave at 140 °C under a pressure of 2 bars for up to 115 hours. No ageing was observed for Al_2O_3/ZrO_2 mixtures using unstabilized ZrO_2. However, significant ageing followed by microcracking was noted at Al_2O_3 grain boundaries for ZrO_2 contents of >15 wt.%, resulting in a pathway for water diffusion from the surface towards the bulk. Compositions exceeding the percolation limit exhibited up to 80 vol.% m-ZrO_2 [460]. All Y_2O_3-doped Al_2O_3/ZrO_2 mixtures showed hydrothermal degradation, reaching levels of up to 25 vol.% for the highest ZrO_2 contents. The most degradation was observed for 22 wt.% 3Y-TZP in Al_2O_3, which corresponded to the percolation limit. Their second study focused on ZTA degradation using only Y- TZP/Al_2O_3 composites [205]. Compositions from 10 to 20 vol.% Y-TZP were aged for up to 80 hours in an autoclave at between 110 °C to 140 °C. All compositions showed surface transformation even for short exposures. Higher ZrO_2 compositions showed the greatest change, from ~10% m-ZrO_2 for sintered samples, increasing to ~25% after ageing; and all samples displayed a rapid rise in m-ZrO_2 during initial exposure, followed by a more gradual increase for the duration of the test. No degradation plateau was observed for any composition.

Additional studies by Pezzotti et al. were conducted on commercially available AMC ceramics from 2007 through 2011 [244,246,461–463] . Femoral heads were subjected to autoclave conditions of 121 °C for up to 300 hours. Using Raman spectroscopy, surfaces were examined for changes in ZrO_2 phase composition. They showed that the $t \rightarrow m$ transformation progressed at a high rate during initial exposure (<30 h) and tended to slow thereafter, but did not plateau. At the conclusion of the test, ~75 vol.% of the

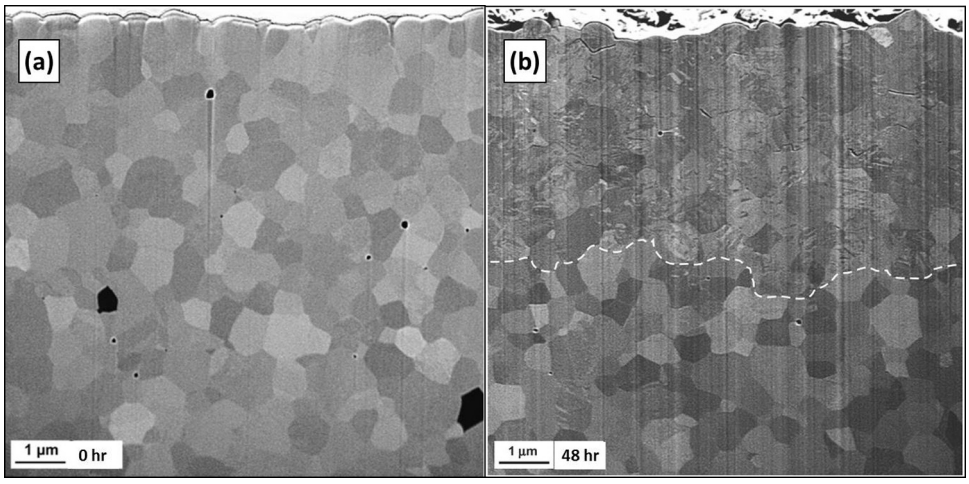

Fig. 13. SEM micrographs of the cross-section of Y-TZP showing progressive evidence of LTD: (a) as-sintered sample with no hydrothermal treatment; and, (b) hydrothermally aged in a saturated steam autoclave at 134 °C and 3 bar for 48 h. Note the clear demarcation between transformed and non-transformed grains and microcracks in (b) [458]. Reprinted with permission.

available ZrO_2 at the surface had transformed. They also found ~28% reduction in surface fracture toughness associated with the transformation. These studies confirmed that AMC was sensitive to hydrothermal degradation; but this result is not unexpected since transformation-toughening is a key feature of this composite ceramic. It also has to be stated that all these *in vitro* conditions were severe, and the effects were only surface related, with bulk properties remaining unaffected. There have been very few *in vivo* failures of AMC femoral heads, and they cannot be correlated so far to LTD. According to one report, approximately 2.2 million devices were implanted by June of 2013, with a reported fracture rate of 0.001% [40]. Retrievals have determined that LTD is operative, but so far, there is no correlation between observed surface transformation and implant functionality [464,465]. Additional research and retrievals will be needed to assess the long-term impact of this phenomenon on the longevity of AMC implants.

It should be noted that Mg-PSZ is also affected by LTD, but its degradation is retarded because of Mg-PSZ's unique microstructure consisting of discrete nano-sized t-ZrO_2 precipitates embedded within larger c-ZrO_2 grains. Moisture must diffuse from grain-boundaries through the cubic matrix to destabilize the precipitates. Its diffusion coefficient is low, so degradation kinetics are expected to be slow [76]. This was experimentally observed by Swain. Severe autoclave exposure of two Mg-PSZ compositions at 400 °C and 6 bar pressure for 4 h showed an increase of ~17% m-ZrO_2 coupled with a modest decline in fracture strength [466].

Returning to Al_2O_3 or using Si_3N_4 might appear to be safe options in avoiding the observed LTD in ZrO_2 based materials. After all, both ceramics are innately phase stable, and presumably immune to attack by moisture. However, as we shall see, this presumption is not entirely correct. Several studies provide insight into the comparative hydrothermal stabilities of Al_2O_3 and Si_3N_4. Sato, et al. examined the hydrothermal stability of a number of Al_2O_3 compositions and Si_3N_4 in caustic alkaline solutions at temperatures up to 200 °C. As expected, they demonstrated no phase change in either bioceramic, and found essentially equivalent dissolution rates for 99.5% Al_2O_3 and hot-isostatically pressed Si_3N_4 [467]. Oda, et al. studied both the hydrothermal corrosion of Al_2O_3 and Si_3N_4 under very severe aqueous conditions (300 °C and up to 85 atm) [416,433]. They showed that both materials degraded by an identical mechanism, which involved attack at the grain boundaries, followed by dislodgement of individual grains. The rate of corrosion for Si_3N_4 was higher than for the alumina, but this was not unexpected given the extreme conditions of the test. Conversely, less severe, and biologically relevant hydrothermal testing was separately conducted on Si_3N_4 by Bal et al. [94], and on Al_2O_3 by Pezzotti [79]. Bal et al. tested dense Si_3N_4 specimens autoclaved at 120 °C in 1 bar steam for 100 h. Components were examined for phase composition and strength both before and after autoclave exposure. There were no observed phase changes, nor were there any differences in the flexural strength (>900 MPa). Using cathodoluminescence spectroscopy on autoclaved samples of Al_2O_3, Pezzotti demonstrated that hydrothermal ageing led to the formation of oxygen vacancies in the alumina lattice. Mechanistically, this is shown in Fig. 14 [79]. Hydrothermal and tribochemical activation of Al_2O_3 results in concurrent hydroxylation of aluminum ions and the release of oxygen along with substitutional inclusion of Mg^{2+} or Ca^{2+} cations forming a spinel-like structure, which is thermodynamically favored over Al_2O_3 [468] . Due to inherently weak grain boundaries and corrosive attack by proton and hydroxyl ions, increased surface roughness and microcracking ensues, which may lead to enhanced wear.

Hydrothermal exposure and/or tribochemical wear of Si_3N_4 also result in marked surface changes. The degradation mechanism is outlined in Fig. 15. As described by Galuskova et al. [410], Dante et al. [469], and also by Pezzotti [79], dissolution of Si_3N_4 occurs by preferential attack of Si–N bonds, with the release of ammonia (NH_3) and hydroxylated silicic acid ($Si(OH_4)\cdot xH_2O$), forming a tribochemical surface film. The presence of this tribofilm leads to low friction for self-mated Si_3N_4, particularly under moderate- speed continuous-motion bearings [114,469,470]; whereas frictional spikes (*i.e.*, stick-slip) are observed with slow-speed non-continuous-motion couples [116]. Also, in contrast to Al_2O_3, which gives up oxygen under hydrothermal conditions, Si_3N_4 is an oxygen scavenger, which may be an advantage in articulation against polyethylene—preventing its premature oxidative deterioration [79].

Few hydrothermal stability studies have been conducted on hard ceramic coatings. At room temperature, these coatings are highly resistant to attack by water, and even offer protective advantages in aqueous abrasive slurries [440]. At higher temperatures and under hydrothermal pressure, DLC films change their carbon coordination from diamond-like to predominately graphitic with a corresponding loss in hardness [471]. In the presence of acids or bases, TiN and ZrN coatings oxidize to form TiO_2 or ZrO_2 at their respective surfaces [409]. However, as discussed previously, the greatest problem associated with these coatings is their discontinuous nature. Localized water penetration and corrosion of

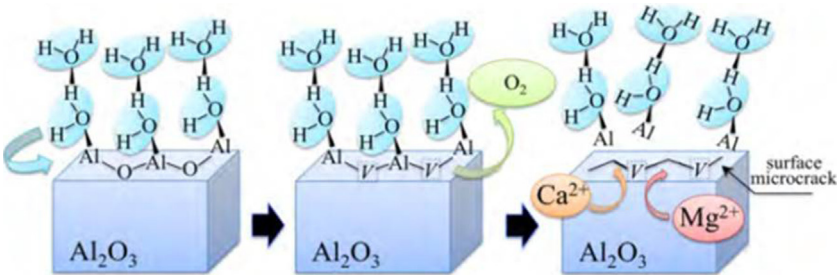

Fig. 14. Tribochemical behavior of Al_2O_3 in a biologic environment [79]. Reprinted with permission.

the underlying metallic substrate is the most common problem *in vitro* [441] or *in vivo* [472]. There are no reported hydrothermal stability studies for OxZr; but this layered ceramic is expected to be highly stable. As discussed previously, perhaps the only concerns for this coating are its thickness and hardness differential between the coating and the substrate, which could lead to delamination [326]. Finally, as presented in the prior section on corrosion, HAp coatings are designed to be hydrothermally active in order to facilitate osseointegration.

In summary, a review of pertinent literature demonstrates that all ceramics and likely all ceramic coatings are susceptible to hydrothermal degradation to a greater or lesser extent. The $t \rightarrow m$ transformation that provides ZrO_2-based materials with enhanced toughness and strength under dry conditions may lead to changes in phase chemistry and properties upon exposure to humid environments. Therefore, under moist conditions, the $t \rightarrow m$ transformation must be assessed during development, or after a process change, and certainly prior to clinical use. Long-term research must also be conducted to assess *in vivo* transformation rates of new ZrO_2 containing materials. Al_2O_3 and Si_3N_4 are phase stable materials under hydrothermal conditions, but are not totally immune to physicochemical surface changes upon interaction with biologic fluids. Similarly, PVD ceramic coatings and OxZr are also stable, but concerns remain about their protective ability over their metallic substrates due to differential hardness, high compressive surface stresses, and deposition defects. However, it should be noted that corrosion and hydrothermal degradation also occur for metal and plastic implants; and on balance, bulk ceramics and ceramic coatings are innately more stable. Consequently, the most important challenges are development of scientific assessments of each material's degradation mechanisms and kinetics, and improving the robustness of their respective processes, in order to eliminate potentially negative consequences to patients.

3.10. Hardness and wear resistance

Hardness is a measure of a material's resistance to elastic or plastic deformation under an applied compressive load [473]. It is a fundamental material property that is related to crystal structure, bonding, and bond density, but can be affected by secondary phases, impurities, grain boundaries, and residual stress [474,475]. Ceramics, which are ionic or covalently bonded, have intrinsically higher hardness than metals or polymers (*cf.*, Tables 1a and 1b). Material hardness plays an important role in artificial joints for one primary reason – wear resistance. All metal, ceramic, and ceramic coatings can be manufactured and polished to extremely fine surface finishes for articulation devices (i.e, <20 nm R_a). *In vitro* hip simulator studies, along with *in vivo* retrievals, demonstrate that polycrystalline ceramics or hard ceramic coatings are more scratch-resistant [150,258,476–478], typically have lower wear rates, and exhibit less osteolysis for self-mated bearing surfaces [247,479–489] and for articulation against polyethylene [150,476,477,490–499] than do CoCr implants. With less than half the hardness of ceramics, CoCr is particularly susceptible to third-body scratching. A scratch in CoCr produces an abrasive gouge below the nominal articulation surface, and also plastically displaces material above the surface. Both effects lead to accelerated wear [500]. Conversely, because of increased hardness, ceramics are more scratch resistant with shallower depths and smaller surface protrusions.

The impact of hardness on wear resistance can be observed from the comparative wear data presented in Tables 1a and 1b.

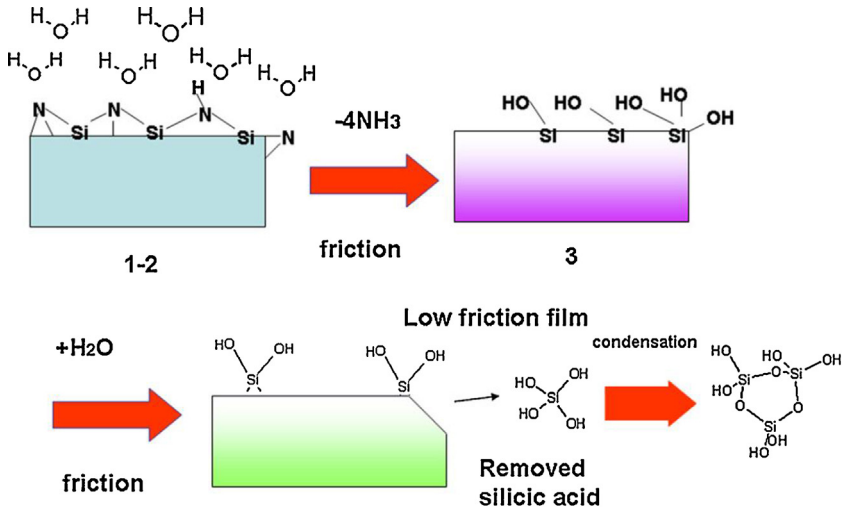

Fig. 15. Tribochemical wear mechanism of Si_3N_4 in a biologic environment in four stages [469]. Reprinted with permission.

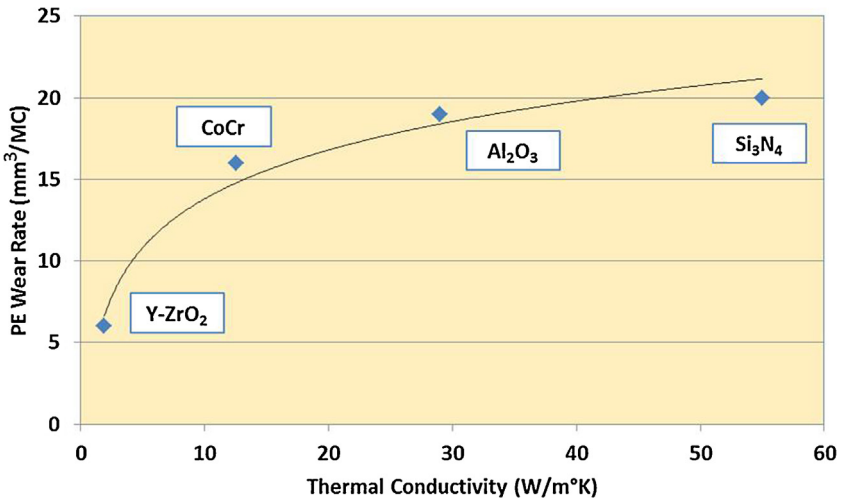

Fig. 16. Polyethylene wear rates versus femoral head thermal conductivity. Adapted from Bowsher et al. [501]. Used with permission.

Wear rates are given for conventional (PE), highly-cross-linked polyethylene (XLPE), and for hard-on-hard bearings using data compiled from hip simulator studies conducted under various protocols during the past 20 years – which partially accounts for the broad range of the observed values. Polyethylene wear is most pronounced for non- or minimally-cross-linked polymers (<40 kGry), and decreases asymptotically for the highly- cross-linked materials (>50 kGry). However, as pointed out by Bowsher et al., any perceived differences in wear need to be tempered with the knowledge that protein precipitation occurs on femoral heads having lower thermal conductivities [501]. This effect is shown in Fig. 16. Less wear is noted for Y-TZP and CoCr in comparison to Al_2O_3 and Si_3N_4 due to greater protein precipitation. Proteins are precipitated because of increased interfacial temperatures. Their presence masks the true wear rate of the bearing. Wear rates for hard-on-hard bearings are lower than XLPE, with AMC and ZTA ceramics providing the best wear performance; however, protein precipitation during *in vitro* wear tests may also play a role in the variability of these wear measurements [502].

Table 1b shows that PVD ceramic coatings or OxZr also provide improved wear resistance because of their high hardness, but only in articulation against polyethylene. Ceramic coatings are unlikely to be effective as hard-on-hard bearings because of the potential for coating failure. Indeed, third-body particles can easily scratch through these thin films, or pit defects can facilitate corrosive penetration, delamination, and catastrophic wear of the underlying metallic substrates. This continues to be a relevant clinical issue as evidenced by several *in vivo* failures. For instance, a clinical trial comparing DLC-coated Ti6Al4V and Al_2O_3 femoral heads articulating against conventional polyethylene showed disastrous results for DLC implants due to corrosive pitting and spallation, leading to a revision rate that was four times the Al_2O_3 control group [133,503]. Several case studies have reported similar poor *in vivo* results for TiN coatings [472,504,505]; and TiNbN coatings were recently found to have completely worn through in another study [506]. OxZr appears to be a solution for these failures due to its substrate coherency and an absence of surface- defects, with clinical results supporting its equivalence to CoCr [144]. However, recent publications have expressed caution over the use of OxZr. Its surface can be easily scratched if: (1) it is malpositioned during insertion; (2) patients experience subluxation or repeated dislocation; or (3) third-body wear particles are present [507–510]. As demonstrated by Lee et al., when an OxZr coating is breached, the underlying soft Zr/2.5Nb alloy can increase polyethylene wear by 161% in comparison to an identically sized CoCr head [150]. These clinical studies and case reports point to the fragile nature of thin hard coatings, and suggest that further development is necessary to improve their reliability. Under ideal laboratory conditions their performance is remarkable; but given on-going *in vivo* failures, clear and convincing clinical evidence will be needed to overcome growing prejudice against their use. Conversely, bulk ceramics provide all of the benefits of thin films with none of the consequences; and the current risk of *in vivo* fracture has become inconsequential. In summary, bulk ceramics should be considered as articulation couples over hard ceramic coatings due to their scratch resistance and low wear, either as self-mated bearings or in articulation against polyethylene.

3.11. Bacteriostasis

Peri-operative or latent infections are a leading cause for hip, knee, and spinal revision surgery [273], with a rate of 2.7–18% [511]. Their occurrence is devastating for patient and practitioner alike, typically requiring surgical removal of the implant, debridement of surrounding tissue, extended hospitalization for antibiotic therapy, followed by re-implantation of an entirely new device [512]. The economic impact to treat infections is typically 4× the cost of primary arthroplasty [513] . While the burden to the healthcare system is large, degradation of the patient's quality of life during treatment, revision, and convalescence has to be considered equally distressing. Nowadays, because of this problem, developing implants with natural or engineered anti-infective properties is garnering considerable attention. Recent reviews have discussed strategies for developing antibacterial devices [514,515]. Interest has focused on preparing composites which perform a dual function, serving both as a structural member (*e.g.*, spinal fusion cage, acetabular cup, coated femoral stem), and incorporating an elutable bactericide (*e.g.*, silver, zinc, copper, iodine, vancomycin, etc.) to prevent biofilm formation or kill planktonic bacteria [516,517]. Elutable calcium from an antimicrobial soda-lime glass–ceramic containing combeite and nepheline crystals was shown by Cabal et al. to effectively resist biofilm formation from five nosocomial strains, while demonstrating excellent biocompatibility towards mesenchymal stem cells [518]. An alternative strategy is to functionalize the implant's surfaces with non-leachable compounds that are contact biocides. Such compounds can be natural or synthetic polymers and include chitosan, peptides, quaternary amines, and *N*-halamines [514,515]. These and similar "active" strategies contrast with more "passive" methods which rely on the material's inherent antibacterial features. Bacteriostasis is the term used to

describe this behavior, and is defined as the property of a material which limits attachment and growth of bacteria without necessarily killing the microorganism. Differences between bactericidal and bacteriostatic materials are significant. Bactericidal compounds often result in large bacteria kill ratios of >99%, whereas bacteriostatic materials only prevent biofilm formation, with reductions from 10% to 90%. There are standardized tests for assessing the effectiveness of implants incorporating bactericidal compounds [519–521]; but, with the exception of a test for plastics [522], none currently exist for comparing bacteriostasis.

In general, ceramics and coatings are considered bacteriostatic. Unlike polymers and metals, they inherently resist biofilm formation. A number of bacteriostasis studies have been conducted on ceramics for arthroplasty and dental applications. Ginebra et al. [523] examined Al_2O_3, Si_3N_4, and AMC *in vitro* for biofilm formation using two bacterial strains (*Staphylococcus epidermidis* and *Escherichia coli*). In comparison to a polystyrene control, all three ceramics showed between 30% and 60% less biofilm formation. In a separate study, Hizal et al. prepared nanostructured and hydrophobic Al_2O_3 and showed that it was effective in repelling *Staphylococcus aureus* and *Escherichia coli* [524]. For dental applications, Yamane et al. completed an *in vivo* human oral study examining titanium, ZrO_2, Al_2O_3, and HAp, all with uniform surface roughness, against Au–Pt alloy as the control. They found no differences among the ceramics as compared to lower adhesion on the Au–Pt alloy [525]. In contrast, Yoshinari et al. demonstrated that Al_2O_3 coated titanium oral implants were significantly more effective in resisting biofilm formation than titanium alone [526]; and Al-Radha et al. found similar results for ZrO_2-coated titanium or ZrO_2-abraded titanium in oral studies [527]. A contrasting bacteriostasis study on several grades of Y-TZP was performed by Karygianni et al. *in vitro* using *Enterococcus faecalis*, *Staphylococcus aureus*, and *Candida albicans*. They observed no anti-adhesive improvement of the ceramics when compared with bovine enamel slabs as controls [528]. Conversely, Gorth et al. tested Si_3N_4, titanium, and PEEK with five separate nosocomial bacterial strains *in vitro* and consistently found lower amounts of biofilm formation (up to 90%), and fewer live bacteria on Si_3N_4 than either of the other two biomaterials. As might be expected, PEEK generated the highest amount of biofilm and harbored the most live bacteria. They postulated that reasons for the observed differences were likely due to: (1) improved hydrophilicity of the ceramic in comparison to the moderately and highly hydrophobic metal and polymer, respectively; (2) chemical moieties on the surface of Si_3N_4 including charged amino and silanol species of $SiNH_3^+$, $SiOH_2^+$, SiO^-, $SiNH_2$, and SiOH, all of which may act to repel microbial attachment; and (3) a micro-textured surface for Si_3N_4, which may also prevent biofilm formation. These features were not observed with the other two biomaterials [107]. Webster et al. pursued this work using an *in vivo* Wistar rat model. Samples of Si_3N_4, PEEK, and titanium were pre-inoculated with 10^4 *S. epidermidis* prior to implantation into the animal's calvaria followed by incubation for up to 3 months. Provided in Fig. 17(a) through (d) are histological analyses conducted subsequent to animal euthanasia, showing a latent infection on the surfaces of the PEEK and titanium implants, whereas none was present for Si_3N_4 [106].

A similar range of results has been observed with the hard ceramic coatings. For instance, a dental study by Grobner-Schreiber et al. using ZrN indicated significant reductions in oral bacteria compared with uncoated samples; but the diversity of the bacterial flora were not affected [529]. For DLC, Love et al. reviewed a number of bacteriostasis studies which showed that hydrophobic carbon coatings with low hydrogen contents were very effective as a bactericide, even when compared with the antibiotic *Gentamicin* [148]. Finally, Shida et al. performed an *in vitro* bacterial adhesion study for OxZr, CoCr alloy, titanium, and stainless steel implants using *S. epidermidis*. All samples were carefully prepared to have similar surface roughness. Reported amounts of *S. epidermidis* that adhered to OxZr and CoCr were significantly lower than for titanium or stainless steel (up to ~60%) [530].

Clearly, the range of observed results for both the ceramics and coatings suggests that exogenous factors play key roles in determining bacterial adhesion. A review of potential parameters governing biofilm formation was conducted by Renner et al. [531], which included physical, chemical, and interactive factors between orthopedic devices and bacteria.

They concluded that interactions between microbes and biomaterials are complex, and the diversity and adaptability of differing bacterial strains to the milieu of the human body make it difficult to construct even simple engineering guidance. For example, it is generally accepted that hydrophilic substrates are more resistant to biofilm formation; but this is not true for all microbes, with common *S. epidermidis* preferring either polar or hydrophobic surfaces [532]. Certainly, the unique physical and chemical environment presented by an implant's surface is important. However, while surface roughness, topography, and chemical properties may dictate bacteria attraction, it is the external functions of the microbe itself (*i.e.*, flagella, fimbriae, and pili) which facilitate its attachment. In this regard, bacteria have an advantage because of their living nature. They have motility, selectivity and are adept at exploiting weaknesses present in inanimate implants or the surrounding environment. Not surprisingly, defensive strategies against their onslaught may need to be as varied as the bacteria themselves. Potential solutions include dense implants coated with bactericidal or bacteriostatic compounds, porous structures infused with elutable antibiotics, or devices engineered with micro- or nano-structured features that resist biofilm formation. These and other strategies are active areas of research. In summary, development of anti- bacterial bioceramics represents a new frontier—one in which necessary structural functions are combined with bacteriostatic or bactericidal features to combat an evolving variety of nosocomial microbial strains.

3.12. Osseointegration

The rigid and permanent fixation of an alloplastic medical device with native bone is referred to as osseointegration (or sometimes as osteointegration). Obviously not all bioceramics and coatings are designed for integration with bone. Some are solely important for articulation and wear. However, at the end of the day, implantable medical devices will ultimately fail if they are not soundly supported by the musculoskeletal system. In this regard, osseointegration is as critical in its function as wear resistance is in its respective role. While significant understanding has been acquired with regards to wear resistance, our knowledge of factors affecting osseointegration is only now coming to light. Interactions between the biological environment and implant surfaces are complex, involving a sequence of events that begins with protein absorption and, if successful, ends with fixation via bone on-growth or in- growth. Previous generations of ceramics were considered efficacious if they were merely classified as being bio-inert or biotolerant, meaning that they did not elicit an inflammatory response. However, this does not suggest there were no reactions. On the contrary, the body's immunological answer to bioinert materials has typically been isolation and fibrous tissue encapsulation. However, to effectively integrate, bioceramics must go beyond this simple one dimensional classification. They must be bioactive and/or bio-resorbable, capable of interacting with tissue, inducing bone formation, and providing fixation.

The biological sequence of events leading to osseointegration is complex and dependent on factors associated with the physicochemical structure of the implant and its interaction with proteins

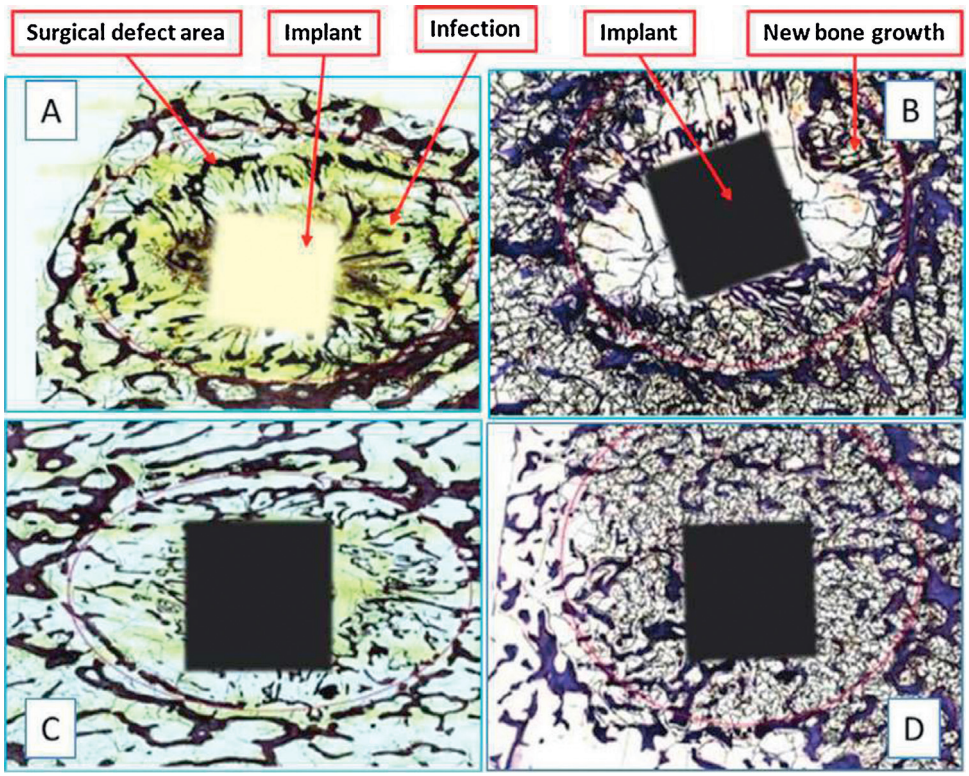

Fig. 17. Effect of biomaterial on latent infection in Wistar rat calvarial defects [106]. Implants were pre-inoculated with 1×104 *Staphylococcus epidermidis*. Histology performed 3 months after implantation: (a) PEEK; (b) Si_3N_4; (c) titanium; and (d) Si_3N_4. Reprinted with permission.

and living cells. The first and immediate biologic reaction to a foreign body is its coating with proteins. For bioceramics, this process has been documented by Wang et al. in detailed review [533]. Fibronectin, a protein found in plasma binds almost instantaneously to all biomaterials, but other proteins including vitronectin, laminin, collagen, and fibrin also quickly adsorb and participate in wound healing [534]. Adsorption of these molecules is induced by the roughness, hydrophilicity, charge, and topography of the biomaterial's surface, with micro- or nano-structured surfaces being the most effective. Proteins orient themselves to local variations in surface charge and topographical features, and adhesion occurs by electrostatic and mechanical means. Specific active sites on these molecules are recognized by mesenchymal stem cells, mainly integrins, which subsequently bind to the proteins. However, as discussed by Kieswetter et al., cell attachment is neither predestined nor immediate. It may take hours to occur [535] . Again, surface chemistry and topography of the implant dictate this timeline, and remarkably, cells can distinguish between different chemistries and surface features [536,537]. As reviewed by Anselme et al., many studies suggest that surface topography may be more important than chemistry, with more mature and differentiated cells adhering to micro- and nano- structured surfaces [538]. However, the presence of soluble calcium phosphates, bioavailable silicon, and magnesium also appear to be key chemical species promoting adhesion and proliferation of progenitor cells, facilitating their eventual differentiation into osteoblasts [539–541]. Provided the chemical environment remains conducive to continued cell function, osteoblasts secrete a calcified osteoid which leads to endochondral ossification and eventual fixation of the implant. Most of our knowledge with respect to the interaction of cells and biomaterials comes from studying titanium alloys, but features that promote its osseointegration appear similar if not identical to those that are likely operative for bioceramics [542–544]. Ceramic scaffolds possessing interconnected porosity have also been shown to be effective in boney in-growth for a number of different materials including bio-glasses and ceramics [545], tantalum [546,547], PEEK [548], and of course, various HAp compositions [60,549]. The integration ability of these scaffolds is dependent upon surface chemistry and the size distribution of engineered porosity. As with on-growth, a chemical environment with appropriate concentrations of Ca, P, Si, and Mg are essential for in-growth, along with porosity that is within a preferred range of ~100 μm to ~500 μm [550]. Although integration occurs for pores smaller than 100 μm, vascularization of the porous structure is most pronounced when openings between the pores exceed this minimum [550] .

A number of the ceramics and coatings have been tested for their ability to interdigitate with living bone, beginning with porous Al_2O_3 in the 1970s [21]. While this early work showed that ossification is possible, the immunological response to Al_2O_3 at that time was encapsulation in fibrous tissue. Bioactive coating strategies have subsequently been employed for Al_2O_3 to alter its local chemical environment and thereby improve boney apposition [551,552]. The use of Y-TZP for dental implants has spawned numerous studies examining its osseointegration characteristics with a review performed by Hisbergues et al. in 2009 [80]. While significant human clinical data are lacking, *in vivo* animal studies suggest that its osseointegration performance is at least equivalent to titanium alloys (*i.e.*, the gold standard for oral surgery). Effective osseointegration has also been demonstrated for mixtures of ZrO_2 and Al_2O_3. For example, using push-out strengths as a measure of integration, Burgkart et al. examined AMC in an ovine model [553] . They showed that a pre-engineered macro-porous structure required approximately eight times the push-out force when compared with smooth implants, and histomorphological evaluations revealed consistent and substantial boney apposition within the porous structure at 12 weeks post-operatively. Similar effective osseointegration for ATZ dental implants has also been reported [554] . For Si_3N_4, several studies demonstrated its osseointegra-

tion capabilities. Anderson et al. showed osseous penetration of up to 3 mm in ~72% porous Si_3N_4 with excellent vascularization twelve weeks after implantation in an ovine model [105]. Similar studies by Guedes e Silva et al. showed good boney apposition for Si_3N_4 samples in rabbits evaluated eight weeks after implantation [103,104]. In Wistar rats, Webster et al. compared the osseointegration of Si_3N_4, PEEK, and titanium, reporting that Si_3N_4 had improved osseointegration over the other two biomaterials at all-time points up to 3 months post-operatively, both under aseptic conditions and when implants were pre-inoculated with 10^4 *S. epidermidis* [106].

There are few reported studies on the osseointegration of hard PVD ceramic coatings. As discussed previously, while these coatings are biocompatible, their ability to fixate to bone is governed by local surface chemistry and topography. From a chemical standpoint, they are largely bioinert, and their surface roughness is determined by the underlying substrate. Consequently, improvements in osseointegration are expected via topography modifications of the substrate or by adjustments to deposition composition. Recent studies suggest that some or all of these strategies may be effective. For example, DLC coated titanium implants showed significantly greater boney apposition and bone thickness growth than comparable bare titanium in an *in vivo* femoral study conducted on rats [555]. An *in vitro* study using DLC suggested that several compositions may provide osseointegration improvements [556]. Alternatively, for TiN coatings, Sovak et al. found excellent mineralization at the interface of implants in Wistar rats, and concluded that TiN was at least as effective in boney fixation as uncoated Ti6Al4V substrates [557]. Finally, for dental implants, Rizzi et al. found that application of a ZrN coating to titanium markedly improved osseointegration and reduced healing time [558]. Similar results might be expected from the other ceramic coatings, but data are currently lacking.

As might be expected, studies on the osseointegration of HAp coatings have been numerous and significant – and no more so than for those that have examined the long-term survivability of HAp-coated hip stems [49,52,559,560]. A number of these studies report Kaplan-Meier survivability of >92% at 20+ years post implantation. Failures were mostly unrelated to the hip stem itself, and either involved anatomical changes, wear, osteolysis, and aseptic loosening of the acetabular cup, or other medical problems. Patient satisfaction with these implants remained high (also at 92%) at final follow-up, with essentially all femoral stems showing signs of stable fixation. Development of HAp coatings is closely related to parallel innovative research into porous synthetic bone scaffolds. Osseointegration is an essential requirement for these devices as well. Today, autograft and allograft are primarily used for rectifying large bone defects due to trauma, tumor resection, osteomyelitis, or necrosis. However, limitations which preclude their wide- spread use include restricted availability, donor site comorbidities, and risks for infection or disease transmission. Consequently, ceramics, glasses, and orthophosphate composites are being extensively investigated as alternative bone-building therapies. The interested reader is referred to a number of recent relevant reviews in this field [44,60,561–567]. There is general agreement that an ideal bone scaffold must be biocompatible and osteoinductive, having a broad range in porosity for cellular proliferation, neovascularization, and bone ingrowth, possessing a strength greater than the bone being repaired, but having a similar elastic modulus to prevent stress shielding. Furthermore, the scaffold must be customized in properties and shape to closely match the osseous defect, and be slowly resorbable concurrent with the ingrowth of new bone. These are challenging requirements given differences in patient age, bone quality, and overall health. HAp and tri-calcium phosphate are commonly used clinically because of their demonstrated biocompatibility, bioactivity, osteoinductivity, and chemical similarity to the apatite phase of living bone. Nanocrystalline HAp particles, fibers and composites having open interconnected porosity, from about 100–900 μm, compounded with bioglass (*i.e.*, 45S5 or β-wollostonite) or synthetic polymers (*e.g.*, polymethylmethacrylate, polyacrylic acid, polyvinyl alcohol, and others) display increased mechanical properties, good biocompatibility, and bioactivity [58,60,566]. Other organic-inorganic multicomponent HAp scaffolds are being explored, including biomimetic adsorption, or seeding of the porous structure with collagen, gelatin, chitosan, growth hormones and factors, bone morphogenetic proteins, genes and mesenchymal stem cells, or various therapeutic drugs. These additives are designed to induce osteo- and angiogenesis, or target disease and prevent infection, respectively [568]. While many of these strategies are exploratory in nature, they demonstrate the breadth of research being conducted on HAp composites, with more than 10,000 scientific publications occurring within the last 4 years [569]. It spite of this progress, utilization of synthetic bone scaffolds remains in its infancy. Challenges that must be overcome include: (1) continued improvement of mechanical properties, particularly fracture toughness, through the use of nanostructured materials, and by developing ceramic–ceramic, ceramic–glass, or ceramic–polymer composites; and (2) enhancement of bioactivity through incorporation of the aforementioned growth factors, genes, cells, or biological agents. Ultimately it should be possible to engineer a new generation of bespoke-based HAp scaffolds to address specific patient pathologies [44]. With attendant developments in bone tissue engineering, the effectiveness of HAp coatings in total joint arthroplasty will undoubtedly improve as well.

To summarize, osseointegration mechanisms for ceramics and ceramic coatings are complex, but dependent principally on two interrelated factors: (1) the biologic environment next to the implant itself, including its hydrophilicity, surface charge, and availability of osteogenic elements (*e.g.*, Ca, P, Si, and Mg) and compounds (*e.g.*, collagen, chitosan, synthetic biocompatible polymers, and therapeutic drugs); and (2) the structure, topography and roughness of the implant's surface, or the size distribution of its pores and connecting channels. These engineered features promote protein adhesion and attract progenitor cells which differentiate into osteoblasts and osteocytes, leading to the firm fixation of orthopaedic devices.

4. New directions in bioceramics

4.1. Novel ceramic materials and composites

Over ten years ago, Dr. Larry Hench, the distinguished researcher and inventor of 45S5 bioglass [570], forecasted the development of a third generation of biomaterials [571]. Whereas the first two generations involved use of bioinert and then bioactive or resorbable materials, respectively, he envisioned a third generation designed to assist in healing the body. His prognostication is becoming a reality, but not by abandonment of first and second generation materials. Indeed, technological progress on all three generations exists on a continuum and are additive. In the following sections, we sequentially discuss new directions in bioinert, bioactive, or resorbable ceramics, and reiterate Dr. Hench's view with respect to the future, which includes "smart ceramics."

4.1.1. Bioinert ceramics

Fifty years of clinical experience has demonstrated that there are no truly bioinert materials. All induce an immunological response, but ceramics tend to minimize this interaction. Bioinert ceramics have evolved through trial and error experimentation from Al_2O_3

(modest strength) to ZrO_2 (high strength, but also high sensitivity to LTD) to ZrO_2–Al_2O_3 composites (high strength with improved LTD resistance). While the current standard in bioinert ceramics is BIOLOX® *delta* (CeramTec, Plochingen, Germany), its position may eventually be challenged by other ZrO_2 and ZTA compositions having both high strength and little or no LTD, or by non-oxide ceramics such as Si_3N_4 with elevated strength and no LTD. As an example of an improved ZrO_2, Matsui et al. demonstrated that addition of a small amount of germanium oxide (0.30 mol%) to a 3 mol% Y_2O_3-doped ZrO_2 coupled with low- temperature sintering produced a fully dense nano- crystalline Y-TZP (grains <300 nm) which exhibited no LTD for 4 years in a steam autoclave at 140 °C [572]. As other examples, ZTA nano- composites which exclude the use of yttria, or which incorporate zirconia nano-particles (<500 nm) evenly dispersed within alumina grains have been developed [154,573]. Both composites result in high strength, tough, and highly LTD resistant ceramics. Torrecillas et al. predict that further developments in nano-structured ceramics and composites should result in a new generation of biomedical implants with lifespans matching the life expectancies of their recipients [574]. Combining Y-TZP with Ta, Ti, or Nb metals to form cermets has also been investigated with promising results. These composites demonstrate improved ageing behavior and mechanical stability, reduced friction against polyethylene, and excellent biocompatibility [575–577]. Even returning to MgO-doped PSZ is a consideration, given its reasonable strength, enhanced toughness, and LTD resistance [578]. Lastly, use of non-oxide Si_3N_4 is also a viable option because it has the requisite strength and toughness, and is absent of any LTD [94].

Overcoming the deficiencies of hard ceramic coatings is also being explored. Recall that thickness, inherent deposition defects (*i.e.*, pinholes and delamination), and wear debris limit the articulation life of these materials. As pointed out by Alakowski et al., the survivability of any thin film under load is proportional to the square of its thickness [579]; with thicker coatings (particularly those composed of multiple interlayers) reducing the likelihood of defects [147,317,580]. Coating thicknesses will need to increase from less than about 5 μm (current state) to greater than 15-20 μm (future state) in order to achieve the goal of being lifetime prostheses. Recognizing a renewed potential for hard surface coatings, a European consortium was formed in 2013 to develop thick PVD Si_3N_4 coatings on cobalt-chromium alloys with a stated objective of introducing them as hip or knee prostheses in clinical trials by about 2018 [581] . This particular bearing surface has the unique advantage of eliminating osteolytic joint debris because Si_3N_4 wears via a tribochemical reaction, the products of which are soluble and resorbable [123,124]. With these ongoing developments, bioinert ceramics and coatings are expected to remain as favored materials for future joint arthroplasty procedures.

4.1.2. Bioactive and resorbable ceramics

Engineered transitions between bioinert and bioactive ceramics represent a new field of endeavor, with advances in the areas of functional gradient materials (FGM) and self-assembled monolayers (SAM). Additionally, while calcium orthophosphates are the standard for bioactive and resorbable ceramics, structural and compositional improvements are enhancing their performance as well.

Functional gradient materials—FGMs are designed by changing the structure or composition within a component to provide variable properties. As discussed by Bahraminasab et al., joint arthroplasty research often tends to be compartmentalized, with some investigators focused solely on bioactivity for improved implant fixation, ignoring problems such as adverse wear or stress-shielding; whereas others concentrate on mechanical properties or friction to reduce stress shielding or wear-induced osteolysis, respetively [582]. Perhaps an optimum solution is introduction of functionally graded materials which address all three issues. For instance, one side of a ceramic acetabular monoblock cup can be engineered to have high porosity, low elastic modulus, and a bioactive coating (*e.g.*, HAp) to promote osseointegration and minimize stress shielding; while the opposite side has low porosity, high elastic modulus, and hardness for wear resistance. Furthermore, such a device has the added advantage of conserving native bone due to elimination of the metallic shell. This idea has proceeded beyond the conceptual stage. Dual porosity ceramic implants are particularly advantageous in spinal fusion [583,584] and are actively being developed as THA acetabular components [585,586]. FGMs based on composition are also being developed. For example, Laurenti et al. designed an innovative reconstructive implant that combines bioactive 45S5 glass fibers and polyurethane. The distal end of the implant is predominately polyurethane, and serves as replacement cartilage, while the proximal end, which has a high concentration of glass fibers, osseointegrates for fixation. They demonstrated excellent performance in an animal model [587]. In another less demanding example, Zhao et al. functionally distributed iron oxide within a dental ZrO_2 to generate a gradient in color [588].

Self-assembled monolayers—use of self-assembled monolayers represents another effective method of bridging the gap between bioinert ceramics and biologic tissue. In fact, SAMs can be considered functional gradient materials themselves, but on the nanometer scale. The technique involves grafting or binding organo- metal molecules to an implant in a single layer in order to activate an otherwise bioinert surface. A recent review of SAM methods as applied to ceramics was prepared by Boke et al. [589]. They focused on SAMs consisting of organo-silane polymers whose silane heads proximally attach themselves covalently to the ceramic's surface, allowing for further functionalization of their distal tails. Silane-based SAMs are effective because of their ability to readily bind with silicate surfaces. However, other inorganic moieties are also available, including thiolates [590] and phosphonates [591]. The phosphonates are particularly valuable in functionalizing many materials including bioinert ceramics and bioactive calcium orthophosphates, with at least one start-up company commercializing their use [592]. The distal tails of the SAM can be functionalized with other molecules to customize surface properties for hydrophilicity or hydrophobicity, for cell adhesion, to selectively promote or repel protein adsorption, and to resist or kill adherent bacteria [591,593,594]. Another SAM, applied to polyethylene, has been shown to favorably reduce friction between acetabular liners and metal femoral heads in total hip arthroplasty. This unique SAM, consisting of 2-methacryloyloxyethyl phosphorylcholine (PMPC) provides hydrophilicity and effective hydrodynamic boundary lubrication between the two articulation surfaces. PMPC grafted liners dramatically reduced polyethylene wear debris by 99.9%, making their performance equivalent or even superior to ceramic-on-ceramic bearings [595]. Three-year clinical and radiographic outcomes for a 76 patient trial using PMPC grafted XLPE liners and CoCr femoral heads showed very high Harris hip scores (95.6), no adverse events, and mean femoral head penetration rates of <0.002 mm/year at the latest follow- up. This is a remarkable achievement given that comparative trials without PMPC grafted liners showed at least an order of magnitude higher penetration rates—from 0.01 to 0.06 mm/year [596]. While the study is still in its early stages, its positive outcomes portend a bright future for this and similar SAM technologies.

Calcium orthophosphates—hydroxyapatite and various calcium phosphates are already considered bioactive because of their osteoinductive and resorbable properties. Yet, these features are being enhanced by elemental substitutions, development of composites, biomimetic processing, and introduction of nanostructures, with several recent exhaustive reviews highlighting these efforts [44,566,597,598]. While pure orthophosphate mixtures are

effective bone inducing agents, they lack other trace elements commonly found in native bone. Consequently, investigators have doped HAp with silicon [539], fluorine [599], strontium [600], magnesium [601], and carbonates [602] among others in attempts to increase bioactivity and osteoinduction. Additions of bone morphogenetic proteins and growth factors [568], mesenchymal stem cells [603], and therapeutic genes [604] have also been explored for similar reasons. Elutable silver [605,606] or antibiotics [607,608] have been incorporated to inhibit nosocomial infections. Composites of synthetic bio-erodible polymers [609] (*e.g.*, polylactic acid, polyglycolic acid, and polylactic-co-glycolide), natural occurring polymers [610–612] (*e.g.*, alginate, collagen, chitosan), or non-resorbing polyurethane [613] have been constructed principally to improve mechanical properties. Similarly, HAp has been admixed with bone cement and antibiotics for fixation and infection prevention, respectively [614]. Magnetic compounds [615] , electrically conductive compositions [616], or carbon nanotubes [617] have been added to HAp with favorable osseous outcomes. Additionally, biomimetic nanocrystalline HAp coatings are among the latest developments that show significant potential. Nano-structures have enhanced mechanical properties, consistent resorption kinetics, and increased osseointegration in comparison to thermally applied coatings [58,261,618]. These various mimeses or modifications have been effective, although few are in clinical use at this time. Each of these concepts will continue to be active areas of research, with future commercial products undoubtedly improving outcomes for joint arthroplasty patients.

4.1.3. Smart ceramics

Smart materials are defined as having adaptable properties that respond to external stimuli (*i.e.*, stress or strain, local chemistry, pH, moisture, temperature, and electric or magnetic fields) [619]. Non-ceramic examples include shape memory alloys and polymers which are designed to expand or contract in response to temperature fluctuations, or to swell or shrink due to changes in moisture or pH. For ceramics, piezoelectric compounds (*e.g.* barium titanate, $BaTiO_3$) which generate a voltage under an applied stress are classic examples. Titanium dioxide (TiO_2) is another smart ceramic. Its photocatalytic behavior is effective for self-cleaning glass, water purification, and in prevention or eradication of biofilms [620,621]. Even ZrO_2-based ceramics (*i.e.*, Y-TZP, ZTA, AMC, and ATZ) and Si_3N_4 are arguably smart biomaterials. They dynamically respond to localized stress and strain changes to minimize catastrophic fracture risk. In ZrO_2, the tensile stress field in front of an advancing crack spontaneously triggers the $t \rightarrow m$ transformation, thereby reducing stress and arresting crack propagation. A different microstructural mechanism is operative in Si_3N_4 (*i.e.*, crack wake bridging) which yields a similar result. These smart mechanisms are effective in ensuring the reliability and longevity of bioinert prostheses. However, the third generation of smart ceramics (according to Dr. Hench) needs to further interact with the human milieu to facilitate healing, not just replace defective or diseased tissues. In keeping with this challenge, several recent reviews provide perceptive viewpoints on this new generation of smart materials. Parvizi et al. envision the use of "self-protective" implants, possessing surfaces with permanent covalently-grafted antibiotics or bacteriostatic molecules [622]. They argue that such moieties will be essential in combating a rising incidence of periprosthetic joint infections (PJI) which result in implant loosening, revision surgery, and replacement. Other researchers have taken on this challenge and effective surface coating strategies against PJI are being realized [515,623,624] . Barrere et al. suggest that biomaterial assisted tissue engineering is in its infancy, and hierarchal constructs are the key to its success [625]. Devices must meet at least three criteria: (1) be recognized and accepted by human tissue; (2) restore tissue utility; and (3) stimulate biological function. Separate pertinent reviews by Wegst et al. [626], Perez et al. [627], and Porter et al. [628] discuss the future of biomaterials by drawing from bioinspired, naturally occurring compounds and structures. They predict synthetic composites will eventually be able to imitate living tissue. To do so, the physical, mechanical, chemical, and biological properties of these composites will need to be engineered (internally and externally) to address unique patient pathologies. Adjustments to mechanical properties (*i.e.*, elastic modulus and strength), tailoring of the morphology and biomimetic functionalization of surfaces with grafted polymers, and inclusion of therapeutic drugs, proteins, or stem cells are all suggested strategies. Finally, Holzapfel et al. promote a multidisciplinary approach in which biologists and biomaterial scientists collaborate to advance beyond biocompatibility and bioactivity, to biomimicry—eventually imitating the extracellular matrix (ECM) of natural tissues [629]. Their stepwise vision is shown diagrammatically in Fig. 18.

While they recognize a long road lies ahead in understanding ECM's complexity, they suggest that this knowledge will ultimately achieve the objective of translating smart biomaterials from the "bench to the bedside." Clearly, one ceramic, HAp, is at the forefront of meeting many of the "smart" criteria outlined by these prognosticators. It can be compositionally modified to resist infection. It can include progenitor cells and genes which provide signaling instruction to *in vivo* cells to differentiate and induce ossification. It can incorporate therapeutic drugs, natural or synthetic polymers, and can be biomimetically deposited to induce native bone growth. Finally, its dissolution kinetics can be tuned so that metabolic resorption occurs consistent with bone reformation. In 2010, a European consortium was formed to explore and conduct clinical trials for a number of these therapies using orthophosphate scaffolds [630]. It is apparent that the modulated features of HAp are living up to Dr. Hench's prediction of a future in which biomaterials aid in repairing instead of replacing living tissue. Although significant research remains, the paradigm shift now occurring with HAp should ultimately be transferrable to other bioceramics.

4.2. Manufacturing processes

There are three general methods for manufacturing ceramic components—subtractive, near-net-shape, and additive. Subtractive manufacturing is the dominant and traditional method. It involves forming of oversized parts followed by material removal to achieve final shapes. Forming methods include dry- or isostatic-pressing, slip-casting, gel-casting, extrusion, and injection molding. Machining is performed on pre-fired parts using cutting, turning, and milling operations (green state), or on fired parts by grinding (dense state). Over the past 30 years, subtractive methods have benefited from innovations in computer-aided design and manufacturing (CAD/CAM) integrated with sophisticated machine tools. Components previously only produced by journeymen machinists and craftsmen are now routinely manufactured by CAM programmers and machine operators. With computer-based technology, intricately shaped parts are now available that previously were considered improbable. Subtractive manufacturing is remarkably flexible and ideal for short production runs and rapid-prototyping [631]. Nowadays, almost all ceramic orthopaedic implants are produced using this method, and it is also extensively used to produce custom dental implants [632]. However, there are drawbacks and limitations. By its very nature, subtractive methods involve waste of raw materials, tooling, energy, labor, and capital equipment. Furthermore, there are constraints to the complexity and feature sizes that can be addressed with this process. Intricate 3-dimensional scaffolds, with sub-millimeter and hidden internal features are nearly impossible, although creative processing, machining, and bonding techniques have been employed to produce prototypes [633,634] .

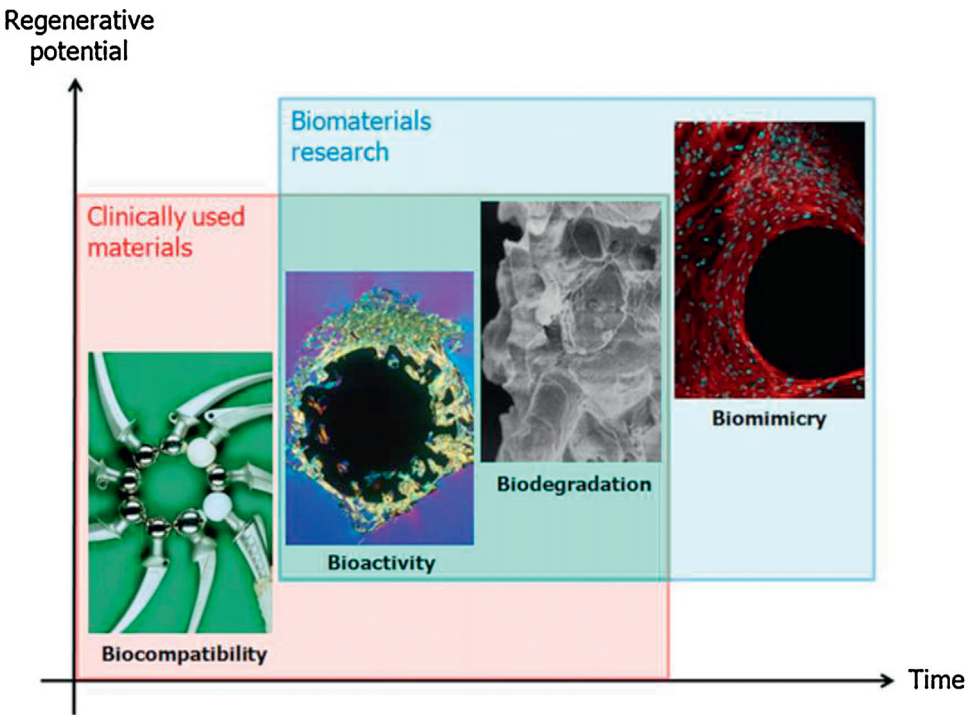

Fig. 18. Evolution of biomaterials. Today's clinical materials will progress from being bioinert and biocompatible to bioactive and biodegradable, to ultimately mimicking or stimulating cellular function [629]. Reprinted with permission.

Near-net-shape fabrication was the next logical progression in ceramic manufacturing. While, it too, involves forming of components by the aforementioned methods, in this case, parts are produced to achieve essentially their final size subsequent to firing. Very little intermediate green machining or final grinding are required, and usually only to remove mold flashings. However, achieving net shape dimensions necessitates tighter process controls and more intensively designed and costly forming tools. This method obviously reduces waste and concomitant costs. Intricately shaped components (particularly produced using injection molding or gel casting) are more common; but they still lack extremely fine or hidden features and close tolerances.

Additive manufacturing is the latest evolutionary development in ceramic production. Also known as solid freeform fabrication (SFF), this method has been exclusively used for prototypes and models until recently. It involves producing solid, porous, or functional gradient components from computer models without the use of special fixtures or tooling. Parts are manufactured by the successive layer-by-layer build-up of ceramic powders. Components can be highly complex, yet still possess fine features. As reviewed by Travitzsky et al., multiple SFF processes have been developed. While a number of SFF methods have been examined for bioceramics, those with particular relevance include 3D printing (3DP), selective laser sintering (SLS), and stereolithography (SLA) [635]. Given in the following paragraphs are brief discussions on each technique along with selected examples.

Three dimensional printing—3DP is perhaps the most widely known method for SFF, and is based on ink-jet printing developed at the Massachusetts Institute of Technology (MIT) in the 1990s [636]. Two deposition methods are employed—direct and indirect. Using the direct method, ceramic powder is dispersed within a liquid binder or wax, and then each layer is successively thermally printed using an injection nozzle. Components having intricate cavities and blind features with excellent surface finish are easily and rapidly formed. However, achieving high-solids content and controlling the rheology of the powder-ink mixture are key challenges. Effective demonstration of this process was recently performed for a Y- TZP ceramic dental crown where the occlusal surfaces were precisely replicated from the computer model [637]. Using the indirect method, components are built by distributing a liquid binder onto successive powder layers. There is no need for admixing powder and ink in this method. Conversely, fine powders are difficult to spread evenly across the work surface, resulting in poor feature definition and lower density. Coarser powders are preferred. Both methods require post-forming sintering to achieve final density. 3DP has been effectively used for construction of hydroxyapatite bone scaffolds [638].

Selective laser sintering—SLS is a process in which particles within a powder bed are fused by the application of a precision laser. Here too, there are two methods—direct and indirect. The direct method relies on localized melting between ceramic particles. A low temperature liquid phase is a prerequisite, which limits the number of ceramic materials that can be employed. High thermal gradients can also result in component distortion and cracking. A polymeric binder is employed in the indirect method. Fusion occurs via melting of the binder between adjacent particles followed by coalescence. Subsequent sintering is required to fully densify the as-formed parts. In either method, the density of the components is directly related to the density of the powder bed. Higher powder bed densities result in higher density parts. Using the direct SLS method, Feng et al. added 45S5 glass into β-tricalcium phosphate (which provided the necessary low-temperature liquid) to form complex bone scaffolds [639]. These were subsequently conventionally sintered to near full-density, yielding excellent mechanical properties and favorable biocompatibility.

Stereolithography—in the SLA method, ceramic powders are dispersed into a photo-sensitive monomer resin. This liquid mixture is then selectively solidified layer by layer upon exposure to an ultraviolet laser. Afterwards, formed components are subjected to general irradiation or a thermal treatment to cure the remaining monomers. Following curing, the monomers are removed in a burn-

out cycle and components are densified by conventional sintering. Similar to the other SFF methods, SLA is capable of forming intricate shapes with hidden features. However, it is not as capable of reproducing computer models as 3DP due to wider photo line widths and flow of uncured resin during part formation. These limitations result in rougher surface finishes with stepped features. Nevertheless, custom-made anatomical ceramic implants, such as hydroxyapatite scaffolds, have been produced using SLA techniques [640], and this method remains broadly applicable for a number of non-ceramic biomedical devices [641].

The one ceramic implant common to all three SFF methods is an orthophosphate bone scaffold. Indeed, SFF technologies offer significant benefits over conventional manufacturing for these devices, and are ideally suited for building complex, patient-customized prostheses [642]. Present-day SFF equipment can readily create sub-millimeter features and internal pore structures which effectively support neovascularization and osteogenesis. However, with the advent of higher precision equipment, building of micron and submicron features is on the horizon [643]. Continued development of these technologies will pave the way for their use in many reconstructive or arthroplastic procedures, including trauma [644], oral [645] , cranio-maxillofacial [646], and spinal [647] surgeries, and ultimately total joint replacement [648].

4.3. Testing methods

Currently, validation of new ceramic orthopaedic prostheses requires conducting a series of independent tests on both samples and components. For example, consider the regulatory requirements for a new ceramic-on-polyethylene total hip arthroplasty system using a titanium hip stem [649]. The ceramic's basic strength is determined by flexural testing of small parallelepiped specimens. Compression burst testing is conducted on actual ceramic femoral heads against mock titanium stems. Separate fatigue testing of the femoral heads is also performed. Corrosion between the femoral heads and hip stems is determined using another test. Additional testing is conducted to assess wear in a hip simulator. While each test is performed in accordance with international standards, the results are independently reported and only weakly correlated. Provided each test meets its successful criteria, the total hip system is considered acceptable for market clearance. Little consideration is given to interactive effects. However, the hip system's real world behavior may differ considerably from these independent evaluations. Multiple physical effects interacting simultaneously might result in unpredicted early failures. As an example, wear, fatigue, and hydrothermal ageing are now known to be the main degradation mechanisms of ceramics used for joint prostheses. All three occur simultaneously *in vivo*, and coupling them in preclinical testing may correctly simulate the complex conditions encountered within the body. Yet, to date, only a few recent papers have highlighted multi-failure mode interactions [248,650]. Realization of this problem has led to the use of multiphysics simulation and experimental verification testing. Multiphysics simulation is a recent approach to computer modeling which simultaneously evaluates the effects of multiple environmental and operating parameters on product performance and reliability [651]. It has been adopted in the aerospace and automotive industries with considerable success [652,653], but is only now beginning to be used for orthopaedics [654]. Recent marked increases in computational power have enabled complex material and system simulations which heretofore have not been possible. Sophisticated multiphysics software is now included with most finite element modeling and CAD systems. These new tools provide biomedical engineers with the ability to *in silco* test and evaluate concepts and conditions simultaneously. It decreases design errors and costs, and minimizes reliance on multiple prototypes and test specimens. However, it does not obviate verification testing. Conversely, it is used to discover the physicochemical and mechanical tests that are most important or overlooked. As described earlier in this review, orthopaedics in general and joint arthroplasty in particular have had products successfully clear independent *in vitro* testing, only to later fail *in vivo*. Adoption and utilization of multiphysics simulation and experimental testing is an important advancement to eliminate the trial and error failures of the past.

5. Conclusions

In the present review, rather than discussing each ceramic material sequentially, a brief history of their evolution was provided, followed by detailed comparisons of respective properties and performance. This was done in order to highlight and contrast differences, advantages, and limitations of these bioceramics. Much of the early work in these materials was directed at total hip arthroplasty. Improvements in wear performance via introduction of Al_2O_3 and osseointegration of hip stems with the advent of HAp coatings are notable milestones. However, other well-intentioned improvements were conducted using trial and error methods, many times with insufficient laboratory and clinical data to support the safety and efficacy of new devices. Notable failures include femoral heads produced using DLC-coated titanium and Y-TZP. Both resulted in considerable patient harm prior to implant removals and the recall of these devices. With the possible exception of OxZr, other hard ceramic surface coatings appear to be headed towards a similar fate, at least from an engineering standpoint, principally due to deposition defects and an inability to withstand third-body wear. Despite improvements in the mechanical properties of ceramics, particularly with the introduction of ZTA, AMC, and Si_3N_4, an unwarranted concern over catastrophic fracture has been an impediment to their adoption by clinicians. Unfortunately, this resulted in further patient suffering associated with failures of metal-on-metal devices. Yet, with exceptions of Al_2O_3 and HAp, both of which have 30+ years of successful clinical history, concerns over newer bioceramics persist because their arthroplastic resumes are no greater than about 10 years. However, unlike prior generations of ceramics, currently available materials have been extensively vetted *in vitro* and *in vivo*, using both standardized and exploratory test methods that are more clinically relevant today than ever before. Regulatory agencies have also commensurately increased their acceptance criteria to ensure the safety and efficacy of devices prior to their release. In turn, the requirements imposed on device manufacturers continue to rise as well. In a recent instructional review by Rajpura et al. [655], the perfect total hip arthroplasty prosthesis needs to be constructed of articulation materials that are reasonably hard, scratch resistant, mechanically tough and strong with excellent *in vivo* biocompatibility and phase stability. It must possess a low friction interface that produces no noise and essentially no wear, with no immunological response to wear debris. In addition, it must have a large femoral head to prevent dislocation, and a head–neck interface that is not susceptible to fretting or electrochemical corrosion. However, while these are demanding requirements, some of which are still unmet, they are likely insufficient for the next generation of bioceramics. No longer will it simply be acceptable to focus on producing biocompatible or bioinert components. In fact, as discussed within this review, no materials are perfectly bioinert. Even the most established bioceramics are subject to chemical or phase instabilities—some of which are detrimental, while others may be beneficial. Indeed, instead of producing bioceramics that are wholly resistant to change, the next generation of ceramics must interact with human tissues and cells. Certainly reducing friction, suppress-

ing noise, and eliminating wear debris are important objectives, but of equivalent importance is eradication of peri-operative and latent infections. While continued improvements in the strength and toughness of bioceramics are desirable, designing them as composite structures to interdigitate with adjacent bone is also needed. The next generation of "smart bioceramics" needs to be customized for specific arthroplasty applications. They should be bioactive, possessing engineered topography and functionalized surface chemistry to selectively and positively interact with adjacent tissue or bone. Only by doing so, will the dream of lifetime implants be realized. Achieving this level of performance for a new generation of ceramics and ceramic coatings will demand the best cooperative efforts from clinicians, manufacturers, and regulatory agencies.

Disclosure

Bryan J. McEntire and B. Sonny Bal are principals of Amedica Corporation, a silicon nitride orthopaedic device manufacturer. None of the other authors have a financial or proprietary interest in the subject matter or materials discussed.

Acknowledgements

Appreciation is expressed to Alan Lakshminarayanan, Ryan Bock, and Erin Jones for their support in literature searches, manuscript organization, and helpful discussions.

References

[1] D.R. Steinberg, M.E. Steinberg, The early history of arthroplasty in the United States, Clin. Orthop. Relat. Res. 374 (2000) 55–89.
[2] J. Charnley, Arthroplasty of the hip: a new operation, Lancet (1961) 1129–1132.
[3] J. Charnley, A. Kamangar, M.D. Longfield, The optimum size of prosthetic heads in relation to the wear of plastic sockets in total replacement of the hip, Med. Biol. Eng. 7 (1969) 31–39.
[4] The Bone and Joint Decade—Global Alliance for Musculoskeletal Health <http://bjdonline.org/key-facts-and-figures/> (2015).
[5] A.J. Weiss, A. Elixhauser, Trends in operating room procedures in U.S. hospitals, 2001–2011, Healthcare Cost Util. Project (March) (2014) 1–14.
[6] S.M. Kurtz, K.L. Ong, E. Lau, K.J. Bozic, Impact of the economic downturn on total joint replacement demand in the United States, J. Bone Jt. Surg. 96A (8) (2014) 624–630.
[7] J. Bernstein, The folly of forecasting, Clin. Orthop. Relat. Res. 471 (5) (2013) 1415–1418.
[8] S. Kim, B. Wise, Y. Zhang, R. Szabo, Increasing incidence of shoulder arthroplasty in the United States, J. Bone Jt. Surg. 93A (24) (2011) 2249–2254.
[9] J.S. Day, E. Lau, K.L. Ong, G.R. Williams, M.L. Ramsey, S.M. Kurtz, Prevalence and projections of total shoulder and elbow arthroplasty in the United States to 2015, J. Shoulder Elb. Surg. 19 (2010) 1115–1120.
[10] S. Mendenhall, Hip and knee implant review, Orthop. Netw. News 25 (3) (2014) 1–20.
[11] J.A. Vetalice, Orthopaedic industry annual report—focus on joint replacement, OrthoKnow (June) (2012) 1–8.
[12] I.D. Learmonth, C. Young, C. Rorabeck, The operation of the century: total hip replacement, Lancet 370 (2007) 1508–1519.
[13] M.N. Smith, Evolution of mould arthroplasty of the hip joint, J. Bone Jt. Surg. 31B (1949) 53–60.
[14] G. Pezzotti, Advanced Materials for Joint Implants, 1st ed., CRC Press, Boca Raton, FLUSA, 2013.
[15] P. Boutin, Total arthroplasty of the hip by fritted aluminum prosthesis. Experimental study and 1st clinical applications, Rev. Chir. Orthop. Reparatrice Appar. Mot. 58 (3) (1971) 229–246.
[16] P. Boutin, P. Christel, J.-M. Dorlot, A. Meunier, A. DeRoquancourt, D. Blanquaert, S. Herman, L. Sedel, et al., The use of dense alumina–alumina ceramic combination in total hip replacement, J. Biomed. Mater. Res. 22 (12) (1988) 1203–1232.
[17] J.T. Scales, D. Goddard, Prosthetic Acetabular Devices US Patent 3698017 (1972).
[18] H. Mittelmeier, K. Karpf, H. Moser, Hip Joint Prosthesis US Patent 3894297 (1975).
[19] A. Zeibig, H. Locke, Ceramic Implant US Patent 3979779 (1976).
[20] J.J. Klawitter, N.A. Bhatti, Ceramic Prosthetic Implant Suitable for a Knee Joint Plateau US Patent 4000525 (1977).
[21] S.F. Hulbert, J.J. Klawitter, B.W. Sauer, J.R. Matthews, Characterization of tissue ingrowth into porous bioceramics, Tech. Rep. Off. Nav. Res. 2 (1972) 1–137, Contract No. N00014-1-A-0339-0001, Proj. No. NR o32-529.
[22] S. Lyng, E. Sudmann, S.F. Hulbert, B.W. Sauer, Fixation of permanent orthopaedic prosthesis use of ceramics in the tibial plateau, Acta Orthop. Scand. 44 (1973) 694–701.
[23] N. Sugano, T. Nishii, K. Nakata, K. Masuhara, K. Takaoka, Polyethylene sockets and alumina ceramic heads in cemented total hip arthroplasty—a ten-year study, J. Bone Jt. Surg. 77B (1995) 548–556.
[24] S. Murphy, Alumina ceramic–ceramic bearings in THA: the new gold standard, Orthopedics 25 (9) (2002) 2–3.
[25] S.B. Murphy, T.M. Ecker, M. Tannast, Two- to nine-year clinical results of alumina ceramic-on-ceramic THA, Clin. Orthop. Relat. Res. 453 (2006) 97–102.
[26] B.S. Bal, J. Garino, M. Ries, H. Oonishi, Ceramic bearings in total knee arthroplasty, J. Knee Surg. 20 (4) (2007) 261–270.
[27] S. Nakamura, M. Kobayashi, H. Ito, K. Nakamura, T. Ueo, T. Nakamura, The Bi-surface total knee arthroplasty: minimum 10 -year follow-up study, Knee 17 (2010) 274–278.
[28] K. Nishida, K. Hashizume, Y. Nasu, M. Kishimoto, T. Ozaki, H. Inoue, A 5–22 year follow-up study of stemmed alumina ceramic total elbow arthroplasties with cement fixation for patients with rheumatoid arthritis, J. Orthop. Sci. 19 (2014) 55–63.
[29] S. Kosugi, A. Taniguchi, K. Tomiwa, H. Kurokawa, Y. Tanaka, TNK ankle – the ceramic 2 – component total ankle prosthesis, Clin. Res. Foot Ankle 2 (3) (2014) 141.
[30] H. Hatano, T. Morita, H. Kobayashi, H. Otsuka, A ceramic prosthesis for the treatment of tumours of the distal radius, J. Bone Jt. Surg. 88B (2006) 1656–1658.
[31] K. Doe, K.N. Kuwata, K. Shinya, Alumina ceramic finger implants: a preliminary biomaterial and clinical evaluation, J. Hand Surg. Am. A9 (1984) 740–749.
[32] N.Q. Nguyen, D. Kafle, J.M. Buchowski, K.-W. Park, B.-S. Chang, C.-K. Lee, J.S. Yeom, Ceramic fracture following cervical disc arthroplasty, J. Bone Jt. Surg. 93 (e132) (2011) 1–4.
[33] Y. oda, S. Miyatake, Y. Tokuriki, H. Handa, Alumina ceramics (bioceram) as the implant material in anterior cervical fusion, Nihon Geka Hokan 50 (2) (1981) 352–357.
[34] R.L. Huckstep, E. Sherry, Replacement of the proximal humerus in primary bone tumours, Aust. N. Z. J. Surg. 66 (1996) 97–100.
[35] Standard Specification for High- Purity Dense Aluminum Oxide for Medical Applications, ASTMF603-00 (2000).
[36] Implants for Surgery – Ceramic Materials – Part 1: Ceramic Materials Based on High Purity Alumina, ISO 6474-1 (2010).
[37] C. Piconi, G. Maccauro, F. Muratori, E.B. DelPrever, Alumina and zirconia ceramics in joint replacements, J. Appl. Biomater. Biomech. 1 (2003) 19–32.
[38] R.S. Roy, A. Mondal, A. Chanda, D. Basu, M.K. Mitra, Sliding wear behavior of submicron-grained alumina in biological environment, J. Biomed. Mater. Res. 83A (2007) 257–262.
[39] K.-H. Koo, Y.-C. Ha, W.H. Jung, S.-R. Kim, J.J. Yoo, H.J. Kim, Isolated fracture of the ceramic head after third- generation alumina-on-alumina total hip arthroplasty, J. Bone Jt. Surg. 90 (2008) 329–3362.
[40] J.P. Garino, The reliability of modern alumina bearings in total hip arthroplasty—update to a 2006 report, Semin. Arthroplasty 24 (2013) 193–201.
[41] Y.L. Jung, S.-Y. Kim, Alumina-on-polyethylene bearing surfaces in total hip arthroplasty, Open Orthop. J. 4 (2010) 56–60.
[42] S.R. Levitt, P.H. Crayton, E.A. Monroe, R.A. Condrate, Forming method for apatite prostheses, J. Biomed. Mater. Res. 3 (4) (1969) 683–684.
[43] S. Dorozhkin, History of calcium phosphates in regenerative medicine, in: B. Ben-Nissan (Ed.), Advance Calcium Phosphate Biomater, Springer, Berlin Heidelberg, 2014, pp. 435–483.
[44] S.V. Dorozhkin, Calcium orthophosphate—based bioceramics, Materials (Basel) 6 (9) (2013) 3840–3942.
[45] R.G. Carrodeguas, S. De Aza, α-Tricalcium phosphate: synthesis, properties and biomedical applications, Acta Biomater. 7 (10) (2011) 3536–3546.
[46] R.G. Carrodeguas, A.H. De Aza, X. Turrillas, P. Pena, S. De Aza, New approach to the $\beta \rightarrow \alpha$ polymorphic transformation in magnesium-substituted tricalcium phosphate and its practical implications, J. Am. Ceram. Soc. 91 (4) (2008) 1281–1286.
[47] E.A. Monroe, W. Votava, D.B. Bass, J. McMullen, New calcium phosphate ceramic material for bone and tooth implants, J. Dent. Res. 50 (4) (1971) 860–861.
[48] R.J. Furlong, J.F. Osborn, Fixation of hip prostheses by hydroxyapatite ceramic coatings, J. Bone Jt. Surg. 77A (5) (1991) 903–910.
[49] J.-P. Vidalain, Twenty-year results of the cementless corail stem, Int. Orthop. 35 (2011) 189–194.
[50] R. Schwarzkopf, P. Olivieri, W.L. Jaffe, Simultaneous bilateral total hip arthroplasty with hydroxyapatite-coated implants: a 20-year follow-up, J. Arthroplasty 27 (7) (2012) 1364–1369.
[51] J.M. Loughead, P.A. O'Connor, K. Charron, C.H. Rorabeck, R.B. Bourne, Twenty-three-year outcome of the porous coated anatomic total hip replacement. a concise follow-up of a previous report, J. Bone Jt. Surg. 94A (2) (2012) 151–155.

[52] J. Buchanan, D. Fletcher, P. Linsley, Review of hydroxyapatite ceramic coated hip implants: a clinical and radiological evaluation with up to twenty-year follow-up, J. Bone Jt. Surg. 94B (Suppl. XXI) (2014) 113.
[53] F. Barrere, C.A. Van-Blitterswijk, K. De-Groot, Bone regeneration: molecular and cellular interactions with calcium phosphate ceramics, Int. J. Nanomed. 1 (3) (2006) 317–332.
[54] R.A. Surmenev, A review of plasma-assisted methods for calcium phosphate-based coatings fabrication, Surf. Coat. Technol. 206 (2012) 2035–2056.
[55] L. Sun, C.C. Berndt, K.A. Gross, A. Kucuk, Material fundamentals and clinical performance of plasma-sprayed hydroxyapatite coatings: a review, J. Biomed. Mater. Res. Appl. Biomater. 58 (2001) 570–592.
[56] R.Z. LeGeros, B. Ben-Nissan, Introduction to synthetic and biologic apatites, in: B. Ben-Nissan (Ed.), Adv. Calcium Phosphate Biomater, Springer, Berlin, Heidelberg, 2014, pp. 1–17.
[57] R.Z. LeGeros, Properties of osteoconductive biomaterials: calcium phosphates, Clin. Orthop. Relat. Res. 395 (2002) 81–98.
[58] H. Zhou, J. Lee, Nanoscale hydroxyapatite particles for bone tissue engineering, Acta Biomater. 7 (2011) 2769–2781.
[59] M. Yamada, T. Ueno, N. Tsukimura, T. Ikeda, K. Nakagawa, N. Hori, T. Suzuki, T. Ogawa, Bone integration capability of nanopolymorphic crystalline hydroxyapatite coated on titanium implants, Int. J. Nanomed. 7 (2012) 859–873.
[60] S.M. Zakaria, S.H.S. Zein, M.R. othman, F. Yang, J.A. Jansen, Nanophase hydroxyapatite as a biomaterial in advanced hard tissue engineering: a review, Tissue Eng. Part B 19 (5) (2013) 431–441.
[61] W.L. Jaffe, D.F. Scott, Total hip arthroplasty with hydroxyapatite–coated prostheses, J. Bone Jt. Surg. 78A (12) (2013) 1918–1934.
[62] J.D. Voigt, M. Mosier, Hydroxyapatite (HA) coating appears to be of benefit for implant durability of tibial components in primary total knee arthroplasty, Acta Orthop. 82 (4) (2011) 448–459.
[63] I. Demnati, D. Grossin, C. Combes, C. Rey, Plasma-sprayed apatite coatings: review of physical–chemical characteristics and their biological consequences, J. Med. Biol. Eng. 34 (1) (2014) 1–7.
[64] B. Cales, Zirconia ceramic for improved hip prosthesis—a review, in: 6th Biomater. Symp.—Ceram. Implant Mater. Orthop. Surg., Gottingen, Germany, 1994, pp. 2–8.
[65] C. Piconi, G. Maccauro, Zirconia as a ceramic biomaterial, Biomaterials 20 (1999) 1–25.
[66] T. Masaki, Mechanical properties of toughened ZrO_2–Y_2O_3 ceramics, J. Am. Ceram. Soc. 69 (8) (1986) 638–640.
[67] J.M. Drouin, B. Cales, Yttria-stabilized zirconia ceramic for improved hip joint head, in: 7th Int. Symp. Ceram. Med. Butterworth–Heinemann, Turku, Finland, 1994, pp. 30–33.
[68] B. Cales, Y. Stefani, E. Lilley, Long term in vivo and in vitro aging of a zirconia ceramic used in orthopaedy, J. Biomed. Mater. Res. 28 (5) (1994) 619–624.
[69] B. Cales, Y. Stefani, Mechanical properties and surface analysis of retrieved zirconia hip joint heads after an implantation time of two to three years, J. Mater. Sci. 5 (1994) 376–380.
[70] R.H.J. Hannink, P.M. Kelly, B.C. Muddle, Transformation toughening in zirconia-containing ceramics, J. Am. Ceram. Soc. 83 (3) (2000) 461–487.
[71] Standard Specification for High- Purity Dense Magnesia Partially Stabilized Zirconia (Mg-PSZ) for Surgical Implant Applications, ASTMF2393-10 (2010).
[72] I.C. Clarke, M. Manaka, D.D. Green, P. Williams, G. Pezzotti, Y.-H. Kim, M. Ries, N. Sugano, et al., Current status of zirconia used in total hip implants, J. Bone Jt. Surg 85A (Suppl. 4) (2003) 73–84.
[73] J. Chevalier, L. Gremillard, S. Deville, Low-temperature degradation of zirconia and implications for biomedical implants, Ann. Rev. Mater. Res. 37 (2007) 1–32.
[74] J.L. Masonis, R.B. Bourne, M.D. Ries, R.W. McCalden, A. Salehi, D.C. Kelman, Zirconia femoral head fractures, J. Arthroplasty 19 (7) (2004) 898–905.
[75] Standard Specification for High- Purity Dense Yttria Tetragonal Zirconium Oxide Polycrystal (Y-TZP) for Surgical Implant Appications, ASTMF1873-98 (2007).
[76] J. Chevalier, L. Gremillard, A.V. Virkar, D.R. Clarke, The tetragonal-monoclinic transformation in zirconia: lessons learned and future trends, J. Am. Ceram. Soc. 92 (9) (2009) 1901–1920.
[77] E.M. Santos, S. Vohra, S.A. Catledge, M.D. McClenny, J. Lemons, K.D. Moore, Examination of surface and material properties of explanted zirconia femoral heads, J. Arthroplasty 9 (Suppl. 2 (7)) (2004) 30–34.
[78] G. Maccauro, C. Piconi, W. Burger, L. Pilloni, E. De Santis, F. Muratori, I.D. Learmonth, Fracture of a Y-TZP ceramic femoral head, J. Bone Jt. Surg. 86B (2004) 1192–1196.
[79] G. Pezzotti, Bioceramics for hip joints: the physical chemistry viewpoint, Materials (Basel) 7 (2014) 4367–4410.
[80] M. Hisbergues, S. Vendeville, P. Vendeville, Zirconia: established facts and perspectives for a biomaterial in dental implantology, J. Biomed. Mater. Res. Part B Appl. Biomater. 88B (2009) 519–529.
[81] P. Kohorst, L. Borchers, J. Strempel, M. Stiesch, T. Hassel, F.-W. Bach, C. Hübsch, Low-temperature degradation of different zirconia ceramics for dental applications, Acta Biomater. 8 (2012) 1213–1220.
[82] B.S. Bal, M.N. Rahaman, Orthopedic applications of silicon nitride ceramics, Acta Biomater. 8 (8) (2012) 2889–2898.
[83] M. Mazzocchi, A. Bellosi, On the possibility of silicon nitride as a ceramic for structural orthopaedic implants. Part I: processing, microstructure, mechanical properties, cytotoxicity, J. Mater. Sci. Mater. Med. 19 (2008) 2881–2887.
[84] M. Mazzocchi, D. Gardini, P.L. Traverso, M.G. Faga, A. Bellosi, On the possibility of silicon nitride as a ceramic for structural orthopaedic implants. Part II: chemical stability and wear resistance in body environment, J. Mater. Sci. Mater. Med. 19 (2008) 2889–2901.
[85] C.C. Sorrell, P.H. Hardcastle, R.K. Druitt, C.R. Howlett, E.R. McCartney, Results of 15-year clinical study of reaction bonded silicon nitride intervertebral spacers, Proc. 7th World Biomater. Conf. 1872 (2004).
[86] D.R. Johnson, Ceramic technology for advanced heat engines project, semi-annual & annual reports for the periods 1988 through, in: Prepared for the U.S. Department of Energy by oak Ridge National Laboratory under Contract DE-AC05-840R21400, Oak Ridge, TN 37831-6285, 1995.
[87] T.S. Kaushal, K.E. Weber, Advanced Diesel Engine Component Development Program, Final Report Tasks 4-14, No. DOE/NASA-0329-2;NASA/CR-191203, National Aeronautics and Space Administration, Cleveland, OH, 1994.
[88] B.J. McEntire, R.W. Wills, R.E. Southam, The development and testing of ceramic components in piston engines, final report, in: Prepared for the U.S. Department of Energy under Contract with Oak Ridge National Laboratories, Contract No. DE?AC05-840R21400, Oak Ridge TN 37831-6285, 1994.
[89] L. Wang, R.W. Snidle, L. Gu, Rolling contact silicon nitride bearing technology: a review of recent research, Wear 246 (2000) 159–173.
[90] F.L. Riley, Silicon nitride and related materials, J. Am. Ceram. Soc. 83 (2) (2000) 245–265.
[91] B.S. Bal, A. Khandkar, R. Lakshminarayanan, I. Clarke, A.A. Hofmann, M.N. Rahaman, Testing of silicon nitride ceramic bearings for total hip arthroplasty, J. Biomed. Mater. Res. Part B Appl. Biomater. 87 (2) (2008) 447–454.
[92] R.M. Taylor, J.P. Bernero, A.A. Patel, D.S. Brodke, A.C. Khandkar, Silicon nitride—a new material for spinal implants, J. Bone Jt. Surg. 92Br (Suppl. I) (2010) 133.
[93] Personal Communication from William Jordan, Director of Regulatory Affairs and Quality Assurance, Amedica Corporation, Salt Lake City, UT 84119 (2014).
[94] B.S. Bal, A. Khandkar, R. Lakshminarayanan, I. Clarke, A.A. Hofmann, M.N. Rahaman, Fabrication and testing of silicon nitride bearings in total hip arthroplasty, J. Arthroplasty 24 (2009) 110–116.
[95] Standard Specification for Silicon Nitride Bearing Balls, ASTMF-2094M-11 (2011).
[96] Fine Ceramics (Advanced Ceramics, Advanced Technical Ceramics)—Silicon Nitride Materials for Rolling Bearing Balls, ISO 26602 (2009).
[97] A. Neumann, T. Reske, M. Held, K. Jahnke, C. Ragoss, H.R. Maier, Comparative investigation of the biocompatibility of various silicon nitride ceramic qualities in vitro, J. Mater. Sci. Mater. Med. 15 (2004) 1135–1140.
[98] C. Santos, S. Ribeiro, J.K.M.F. Daguano, S.O. Rogero, K. Strecker, C.R.M. Silva, Development and cytotoxicity evaluation of SiAlONs ceramics, Mater. Sci. Eng. C27 (2007) 148–153.
[99] B. Cappi, S. Neuss, J. Salber, R. Telle, R. Knüchel, H. Fischer, Cytocompatibility of high strength non-oxide ceramics, J. Biomed. Mater. Res. 93A (2010) 67–76.
[100] C.R. Howlett, E. McCartney, W. Ching, The effect of silicon nitride ceramic on rabbit skeletal cells and tissue, Clin. Orthop. Relat. Res. 244 (1989) 293–304.
[101] A. Neumann, M. Kramps, C. Ragoß, H.R. Maier, K. Jahnke, Histological and microradiographic appearances of silicon nitride and aluminum oxide in a rabbit femur implantation model, Materwiss. Werksttech. 35 (9) (2004) 569–573.
[102] A. Neumann, C. Unkel, C. Werry, C.U. Herborn, H.R. Maier, C. Ragoss, K. Jahnke, Prototype of a silicon nitride ceramic-based miniplate osteofixation system for the midface, Otolaryngol. Neck Surg. 134 (2006) 923–930.
[103] C.C. Guedes e Silva, B. Konig, M.J. Carbonari, M. Yoshimoto, S. Allegrini, J.C. Bressiani, Tissue response around silicon nitride implants in rabbits, J. Biomed. Mater. Res. 84A (2008) 337–343.
[104] C.C. Guedes e Silva, B. König, M.J. Carbonari, M. Yoshimoto, S. Allegrini, J.C. Bressiani, Bone growth around silicon nitride implants—an evaluation by scanning electron microscopy, Mater. Charact. 59 (2008) 1339–1341.
[105] M.C. Anderson, R. Olsen, Bone ingrowth into porous silicon nitride, J. Biomed. Mater. Res. 92A (2010) 1598–1605.
[106] T.J. Webster, A.A. Patel, M.N. Rahaman, B.S. Bal, Anti-infective and osteointegration properties of silicon nitride, poly(ether ether ketone), and titanium implants, Acta Biomater. 8 (12) (2012) 4447–4454.
[107] D.J. Gorth, S. Puckett, B. Ercan, T.J. Webster, M. Rahaman, B.S. Bal, Decreased bacteria activity on si3n4 surfaces compared with peek or titanium, Int. J. Nanomed. 7 (2012) 4829–4840.
[108] J. Takadoum, H. Houmid-Bennani, D. Mairey, The wear characteristics of silicon nitride, J. Eur. Ceram. Soc. 18 (1998) 553–556.
[109] T. Satoh, S. Sakaguchi, K. Hirao, M. Toriyama, S. Kanzaki, Influence of aluminum–oxygen–yttrium solid solution on the aqueous tribological behavior of silicon nitride, J. Am. Ceram. Soc. 84 (2) (2001) 462–464.
[110] T.E. Fischer, H. Tomizawa, Interaction of tribochemistry and microfracture in the friction and wear of silicon nitride, Wear 105 (1985) 29–45.
[111] I.C. Clarke, J.G. Bowsher, A 5 million cycle wear study of silicon nitride and cobalt chrome femoral heads on UHMWPE liners, LLUMC Final Report HE 177 (2005).
[112] P.A. Williams, R. Lakshminarayanan, A. Khandkar, D.D. Green, I.C. Clarke, Wear debris morphology of silicon–nitride generated from a hip simulator

model, Ann. Meet. Soc. Biomater. Conjunction Int. Biomater. Symp. 29 (2) (2006) 1–2.
[113] H. Tomizawa, E. Fischer, Friction and wear of silicon nitride and silicon carbide in water: hydrodynamic lubrication at low sliding speed obtained by tribochemical wear, ASLE Trans. 30 (1) (1987) 41–46.
[114] T. Saito, Y. Imada, F. Honda, An analytical observation of the tribochemical reaction of silicon nitride sliding with low friction in aqueous solutions, Wear 205 (1997) 153–159.
[115] H. Ishigaki, R. Nagata, M. Iwasa, Effect of adsorbed water on friction of hot-pressed silicon nitride and silicon carbide at slow speed sliding, Wear 121 (1988) 107–116.
[116] S. Jahanmir, Y. Ozmen, L.K. Ives, Water lubrication of silicon nitride in sliding, Tribol. Lett. 17 (3) (2004) 409–417.
[117] Y.S. Zhou, M. Ohashi, N. Tomita, K. Ikeuchi, K. Takashima, Study on the possibility of silicon nitride—silicon nitride as a material for hip prostheses, Mater. Sci. Eng. C 5 (1997) 125–129.
[118] Y.S. Zhou, K. Ikeuchi, M. Ohashi, Comparison of the friction properties of four ceramic materials for joint replacements, Wear 210 (1) (1997) 171–177.
[119] G. Roebben, C. Sarbu, T. Lube, O. Van der Biest, Quantitative determination of the volume fraction of intergranular amorphous phase in sintered silicon nitride, Mater. Sci. Eng. A 370 (1) (2004) 453–458.
[120] P.F. Becher, E.Y. Sun, K.P. Plucknett, K.B. Alexander, C. Hsueh, H. Lin, S.B. Waters, C.G. Westmoreland, Microstructural design of silicon nitride with improved fracture toughness: I, effects of grain shape and size, J. Am. Ceram. Soc. 81 (11) (1998) 2821–2830.
[121] E.Y. Sun, P.F. Becher, K.P. Plucknett, C.-H. Hsueh, K.B. Alexander, S.B. Waters, Microstructural design of silicon nitride with improved fracture toughness: II, effects of yttria and alumina additives, J. Am. Ceram. Soc. 81 (11) (1998) 2831–2840.
[122] P.F. Becher, Microstructural design of toughened ceramics, J. Am. Ceram. Soc. 74 (2) (1991) 255–269.
[123] J. Olofsson, M. Pettersson, N. Teuscher, A. Heilmann, K. Larsson, K. Grandfield, C. Persson, S. Jacobson, et al., Fabrication and evaluation of SixNy coatings for total joint replacements, J. Mater. Sci. Mater. Med. 23 (8) (2012) 1879–1889.
[124] J. Olofsson, T. Grehk, T. Berlind, Evaluation of silicon nitride as a wear resistant and resorbable alternative for total hip joint replacement, Biomatter 2 (2) (2012) 94–102.
[125] M. Pettersson, T. Berlind, S. Schmidt, S. Jacobson, L. Hultman, C. Persson, H. Engqvist, Structure and composition of silicon nitride and silicon carbon nitride coatings for joint replacements, Surf. Coatings Technol. 235 (2013) 827–834.
[126] Z. Shi, Y. Wang, C. Du, N. Huang, L. Wang, C. Ning, Silicon nitride films for the protective functional coating: blood compatibility and biomechanical property study, J. Mech. Behav. Biomed. Mater. 16 (2012) 9–20.
[127] J.M. Maloney, S.A. Lipka, S.P. Baldwin, In vivo biostability of CVD silicon oxide and silicon nitride films, Mater. Res. Soc. Proc. 872 (2005) J14.3.1.
[128] B.F. Coll, P. Jacquot, Surface modification of medical implants and surgical devices using TiN layers, Surf. Coatings Technol. 36 (1988) 867–878.
[129] F.F. Buechel, Hip resurfacing revisited, Orthopedics 19 (9) (1996) 753–756.
[130] F.F. Buechel, T.E. Helbig, J. D'Alessio, M.J. Pappas, Two- to 12-year evaluation of cementless buechel–pappas total hip arthroplasty, J. Arthroplasty 19 (8) (2004) 1017–1027.
[131] F.F. Buechel, T.E. Helbig, M.J. Pappas, K. Trier, S.W. Dean, 31 Year evolution of the rotating–platform total knee replacment: coping with 'Spinout' and wear, JASTM Int. 9 (2) (2012) 1–14.
[132] R. Hauert, A review of modified DLC coatings for biological applications, Diam. Relat. Mater. 12 (3) (2003) 583–589.
[133] G. Taeger, L.E. Podleska, B. Schmidt, M. Ziegler, D. Nast-Kolb, Comparison of diamond-like-carbon and alumina- oxide articulating with polyethylene in total hip arthroplasty, Materwiss. Werksttech. 34 (12) (2003) 1094–1100.
[134] A.S. Aesculap, Advanced surface, Aescul. Corp. Broch. (2012) https://www.aesculapimplantsystems.com/products/.
[135] K.J. Hamelynck, R.G. Woering, Ceramic surface engineered metal-on-metal hips system for total hip arthroplasty and resurfacing hip arthroplasty, ACCIS White Paper (2009) http://www.accis.nl.
[136] A.P. Serro, C. Completo, R. Colaço, F. dos Santos, C.L. da Silva, J.M.S. Cabral, H. Araújo, E. Pires, et al., A comparative study of titanium nitrides, TiN, TiNbN and TiCN, as coatings for biomedical applications, Surf. Coatings Technol. 203 (24) (2009) 3701–3707.
[137] S. Mukherjee, M.F. Maitz, M.T. Pham, E. Richter, F. Prokert, W. Moeller, Development and biocompatibility of hard Ti-based coatings using plasma immersion ion implantation-assisted deposition, Surf. Coatings Technol. 196 (1) (2005) 312–316.
[138] Z. Kertzman, J. Marchal, M. Suarez, M. Staia, P. Filip, P. Kohli, S. Aouadi, Mechanical, tribological, and biocompatibility properties of ZrN–Ag nanocomposite films, J. Biomed. Mater. Res. 84A (4) (2005) 1061–1067.
[139] M. Allen, B. Myer, N. Rushton, In vitro and in vivo investigations into the biocompatibility of diamond-like carbon (DLC) coatings for orthopedic applications, J. Biomed. Mater. Res. 58 (3) (2001) 319–328.
[140] R.S. Laskin, An oxidized Zr ceramic surfaced femoral component for total knee arthroplasty, Clin. Orthop. Relat. Res. 416 (2003) 191–196.
[141] P. Hernigou, G. Mathieu, A. Poignard, O. Manicom, P. Filippini, A. Demoura, Oxinium, a new alternative femoral bearing surface option for hip replacement, Eur. J. Orthop. Surg. Traumatol. 17 (3) (2007) 243–246.
[142] Oxinium Femoral Heads, Smith Nephew Corp. Broch. <http://smith-nephew.com> (2003).
[143] C.B. Rieker, Is the oxinium technology a useful technology in total joint arthroplasty? in: J.-Y. Lazennec, M. Dietrich (Eds.), Bioceram. Jt. Arthroplast. Proc. 9th Biol. Symp., Steinkopff, Paris, France, 2004, pp. 99–104.
[144] Z.A. Morison, S. Patil, H.A. Khan, E.R. Bogoch, E.H. Schemitsch, J.P. Waddell, A randomized controlled trial comparing oxinium and cobalt–chrome on standard and cross-linked polyethylene J. Arthroplasty 29 (9) (2014) 164–168.
[145] D.H. Park, J. Leong, S.J. Palmer, Total knee arthroplasty with an oxidised zirconium femoral component: a 5-year follow-up study, J. Orthop. Surg. 22 (1) (2014) 75–79.
[146] U. Türkan, O. Öztürk, A.E. Eroğlu, Metal ion release from TiN Coated CoCrMo orthopedic implant material, Surf. Coatings Technol. 200 (16) (2006) 5020–5027.
[147] R.A. Antunes, M.C.L. de Oliveira, Corrosion processes of physical vapor deposition-coated metallic implants, Crit. Rev. Biomed. Eng. 37 (6) (2009) 425–460.
[148] C.A. Love, R.B. Cook, T.J. Harvey, P.A. Dearnley, R.J.K. Wood, Diamond like carbon coatings for potential application in biological implants—a review, Tribol. Int. 63 (2013) 141–150.
[149] E. Alvarez, Surface Damage in Retrieved Total Knee Replacement Femoral Components, Ph.D Diss, Clemson Univeristy, 2012, pp. 1–240.
[150] R. Lee, A. Essner, A. Wang, W.L. Jaffe, Scratch and wear performance of prosthetic femoral head components against crosslinked UHMWPE sockets, Wear 267 (11) (2009) 1915–1921.
[151] J.N. Weisenburger, S.M. Hovendick, K.L. Garvin, H. Haider, How durable are titanium nitride coatings on total hip replacements, J. Bone Jt. Surg. 93Br (Suppl. IV) (2011) 474.
[152] M. Kuntz, Validation of a new high performance alumina matrix composite for use in total joint replacement, Semin. Arthroplasty 17 (3) (2006) 141–145.
[153] G.M. Insley, R.M. Streicher, Next generation ceramics based on zirconia toughened alumina for hip joint prostheses, Key Eng. Mater. 254 (2004) 675–678.
[154] T. Nakanishi, M. Sasaki, J. Ikeda, F. Miyaji, M. Kondo, Mechanical and phase stability of zirconia toughened alumina, Key Eng. Mater. 330–332 (2007) 1267–1270.
[155] S. Hori, M. Yoshimura, S. Somiya, Strength-toughness relations in sintered and isostatically hot-process ZrO_2-toughened Al_2O_3, J. Am. Ceram. Soc. 69 (3) (1986) 169–172.
[156] G. Magnani, A. Brillante, Effect of the composition and sintering process on mechanical properties and residual stresses in zirconia–alumina composites, J. Eur. Ceram. Soc. 25 (15) (2005) 3383–3392.
[157] R.L.K. Matsumoto, Aging behavior of ceria-stabilized tetragonal zirconia polycrystals, J. Am. Ceram. Soc. 71 (3) (2005) C128–C129.
[158] M. Nawa, S. Nakamoto, T. Sekino, K. Niihara, Tough and strong Ce–TZP/alumina nanocomposites doped with titania, Ceram. Int. 24 (7) (1998) 497–506.
[159] R. Gadow, F. Kern, Novel zirconia–alumina nanocomposites combining high strength and toughness, Adv. Eng. Mater. 12 (12) (2010) 1220–1223.
[160] M. Kuntz, N. Shneider, R. Heros, Controlled zirconia phase transformation in BIOLOX® delta? A feature of safety, in: Bioceram. Altern. Bear. Jt. Arthroplast. Steinkopff, New York, 2005, pp. 79–84.
[161] Implants for Surgery – Ceramic Materials – Part 2: Composite Materials Based on a high Purity Alumina Matrix with Zirconia Reinforcement, ISO/DIS 6474-2.2 (2001) 1–17.
[162] S. Begand, T. Oberbach, W. Glien, ATZ—a new material with a high potential in joint replacement, Key Eng. Mater. 284 (2005) 983–986.
[163] G. Willmann, W. Von-Chamier, H. Pfaff, R. Rack, Biocompatibility of a new alumina matrix biocomposite AMC, Key Eng. Mater. 192–195 (2002) 569–574.
[164] R.J. Kohal, M. Baechle, J.S. Han, D. Hueren, U. Huebner, F. Butz, In vitro reaction of human osteoblasts on alumina- toughened zirconia, Clin. Oral Implants Res. 20 (11) (2009) 1265–1271.
[165] M. Kuntz, T. Pandorf, W. Chen, Material properties and life time of a high performance alumina matrix composite for use in total joint replacement, J. Med. Biomech. 24 (5) (2009) 363–368.
[166] S. Begand, T. Oberbach, W. Glien, Investigatons of the mechanical properties of an alumina toughned zirconia ceramic for an application in joint prostheses, Key Eng. Mater. 284–286 (2005) 1019–1022.
[167] H. Kamiya, M. Sakakibara, Y. Sakurai, G. Jimbo, S. Wada, Erosion wear properties of tetragonal ZrO_2 (Y_2O_3)–toughened Al_2O_3 composites, J. Am. Ceram. Soc. 77 (3) (1994) 666–672.
[168] B. Kerkwijk, L. Winnubst, E.J. Mulder, H. Verweij, Processing of homogeneous zirconia-toughened alumina ceramics with high sliding wear resistance, J. Am. Ceram. Soc. 82 (8) (1999) 2087–2093.
[169] G.M. Insley, I. Turner, J. Fisher, R.M. Streicher, In-vitro testing and validation of zirconia toughened alumina (ZTA), in: J.P. Garino, G. Willmann (Eds.), Bioceram. Jt. Arthroplast. Proc. 7th Int. Biol. Symp., Thieme Publishing Group, 2015, pp. 26–31.
[170] I.C. Clarke, G. Pezzotti, D.D. Green, H. Shirasu, T. Donaldson, Severe simulation test for run-in wear of all- alumina compared to alumina composite THR, in: J.A. D'Antonio, M. Dietrich (Eds.), Bioceram. Altern. Bear. Jt. Arthroplast, Steinkopff Verlag, Darmstadt, 2006, pp. 11–20.

[171] I.C. Clarke, D. Green, P. Williams, T. Donaldson, G. Pezzotti, US perspective on hip simulator wear testing of BIOLOX® delta in 'Severe' test modes, in: F. Benazzo, F. Falez, M. Dietrich (Eds.), Bioceram. Altern. Bear. Jt. Arthroplast, Steinkopff Verlag, Darmstadt, 2006, pp. 189–205.

[172] I.C. Clarke, D.D. Green, P.S. Williams, K. Kubo, G. Pezzotti, A. Lombardi, A. Turnbull, T.K. Donaldson, Hip-simulator wear studies of an alumina–matrix composite (AMC) ceramic compared to retrieval studies of amc balls with 1–7 years follow-up, Wear 267 (5–8) (2009) 702–709.

[173] T. Oberbach, S. Begand, W. Glien, In-vitro wear of different ceramic couplings, Key Eng. Mater. 330–332 (2007) 1231–1234.

[174] S. Begand, T. Oberbach, W. Glien, Tribological behaviour of an alumina toughened zirconia ceramic for an application in joint prostheses, Key Eng. Mater. 309–311 (2006) 1261–1264.

[175] W.G. Hamilton, J.P. McAuley, D.A. Dennis, J.A. Murphy, T.J. Blumenfeld, J. Politi, THA with delta ceramic on ceramic: results of a multicenter investigational device exemption trial, Clin. Ortho. Relat. Res. 468 (2010) 358–366.

[176] J.J. Callaghan, S.S. Liu, Ceramic on crosslinked polyethylene in total hip replacement: any better than metal on crosslinked polyethylene? Iowa Orthop. J. 29 (2009) 1–4.

[177] P. Bergschmidt, C. Lohmann, R. Bader, S. Finze, C. Lukas, W. Ruther, W. Mittelmeier, Preliminary clinical results of the multigen plus total knee system with a ceramic femoral component – a national duo – centre study, Eur. Musculoskelet. Rev. 1 (2009) 82–85.

[178] I. Thomas, J. Milan, R. Thomas- Peter, R. Martin, L. van den Daeelen, B. Stockl, Preliminary Results of a New Nanocrystalline Dispersion Ceramic 'Ceramys,' <http://www.mathysmedical.com/> (2009) 1–4.

[179] J. Chevalier, L. Gremillard, Ceramics for medical applications: a picture for the next 20 years, J. Eur. Ceram. Soc. 29 (7) (2009) 1245–1255.

[180] G. Hunter, J. Dickinson, B. Herb, R. Graham, Creation of oxidized zirconium orthopaedic implants, JASTM Int. 2 (7) (2005), Paper ID: JAI12775.

[181] P. Kutilek, J. Miksovsky, The procedure of evaluating the practical adhesion strength of new biocompatible nano-and micro-thin films in accordance with international standards, Acta Bioeng. Biomech. 13 (3) (2011) 87–94.

[182] A.P. Druschitz, J.G. Schroth, Hot isostatic pressing of a presintered yttria-stabilized zirconia ceramic, J. Am. Ceram. Soc. 72 (9) (1989) 1591–1597.

[183] Y. Matsumoto, K. Hirota, O. Yamaguchi, S. Inamura, H. Miyamoto, N. Shiokawa, K. Tsuji, Mechanical properties of hot isostatically pressed zirconia-toughened alumina ceramics prepared from coprecipitated powders, J. Am. Ceram. Soc. 76 (10) (1993) 2677–2680.

[184] D.-W. Shin, K.K. Orr, H. Schubert, Microstructure-mechanical property relationships in hot isostatically pressed alumina and zirconia-toughened alumina, J. Am. Ceram. Soc. 73 (5) (1990) 1181–1188.

[185] F. Castro, I. Iturriza, HIP of Si_3N_4 and Si_3N_4 + 1 w/o Y_2O_3 to full density, J. Mater. Sci. Lett. 9 (1990) 600–602.

[186] J. Garino, M.N. Rahaman, B.S. Bal, The reliability of modern alumina bearings in total hip arthroplasty, Semin. Arthroplasty 17 (3–4) (2006) 113–119.

[187] M.N. Rahaman, A. Yao, B.S. Bal, J.P. Garino, M.D. Ries, Ceramics for prosthetic hip and knee joint replacement, J. Am. Ceram. Soc. 90 (7) (2007) 1965–1988.

[188] P.H. Mayrhofer, C. Mitterer, H. Clemens, Self-organized nanostructures in hard ceramic coatings, Adv. Eng. Mater. 7 (12) (2005) 1071–1082.

[189] S.Y. Sharivker, V.G. Zil'berberg, M.I. Olievskii, The density of ceramic coatings applied with a plasma, Sov. Powder Metall. Met. Ceram. 8 (1) (1969) 30–33.

[190] L.W. Hobbs, V.B. Rosen, S.P. Mangin, M. Treska, G. Hunter, Oxidation microstructures and interfaces in the oxidized zirconium knee, Int. Appl. Cerem. Technol. 2 (3) (2005) 221–246.

[191] G. Montavon, S. Sampath, C.C. Bemdt, C. Coddet, Effects of vacuum plasma spray processing parameters on splat morphology, J. Therm. Spray Technol. 4 (1) (1995) 67–74.

[192] A. Dey, A.K. Mukhopadhyay, Fracture toughness of microplasma-sprayed hydroxyapatite coating by nanoindentation, Int. J. Appl. Ceram. Technol. 8 (3) (2011) 572–590.

[193] A. Dey, A.K. Mukhopadhyay, Anisotropy in nanohardness of microplasma sprayed hydroxyapatite coating, Adv. Appl. Ceram. 109 (6) (2010) 346–354.

[194] V.P. Orlovskii, V.S. Komlev, S.M. Barinov, Hydroxyapatite and hydroxyapatite-based ceramics, Inorg. Mater. 38 (10) (2002) 973–984.

[195] K. Bodišová, M. Kašiarová, M. Domanická, M. Hnatko, Z. Lenčéš, Z.V. Nováková, J. Vojtaššák, S. Gromošová, et al., Porous silicon nitride ceramics designed for bone substitute applications, Ceram. Int. 39 (7) (2013) 8355–8362.

[196] J.E. Kiwerski, A. Ogonowski, The use of porous corundum ceramics in spinal surgery, Int. Orthop. 18 (1) (1994) 10–13.

[197] D.C. Tancred, B.A. McCormack, A.J. Carr, A synthetic bone implant macroscopically identical to cancellous bone, Biomaterials 19 (24) (1998) 2303–2311.

[198] R. Huet, A. Sakona, S.M. Kurtz, Strength and reliability of alumina ceramic femoral heads: review of design, testing, and retrieval analysis, J. Mech. Behav. Biomed. Mater. 4 (3) (2011) 476–483.

[199] D. Kovar, M.J. Ready, Role of grain size in strength variability of alumina, J. Am. Ceram. Soc. 77 (7) (1994) 1928–1938.

[200] P. Chantikul, S.J. Bennison, B.R. Lawn, Role of grain size in the strength and R-curve properties of alumina, J. Am. Ceram. Soc. 73 (8) (1990) 2419–2427.

[201] F. Meschke, G. De Portu, N. Claussen, Microstructure and thermal stability of fine-grained (Y, Mg)-PSZ ceramics with alumina additions, J. Eur. Ceram. Soc. 11 (5) (1993) 481–486.

[202] F. Meschke, N. Claussen, G. De Portu, J. Rödel, Phase stability of fine-grained (Mg,Y)-PSZ, J. Am. Ceram. Soc. 78 (7) (1995) 1997–1999.

[203] J. Eichler, J. Rödel, U. Eisele, M. Hoffman, Effect of grain size on mechanical properties of submicrometer 3Y-TZP: fracture strength and hydrothermal degradation, J. Am. Ceram. Soc. 90 (9) (2007) 2830–2836.

[204] A. Paul, B. Vaidhyanathan, J.G.P. Binner, Hydrothermal aging behavior of nanocrystalline Y-TZP ceramics, J. Am. Ceram. Soc. 94 (7) (2011) 2146–2152.

[205] S. Deville, J. Chevalier, C. Dauvergne, G. Fantozzi, J.F. Bartolome, J.S. Moya, R. Torrecillas, Microstructural investigation of the aging behavior of (3Y-TZP)-Al_2O_3 composites, J. Am. Ceram. Soc. 88 (5) (2005) 1273–1280.

[206] D. Casellas, M.M. Nagl, L. Llanes, M. Anglada, Fracture toughness of alumina and ZTA ceramics: microstructural coarsening effects, J. Mater. Process. Technol. 143–144 (1) (2003) 148–152.

[207] M. Nawa, H. Nakanishi, Y. Suehiro, ZrO_2–Al_2O_3 composite ceramic material and production method therefor US Patent 8093168 (2012).

[208] M.M. Hasan, F. Islam, Effect of sintering temperature and time on the microstruture and properties of zirconia toughened alumina (ZTA), in: R.K. Bordia, E.A. olevsky (Eds.), Adv. Sinter. Sci. Technol., American Ceramic Society Press, Columbus, OH, 2010, pp. 283–290.

[209] W. Burger, H.G. Richter, High Strength and toughness alumina matrix composites by transformation toughening and 'in situ' platelet reinforcement (ZPTA)—the new generation of bioceramics, Key Eng. Mater. 192–195 (2001) 545–548.

[210] G. Pezzotti, On the actual contribution of crack deflection in toughening platelet-reinforced brittle-matrix composites, Acta Metall. Mater. 41 (6) (1993) 1826–1839.

[211] A. Kirsten, S. Begand, T. Oberbach, R. Telle, H. Fischer, Subcritical crack growth behavior of dispersion oxide ceramics, J. Biomed. Mater. Res. 95B (1) (2010) 202–206.

[212] A.H. De Aza, J. Chevalier, G. Fantozzi, M. Schehl, R. Torrecillas, Crack growth resistance of alumina, zirconia and zirconia toughened alumina ceramics for joint prostheses, Biomaterials 23 (3) (2002) 937–945.

[213] M. Dehestani, E. Adolfsson, Phase stability and mechanical properties of zirconia and zirconia composites, Int. J. Appl. Ceram. Technol. 10 (1) (2013) 129–141.

[214] H.-D. Kim, B.-D. Han, D.-S. Park, B.-T. Lee, P.F. Becher, Novel two-step sintering process to obtain a bimodal microstructure in silicon nitride, J. Am. Ceram. Soc. 85 (1) (2002) 245–252.

[215] D.M. Mattox, Handbook of Physical Vapor Deposition (PVD) Processing, 2nd ed., Elsevier, Burlington, MA, 2010.

[216] J. Robertson, Diamond-like amorphous carbon, Mater. Sci. Eng. R. 37 (4–6) (2002) 129–281.

[217] V.-H. Pham, S.-W. Yook, E.-J. Lee, Y. Li, G. Jeon, J.-J. Lee, H.-E. Kim, Y.-H. Koh, Deposition of TiN films on Co–Cr for improving mechanical properties and biocompatibility using reactive DC sputtering, J. Mater. Sci. Mater. Med. 22 (10) (2011) 2231–2237.

[218] M. Fenker, Properties of oxynitride thin films for biomedical applications, in: F. Vaz, N. Martin, M. Fenker (Eds.), Met. Oxynitride Thin Film by React. Sputtering Relat. Depos. Methods, Bentham Science Publishers, 2013, pp. 254–264.

[219] D.-Y. Wang, Y.-Y. Chang, C.-L. Chang, Y.-W. Huang, Deposition of diamond-like carbon films containing metal elements on biomedical Ti alloys, Surf. Coatings Technol. 200 (7) (2005) 2175–2180.

[220] J. Lützner, A. Hartmann, G. Dinnebier, P. Spornraft-Ragaller, C. Hamann, S. Kirschner, Metal hypersensitivity and metal ion levels in patients with coated or uncoated total knee arthroplasty: a randomised controlled study, Int. Orthop. 37 (10) (2013) 1925–1931.

[221] L.C. Hernández, L. Ponce, A. Fundora, E. López, E. Pérez, Nanohardness and residual stress in TiN coatings, Materials (Basel) 4 (5) (2011) 929–940.

[222] S. Zhang, D. Sun, Y. Fu, H. Du, Toughening of hard nanostructural thin films: a critical review, Surf. Coatings Technol. 198 (1–3) (2005) 2–8.

[223] J. Menghani, K.B. Pai, M.K. Totlani, Corrosion and wear behaviour of ZrN thin films, Tribol.–Mater. Surf. Interfaces 5 (3) (2011) 122–128.

[224] J. Bolton, X. Hu, In vitro corrosion testing of PVD coatings applied to a surgical grade Co–Cr–Mo alloy, J. Mater. Sci. Mater. Med. 13 (6) (2002) 567–574.

[225] M. Iwasaki, A. Hirata, Deposition of high-density amorphous carbon films by sputtering in electron-beam-excited plasma, New Diam. Front. Carbon Technol. 15 (3) (2005) 139–149.

[226] V. Chawla, R. Jayaganthan, R. Chandra, Microstructural characteristics and mechanical properties of magnetron sputtered nanocrystalline TiN films on glass substrate, Bull. Mater. Sci. 32 (2) (2009) 117–123.

[227] P.H. Mayrhofer, C. Mitterer, J. Musil, Structure-property relationships in single- and dual- phase nanocrystalline hard coatings, Surf. Coatings Technol. 174–175 (2003) 725–731.

[228] S. Kamiya, H. Hanyu, S. Amaki, H. Yanase, Statistical evaluation of the strength of wear- resistant hard coatings, Surf. Coatings Technol. 202 (4) (2007) 1154–1159.

[229] S.W.K. Kweh, K.A. Khor, P. Cheang, Plasma-sprayed hydroxyapatite (HA) coatings with flame-spherodized feedstock: microstructure and mechanical properties, Biomaterials 21 (12) (2000) 1223–1234.

[230] C.-C. Chen, S.-J. Ding, Effect of heat treatment on characteristics of plasma sprayed hydroxyapatite coatings, Mater. Trans. 47 (3) (2006) 935–940.

[231] Z.L. Dong, K.A. Khor, C.H. Quek, T.J. White, P. Cheang, TEM and STEM analysis on heat-treated and in vitro plasma-sprayed hydroxyapatite/Ti-6Al-4V composite coatings, Biomaterials 24 (1) (2003) 97–105.

[232] A. Rabiei, S. Sandukas, Processing and evaluation of bioactive coatings on polymeric implants, J. Biomed. Mater. Res. 101A (9) (2013) 2621–2629.
[233] S. Barkarmo, M. Andersson, F. Currie, P. Kjellin, R. Jimbo, C.B. Johansson, V. Stenport, Enhanced bone healing around nanohydroxyapatite- coated polyetheretherketone implants: an experimental study in rabbit bone, J. Biomater. Appl. 29 (5) (2014) 737–747.
[234] S. Yu, K.P. Hariram, R. Kumar, P. Cheang, K.K. Aik, In vitro apatite formation and its growth kinetics on hydroxyapatite/polyetheretherketone biocomposites, Biomaterials 26 (15) (2005) 2343–2352.
[235] HA/PEEK-Optima, Invibio Corp. Present <http://invibio.com/ortho/materials/peek-optima-ha> (2012).
[236] S.M. Kurtz, J.N. Devine, PEEK biomaterials in trauma, orthopedic, and spinal implants, Biomaterials 28 (32) (2007) 4845–4869.
[237] Standard Test Method for Flexural Strength of Advanced Ceramics at Ambient Temperature, ASTMC1161-02 (reapproved) (2008).
[238] Fine Ceramics (Advanced Ceramics, Advanced Technical ceramics) – Test Method for Flexural Strength of Monolithic Ceramics at Room Temperature, ISO 147042008 (2008).
[239] Y. Katayama, Y. Hattori, Effects of specimen size on strength of sintered silicon nitride, J. Am. Ceram. Soc. 65 (10) (1982) C164–C165.
[240] G.D. Quinn, R. Morrell, Design data for engineering ceramics: a review of the flexure test, J. Am. Ceram. Soc. 74 (9) (1991) 2037–2066.
[241] G. Willmann, Ceramic femoral head retrieval data, Clin. Orthop. Relat. Res. 379 (2000) 22–28.
[242] Recall of Zirconia Ceramic Femoral Heads for Hip Implants, Bull. Am. Ceram. Soc., 80(12) (2001) 14.
[243] B. Masson, M. Kuntz, Long-term stability of ceramic composite in total hip arthroplasty, in: K. Knahr (Ed.), Total Hip Arthroplasty, Springer, Berlin, Heidelberg, 2012, pp. 145–153.
[244] G. Pezzotti, K. Yamada, S. Sakakura, R.P. Pitto, Raman spectroscopic analysis of advanced ceramic composite for hip prosthesis, J. Am. Ceram. Soc. 91 (4) (2008) 1199–1206.
[245] K. Yamada, G. Pezzotti, Environmental phase stability of ceramics composite for hip prostheses in presence of surface damage, Key Eng. Mater. 361–363 (2008) 783–786.
[246] G. Pezzotti, T. Saito, Y. Takahashi, K. Fukatsu, N. Sugano, Surface topology of advanced alumina/zirconia composite femoral head as compared with commercial femoral heads made of monolithic zirconia, J. Am. Ceram. Soc. 94 (3) (2011) 945–950.
[247] S. Affatato, E. Modena, A. Toni, P. Taddei, Retrieval analysis of three generations of biolox® femoral heads: spectroscopic and SEM characterisation, J. Mech. Behav. Biomed. Mater. 13 (2012) 118–128.
[248] T. Douillard, J. Chevalier, A. Descamps-Mandine, I. Warner, Y. Galais, P. Whitaker, J.J.J. Wu, Q.Q. Wang, Comparative ageing behaviour of commercial, unworn and worn 3Y-TZP and zirconia-toughened alumina hip joint heads, J. Eur. Ceram. Soc. 320 (8) (2012) 1529–1540.
[249] M. Cecilia, C. De Sá, D. Moraes, C. Nelson, J. Duailibi, L. Guimarães, G. DeOliveira, Mechanical properties of alumina–zirconia composites for ceramic abutments, Mater. Res. 7 (4) (2004) 643–649.
[250] J. Schneider, S. Begand, R. Kriegel, C. Kaps, W. Glien, T. Oberbach, Low-temperature aging behavior of alumina-toughened zirconia, J. Am. Ceram. Soc. 91 (11) (2008) 3613–3618.
[251] Standard Test Method for Monotonic Equibiaxial Flexural Strength of Advanced Ceramics at Ambient Temperature, ASTMC1499-09 (2013).
[252] I.Y. Prokhorov, Zirconia ceramics from coprecipitated powders, Refract. Ind. Ceram. 38 (1997) 453–459.
[253] S.R. Choi, J.A. Salem, Crack – growth resistance of in situ – toughened silicon nitride, J. Am. Ceram. Soc. 77 (4) (1994) 1042–1046.
[254] O. Borrero-Lopez, M. Hoffman, Measurement of fracture strength in brittle thin films, Surf. Coatings Technol. 254 (2014) 1–10.
[255] U. Wiklund, M. Bromark, M. Larsson, P. Hedenqvist, S. Hogmark, Cracking resistance of thin hard coatings estimated by four-point bending, Surf. Coatings Technol. 91 (1–2) (1997) 57–63.
[256] H.D. Espinosa, B. Peng, N. Moldovan, T.A. Friedmann, X. Xiao, D.C. Mancini, O. Auciello, J. Carlisle, et al., Elasticity, strength, and toughness of single crystal silicon carbide, ultrananocrystalline diamond, and hydrogen-free tetrahedral amorphous carbon, Appl. Phys. Lett. 89 (7) (2006) o73111.
[257] Standard Test Method for Adhesion Strength and Mechanical Failure Modes of Ceramic Coatings by Quantitative Single Point Scratch Testing, ASTMC1624-05 (reapproved 2010) (2010).
[258] M.E. Roy, L.A. Whiteside, B.J. Katerberg, Diamond-like carbon coatings enhance scratch resistance of bearing surfaces for use in joint arthroplasty: hard substrates outperform soft, J. Biomed. Mater. Res. Part B Appl. Biomater. 89 (2) (2009) 527–535.
[259] T. Utsumi, Y. Oka, E. Fujiwara, M. Yatsuzuka, Effect of a hard supra-thick interlayer on adhesion of DLC film prepared with PBIID process, Nucl. Instr. Methods Phys. Res. B Beam Interact. Mater. Atoms 257 (1–2) (2007) 706–709.
[260] M. Akao, H. Aoki, K. Kato, Mechanical properties of sintered hydroxyapatite for prosthetic applications, J. Mater. Sci. 16 (3) (1981) 809–812.
[261] A.A. Chaudhry, H. Yan, K. Gong, F. Inam, G. Viola, M.J. Reece, J.B.M. Goodall, I. ur Rehman, et al., High-strength nanograined and translucent hydroxyapatite monoliths via continuous hydrothermal synthesis and optimized spark plasma sintering, Acta Biomater. 7 (2) (2011) 791–799.
[262] L. Boilet, V. Lardot, A. Tricoteaux, A. Leriche, F. Cambier, M. Descamps, Processing and properties of calcium phosphates bioceramics by hot isostatic pressing, MATEC Web Conf. 7 (2013) o4020.
[263] H.-W. Kim, Y.-M. Kong, Y.-H. Koh, H.E. Kim, H.-M. Kim, J.S. Ko, Pressureless sintering and mechanical and biological properties of fluor-hydroxyapatite composites with zirconia, J. Am. Ceram. Soc. 86 (12) (2003) 2019–2026.
[264] S. Kim, Y.-M. Kong, I.-S. Lee, H.-E. Kim, Effect of calcinations of starting powder on mechanical properties of hydroxyapatite-alumina bioceramic composite, J. Mater. Sci. Mater. Med. 13 (2002) 307–310.
[265] Y.-M. Kong, S. Kim, H.-E. Kim, I.-S. Lee, Reinforcement of hydroxyapatite bioceramic by addition of ZrO_2 Coated with Al_2O_3, J. Am. Ceram. Soc. 82 (11) (1999) 2963–2968.
[266] Implants for Surgery – Hydroxyapatite – Part 4: Determination of Coating Adhesion Strength, ISO 1379-4 (2002).
[267] Standard Test Method for Adhesion or Cohesion Strength of Thermal Spray Coatings, ASTMC633-13 (2013).
[268] E. Mohseni, E. Zalnezhad, A.R. Bushroa, Comparative investigation on the adhesion of hydroxyapatite coating on Ti–6Al–4V implant: a review paper, Int. J. Adhes. Adhes. 48 (2014) 238–257.
[269] M. Roy, A. Bandyopadhyay, S. Bose, Induction plasma sprayed nano hydroxyapatite coatings on titanium for orthopaedic and dental implants, Surf. Coatings Technol. 205 (8–9) (2011) 2785–2792.
[270] Y. Yang, J.L. Ong, Bond Strength, compositional, and structural properties of hydroxyapatite coating on Ti, ZrO_2-coated Ti, and TPS-coated Ti substrate, J. Biomed. Mater. Res. 64A (3) (2003) 509–516.
[271] B.-D. Hahn, D.-S. Park, J.-J. Choi, J. Ryu, W.-H. Yoon, J.-H. Choi, J.-W. Kim, Y.-L. Cho, et al., Preparation and in vitro characterization of aerosol-deposited hydroxyapatite coatings with different surface roughnesses, Appl. Surf. Sci. 257 (17) (2011) 7792–7799.
[272] M. Vilotijević, P. Marković, S. Zec, S. Marinković, V. Jokanović, Hydroxyapatite coatings prepared by a high power laminar plasma jet, J. Mater. Process. Technol. 211 (6) (2011) 996–1004.
[273] M. Borroff, M. Green, P. Gregg, A. MacGregor, M. Porter, K. Tucker, N. Wishart (Eds.), National Joint Registry for England, Wales and Northern Ireland, 11th Annual Report. Published Online at: <www.njrcentre.org.uk>, London (2014).
[274] Australian Orthopaedic Association National Joint Replacement Registry, Annual Report, in: S. Graves (Ed.), AOA Press, Adelaide, 2014, Published online at: <www.aoa.org.au>.
[275] J.S. Melvin, T. Karthikeyan, R. Cope, T.K. Fehring, Early failures in total hip arthroplasty—a changing paradigm, J. Arthroplasty 2988 (6) (2014) 1285–1288.
[276] Standard Practice for Reporting Uniaxial Strength Data and Estimating Weibull Distribution Parameters for Advanced Ceramics, ASTMC1239-13 (2013).
[277] M. Ambrožič, L. Gorjan, M. Gomilšek, Bend strength variation of ceramics in serial fabrication, J. Eur. Ceram. Soc. 34 (7) (2014) 1873–1879.
[278] G.D. Quinn, Flexure Strength of Advanced Ceramics – A Round Robin Exercise, Rep. No. MTLTR 89-62, AD-A212-101, US Arm Mater. Technol. Lab. (1989).
[279] S. Verma, M.N. Sahu, P.K. Jain, Silicon nitride/SiAlON ceramics—a review, Indian J. Eng. Mater. Sci. 8 (February) (2001) 36–45.
[280] S. Ban, Y. Suehiro, H. Nakanishi, M. Nawa, Fracture toughness of dental zirconia before and after autoclaving, J. Ceram. Soc. Japan 118 (1378) (2010) 406–409.
[281] C.-W. Li, J. Yamanis, Super-tough silicon nitride with R-curve behavior, Ceram. Eng. Sci. Proc. 105 (7–8) (1989) 632–645.
[282] C.-W. Li, S.-C. Lui, J. Goldacker, Relation between strength, microstructure, and grain-bridging characteristics in in situ reinforced silicon nitride, J. Am. Ceram. Soc. 78 (2) (1995) 449–459.
[283] N. Hirosaki, Y. Akimune, M. Mitomo, Effect of grain growth of β-silicon nitride on strength, weibull modulus, and fracture toughness, J. Am. Ceram. Soc. 76 (7) (1993) 1892–1894.
[284] Z. Krstic, Z. Yu, V.D. Krstic, Effect of grain width and aspect ratio on mechanical properties of Si_3N_4 ceramics, J. Mater. Sci. 42 (42) (2007) 5431–5436.
[285] I. Tanaka, G. Pezzotti, T. Okamoto, Y. Miyamoto, M. Koizumi, Hot isostatic press sintering and properties of silicon nitride without additive, J. Am. Ceram. Soc 72 (9) (1989) 1656–1660.
[286] O. Borrero-López, M. Hoffman, A. Bendavid, P.J. Martin, A simple nanoindentation-based methodology to assess the strength of brittle thin films, Acta Mater. 56 (7) (2008) 1633–1641.
[287] C. Yatongchai, A.W. Wren, D.J. Curran, J.-C. Hornez, M.R. Towler, Comparison of the weibull characteristics of hydroxyapatite and strontium doped hydroxyapatite, J. Mech. Behav. Biomed. Mater. 21 (2013) 95–108.
[288] C.-W. Yang, T.-S. Lui, Effect of hydrothermal self-healing and intermediate strengthening layers on adhesion reinforcement of plasma-sprayed hydroxyapatite coatings, in: H. Jazi (Ed.), Adv. Plasma Spray Appl., InTech, Shanghai, China, 2012, pp. 123–147, Published online at: <http://www.intechopen.com>.
[289] A. Dey, A.K. Mukhopadhyay, S. Gangadharan, M.K. Sinha, D. Basu, Weibull modulus of nano-hardness and elastic modulus of hydroxyapatite coating, J. Mater. Sci. 44 (18) (2009) 4911–4918.
[290] M. Naito, M. Okumiya, H. Abe, A. Kondo, Powder processing issues for high quality advanced ceramics, KONA Powder Part. J. 28 (2010) 143–154.

[291] J.E. Maye, G.-P. Fang, Effect of grinding parameters on strength and finish of ceramics, in: 1st Int. Mach. Grind. Conf. SME, Dearborn, Michiga, 1995, pp. MR95–170.
[292] T. Strakna, S. Jahanmir, R. Allor, K. Kumar, Effect of grinding on strength of silicon nitride, in: NAMRCXXIII, SME Press, Houghton, MI, 1995, pp. MR95–138.
[293] T. Kosmac, C. Oblak, P. Jevnikar, N. Funduk, L. Marion, The effect of surface grinding and sandblasting on flexural strength and reliability of Y-TZP zirconia ceramic, Dent. Mater. 15 (6) (1999) 426–433.
[294] H. Richter, Application of proof-testing to ceramic hip joint heads, in: 3rd Int. Biol. Symp. Ceram. Wear Couple, 1998, pp. 7–12.
[295] B. Weisse, C. Affolter, R.E. Koller, A. Stutz, Proof testing of ceramic femoral heads for hip joint implants, Proc. Inst. Mech. Eng. Part HJ. Eng. Med. 224 (9) (2010) 1051–1059.
[296] S. Wiederhorn, Brittle fracture and toughening mechanisms in ceramics, Ann. Rev. Mater. Sci. 14 (1) (1984) 373–403.
[297] T. Fujii, T. Nose, Evaluation of fracture toughness for ceramic materials, ISIJ Int. 29 (9) (1989) 717–725.
[298] M. Sakai, R.C. Bradt, Fracture toughness testing of brittle materials, Int. Mater. Rev. 38 (2) (1993) 53–78.
[299] G.A. Gogotsi, Fracture toughness of ceramics and ceramic composites, Ceram. Int. 29 (7) (2003) 777–784.
[300] G.D. Quinn, R.C. Bradt, On the Vickers indentation fracture toughness test, J. Am. Ceram. Soc. 90 (3) (2007) 673–680.
[301] R. Morrell, Fracture toughness testing for advanced technical ceramics: internationally agreed good practice, Adv. Appl. Ceram. 105 (2) (2006) 88–98.
[302] J.J. Kruzic, D.K. Kim, K.J. Koester, R.O. Ritchie, Indentation techniques for evaluating the fracture toughness of biomaterials and hard tissues, J. Mech. Behav. Biomed. Mater. 2 (4) (2009) 384–395.
[303] G.D. Quinn, J. Salem, I. Bar- on, K. Cho, M. Foley, H. Fang, Fracture toughness of advanced ceramics at room temperature, J. Res. Natl. Inst. Stand. Technol. 97 (5) (1992) 579–607.
[304] R.J. Primas, R. Gstrein, ESISTC6 round robin on fracture toughness of ceramics, ECF11, Mech. Mech. Damage Fail (1996) 747–752.
[305] J. Kübler, Fracture Toughness of Ceramics Using the SEVNB Method, Round Robin ECF13, San Sebastian 2000, 2013.
[306] J.J. Swab, J. Tice, A.A. Wereszczak, R.H. Kraft, Fracture toughness of advanced structural ceramics: applying ASTMC 1421, J. Am. Ceram. Soc. (2014) 1–9, http://dx.doi.org/10.1111/jace.13293.
[307] A.G. Evans, Perspective on the development of high-toughness ceramics, J. Am. Ceram. Soc. 73 (2) (1990) 187–206.
[308] D. Munz, What can we learn from R-curve measurements? J. Am. Ceram. Soc. 90 (1) (2007) 1–15.
[309] Y. Morita, K. Nakata, Y.-H. Kim, T. Sekino, K. Niihara, K. Ikeuchi, Wear properties of alumina/zirconia composite ceramics for joint prostheses measured with an end-face apparatus, Biomed. Mater. Eng. 14 (3) (2004) 263–270.
[310] J. Chevalier, P. Taddei, L. Gremillard, S. Deville, G. Fantozzi, J.F. Bartolomé, C. Pecharroman, J.S. Moya, et al., Reliability assessment in advanced nanocomposite materials for orthopaedic applications, J. Mech. Behav. Biomed. Mater. 4 (3) (2011) 303–314.
[311] G. Pezzotti, K. Yamamoto, Artificial hip joints: the biomaterials challenge, J. Mech. Behav. Biomed. Mater. 31 (2014) 313–320.
[312] E. Apel, C. Ritzberger, N. Courtois, H. Reveron, J. Chevalier, M. Schweiger, F. Rothbrust, V.M. Rheinberger, et al., Introduction to a tough, strong and stable Ce-TZP/MgAl2O4 composite for biomedical applications, J. Eur. Ceram. Soc. 32 (11) (2012) 2697–2703.
[313] G. Pezzotti, H. Ichimaru, L.P. Ferroni, K. Hirao, O. Sbaizero, Raman microprobe evaluation of bridging stresses in highly anisotropic silicon nitride, J. Am. Ceram. Soc. 84 (8) (2001) 1785–1790.
[314] A. Riedl, R. Daniel, M. Stefenelli, T. Schöberl, O. Kolednik, C. Mitterer, J. Keckes, A novel approach for determining fracture toughness of hard coatings on the micrometer scale, Scr. Mater. 67 (7–8) (2011) 708–711.
[315] S. Zhang, X. Zhang, Toughness evaluation of hard coatings and thin films, Thin Solid Films 520 (2012) 2375–2389.
[316] S. Zhang, D. Sun, Y. Fu, H. Du, Toughness measurement of thin films: a critical review, Surf. Coatings Technol. 198 (1–3) (2005) 74–84.
[317] Y.X. Wang, S. Zhang, Toward hard yet tough ceramic coatings, Surf. Coatings Technol. 258 (2014) 1–16.
[318] J. Ding, Y. Meng, S. Wen, Mechanical properties and fracture toughness of multilayer hard coatings using nanoindentation, Thin Solid Films 371 (1–2) (2000) 178–182.
[319] P. Panjan, M. Čekada, B. Navinšek, A new experimental method for studying the cracking behaviour of PVD multilayer coatings, Surf. Coatings Technol. 174–175 (2003) 55–62.
[320] G. Jaeger, I. Endler, M. Heilmaier, K. Bartsch, A. Leonhardt, A new method of determining strength and fracture toughness of thin hard coatings, Thin Solid Films 377–378 (2000) 382–388.
[321] L. Zhang, H. Yang, X. Pang, K. Gao, A.A. Volinsky, Microstructure, residual stress, and fracture of sputtered TiN films, Surf. Coatings Technol. 224 (2013) 120–125.
[322] S. Baek, C. ?S. Seok, Fracture characteristics of DLC on silicon using nano-indentation and FEA, Int. J. Mod. Phys. B 20 (25–27) (2006) 4213–4218.
[323] Y. Tang, G.-J. Zhang, J.-X. Xue, X.-G. Wang, C.-M. Xu, X. Huang, Densification and mechanical properties of hot-pressed ZrN ceramics doped with Zr or Ti, J. Eur. Ceram. Soc. 33 (7) (2013) 1363–1371.
[324] P.K. Yalamanchili, ZrN based nanostructured hard coatings structure–property relationship, in: Thesis, Department of Physics, Chemistry and Biology, Linkoping University, Sweden, 2014.
[325] H.H. Mofidi, A.S. Rouhaghdam, S. Ahangarani, M. Bozorg, M. Azadi, Fracture toughness of TiN coating as a function of interlayer thickness, Adv. Mater. Res. 829 (2014) 466–470.
[326] A. Leto, W. Zhu, M. Matsubara, G. Pezzotti, Bioinertness and fracture toughness evaluation of the monoclinic zirconia surface film of oxinium™ femoral head by raman and cathodoluminescence spectroscopy, J. Mech. Behav. Biomed. Mater. 31 (2014) 135–144.
[327] J. Eichler, U. Eisele, J. Rödel, Mechanical properties of monoclinic zirconia, J. Am. Ceram. Soc. 87 (7) (2004) 1401–1403.
[328] R.K. Roeder, G.L. Converse, R.J. Kane, W. Yue, Hydroxyapatite-reinforced polymer biocomposites for synthetic bone substitutes, JOM 60 (3) (2008) 38–45.
[329] D. Arola, D. Bajaj, J. Ivancik, H. Majd, D. Zhang, Fatigue of biomaterials: hard tissues, Int. J. Fatigue 32 (9) (2010) 1400–1412.
[330] D.C. Wirtz, N. Schiffers, T. Pandorf, K. Radermacher, D. Weichert, R. Forst, Critical evaluation of known bone material properties to realize anisotropic FE-simulation of the proximal femur, J. Biomech. 33 (10) (2000) 1325–1330.
[331] J.Y. Rho, T.Y. Tsui, G.M. Pharr, Elastic properties of human cortical and trabecular lamellar bone measured by nanoindentation, Biomaterials 18 (20) (1997) 1325–1330.
[332] T.S. Keller, Z. Mao, D.M. Spengler, Young's modulus, bending strength, and tissue physical properties of human compact bone, J. Orthop. Res. 8 (4) (1990) 592–603.
[333] J. Peterson, P.C. Dechow, Material properties of the inner and outer cortical tables of the human parietal bone, Anat. Rec. 268 (1) (2002) 7–15.
[334] F.G. Evans, Factors affecting the mechanical properties of bone, Bull. N. Y. Acad. Med. 49 (9) (1973) 751–764.
[335] H.S. Gupta, P. Zioupos, Fracture of bone tissue: The 'Hows' and the 'Whys', Med. Eng. Phys. 30 (10) (2008) 1209–1226.
[336] L.P. Mullins, M.S. Bruzzi, P.E. McHugh, Measurement of the microstructural fracture toughness of cortical bone using indentation fracture, J. Biomech. 40 (14) (2007) 3285–3288.
[337] K.J. Koester, H.D. Barth, R.O. Ritchie, Effect of aging on the transverse toughness of human cortical bone: evaluation by R-curves, J. Mech. Behav. Biomed. Mater. 4 (7) (2011) 1504–1513.
[338] C.E. Hoffler, K.E. Moore, K. Kozloff, P.K. Zysset, M.B. Brown, S.A. Goldstein, Heterogeneity of bone lamellar-level elastic moduli, Bone 26 (6) (2000) 603–609.
[339] R.O. Ritchie, Mechanisms of fatigue–crack propagation in ductile and brittle solids, Int. J. Fract. 100 (1999) 55–83.
[340] R.O. Ritchie, C.J. Gilbert, J.M. McNaney, Mechanics and mechanisms of fatigue damage and crack growth in advanced materials, Int. J. Solids Struct. 37 (1–2) (2000) 311–329.
[341] R.O. Ritchie, J.O. Peters, Small fatigue cracks: mechanics, mechanisms and engineering applications, Mater. Trans. 42 (1) (2001) 58–67.
[342] P.C. Paris, F. Erdogan, A critical analysis of crack propagation laws, J. Fluids Eng. 85 (4) (1963) 528–533.
[343] J.J. Kruzic, R.M. Cannon, R.O. Ritchie, Effects of moisture on grain-boundary strength, fracture, and fatigue properties of alumina, J. Am. Ceram. Soc. 88 (8) (2005) 2236–2245.
[344] D.S. Jacobs, I.-W. Chen, Mechanical and environmental factors in the cyclic and static fatigue of silicon nitride, J. Am. Ceram. Soc. 77 (5) (1994) 1153–1161.
[345] S. Ramalingam, I.E. Reimanis, E.R. Fuller, J.D. Haftel, Slow crack growth behavior of zirconia-toughened alumina and alumina using the dynamic fatigue indentation technique, J. Am. Ceram. Soc. 94 (2) (2011) 576–583.
[346] J. Chevalier, C. Olagnon, G. Fantozzi, Subcritical crack propagation in 3Y-TZP ceramics: static and cyclic fatigue, J. Am. Ceram. Soc. 82 (11) (1999) 3129–3138.
[347] A. Bhatnagar, M.J. Hoffman, R.H. Dauskardt, Fracture and subcritical crack-growth behavior of Y–Si–Al–O–N glasses and Si_3N_4 ceramics, J. Am. Ceram. Soc. 83 (3) (2000) 585–596.
[348] A.H. De Aza, J. Chevalier, G. Fantozzi, Slow-crack-growth behavior of zirconia-toughened alumina ceramics processed by different methods, J. Am. Ceram. Soc. 86 (1) (2003) 115–120.
[349] S. Hampshire, Oxynitride gasses, J. Eur. Ceram. Soc. 28 (7) (2008) 1475–1483.
[350] D. Graaf, H.T. Hintzen, G. With, Subcritical crack growth and power law exponent of Y–Si–Al–O(–N) glasses in aqueous environment, J. Mater. Sci. 41 (18) (2006) 6031–6034.
[351] S. Ishihara, A.J. Mcevily, T. Goshima, Effect of atmospheric humidity on the fatigue crack propagation behavior of short cracks in silicon nitride, J. Am. Ceram. Soc. 83 (3) (2000) 571–577.
[352] S. Horibe, R. Hirahara, Fatigue crack propagation of sintered silicon nitride in vacuum and air, Fatigue Fract. Eng. Mater. Struct. 14 (8) (1991) 863–870.
[353] S. Horibe, Fatigue of silicon nitride ceramics under cyclic loading, J. Eur. Ceram. Soc. 6 (2) (1990) 89–95.
[354] C.J. Gilbert, R.H. Dauskardt, R.O. Ritchie, Behavior of cyclic fatigue cracks in monolithic silicon nitride, J. Am. Ceram. Soc. 78 (9) (1995) 2291–2300.
[355] J. Chevalier, S. Deville, G. Fantozzi, J.F. Bartolomé, C. Pecharroman, J.S. Moya, L.A. Diaz, R. Torrecillas, Nanostructured ceramic oxides with a slow crack

growth resistance close *t* covalent materials, Nano Lett. 5 (7) (2005) 1297–1301.
[356] K.-T. Wan, S. Lathabai, B.R. Lawn, Crack velocity functions and thresholds in brittle solids, J. Eur. Ceram. Soc. 6 (4) (1990) 259–268.
[357] D.A. Krohn, D.P.H. Hasselman, Static and cyclic fatigue behavior of a polycrystalline alumina, J. Am. Ceram. Soc. 55 (4) (1972) 208–211.
[358] S. Suresh, E.K. Tschegg, Combined mode I–mode III fracture of fatigue-precracked alumina, J. Am. Ceram. Soc. 70 (10) (1987) 726–733.
[359] M.J. Reece, F. Guiu, M.F.R. Sammurt, Cyclic fatigue crack propagation in alumina under direct tension-compression loading, J. Am. Ceram. Soc. 2 (2) (1989) 348–352.
[360] S. Lathabai, Y.-W. Mai, B.R. Lawn, Cyclic fatigue behavior of an alumina ceramic with crack-resistance characteristics, J. Am. Ceram. Soc. 72 (9) (1989) 1760–1763.
[361] S. Lathabai, J. Rodel, B.R. Lawn, Cyclic fatigue from frictional degradation at bridging grains in alumina, J. Am. Ceram. Soc. 74 (6) (1991) 1340–1348.
[362] C.J. Gilbert, R.O. Ritchie, Mechanisms of cyclic fatigue–crack propagation in a fine-grained alumina ceramic: the role of crack closure, Fatigue Fract. Eng. Mater. Struct. 20 (10) (1997) 1453–1466.
[363] R.H. Dauskardt, D.B. Marshall, R.O. Ritchie, Cyclic fatigue–crack propagation in magnesia-partially-stabilized zirconia ceramics, J. Am. Ceram. Soc. 73 (4) (1990) 893–903.
[364] A.A. Steffen, R.H. Dauskardt, R.O. Ritchie, Cyclic fatigue life and crack-growth behavior of microstructurally small cracks in magnesia-partially-stabilized zirconia ceramics, J. Am. Ceram. Soc. 74 (6) (1991) 1259–1268.
[365] M. Hoffman, Y.-W. Mai, S. Wakayama, M. Kawahara, T. Kishi, Crack-tip degradation processes observed during in situ cyclic fatigue of partially stabilized zirconia, J. Am. Ceram. Soc. 78 (10) (1995) 2801–2810.
[366] T. Liu, Y.-W. Mai, G. Grathwohl, Cyclic fatigue crack propagation behavior of 9Ce- TZP ceramics with different grain size, J. Am. Ceram. Soc. 76 (10) (1993) 2601–2606.
[367] S.-Y. Liu, I.-W. Chen, Plasticity-induced fatigue damage in ceria-stabilized tetragonal zirconia polycrystals, J. Am. Ceram. Soc. 77 (8) (1994) 2025–2035.
[368] R.H. Dauskardt, W. Yu, R.O. Ritchie, Fatigue crack propagation in transformation- toughened zirconia ceramic, J. Am. Ceram. Soc. 70 (10) (1987) C248–C252.
[369] S.-Y. Liu, I.-W. Chen, Fatigue of yttria-stabilized zirconia: I, fatigue damage, fracture origins, and lifetime prediction, J. Am. Ceram. Soc. 74 (6) (1991) 1197–1205.
[370] S.-Y. Liu, I.-W. Chen, Fatigue of yttria-stabilized zirconia: ii, crack propagation, fatigue striations, and short-crack behavior, J. Am. Ceram. Soc. 74 (3) (1991) 1206–1216.
[371] G. Grathwohl, T. Liu, Crack resistance and fatigue of transforming ceramics: I, materials in the ZrO_2–Y_2O_3–Al_2O_3 System, J. Am. Ceram. Soc. 74 (2) (1991) 318–325.
[372] R. Benzaid, J. Chevalier, M. Saadaoui, G. Fantozzi, M. Nawa, L.A. Diaz, R. Torrecillas, M. Saâdaoui, Fracture toughness, strength and slow crack growth in a ceria stabilized zirconia-alumina nanocomposite for medical applications, Biomaterials 29 (27) (2008) 3636–3641.
[373] T. Kawakubo, K. Komeya, Static and cyclic fatigue behavior of a sintered silicon nitride at room temperature, J. Am. Ceram. Soc. 70 (6) (1987) 400–405.
[374] M. Okazaki, A.J. Mcevily, T. Tanaka, On the mechanism of fatigue crack growth in silicon nitride, Metall. Trans. A 22 (6) (1991) 1425–1434.
[375] R.V. Marrey, R. Burgermeister, R.B. Grishaber, R.O. Ritchie, Fatigue and life prediction for cobalt–chromium stents: a fracture mechanics analysis, Biomaterials 27 (9) (2006) 1988–2000.
[376] R.O. Ritchie, D.L. Davidson, B.L. Boyce, J.P. Campbell, O. Roder, High-cycle fatigue of Ti–6Al–4V, Fatigue Fract. Eng. Mater. Struct. 22 (7) (1999) 621–631.
[377] K. Wang, F. Wang, W. Cui, T. Hayat, B. Ahmad, Prediction of short fatigue crack growth of Ti–6Al–4V, Fatigue Fract. Eng. Mater. Struct. 37 (10) (2014) 1075–1086.
[378] M.S. Abu Bakar, M.H.W. Cheng, S.M. Tang, S.C. Yu, K. Liao, C.T. Tan, K.A. Khor, P. Cheang, Tensile properties, tension–tension fatigue and biological response of polyetheretherketone–hydroxyapatite composites for load-bearing orthopedic implants, Biomaterials 24 (13) (2003) 2245–2250.
[379] M. Sobieraj, S.M. Kurtz, C.M. Rimnac, Notch sensitivity of PEEK in monotonic tension, Biomaterials 30 (33) (2009) 6485–6494.
[380] M.C. Sobieraj, J.E. Murphy, J.G. Brinkman, S.M. Kurtz, C.M. Rimnac, Notched fatigue behavior of PEEK, Biomaterials 31 (35) (2010) 9156–9162.
[381] M.B. Schaffler, E.L. Radin, D.B. Burr, Mechanical and morphological effects of strain rate on fatigue of compact bone, Bone 10 (3) (1989) 207–214.
[382] K. Choi, S.A. Goldstein, A comparison of the fatigue behavior of human trabecular and cortical bone tissue, J. Biomech. 25 (2) (1992) 1371–1381.
[383] P. Zioupos, M. Gresle, K. Winwood, Fatigue strength of human cortical bone: age, physical, and material heterogeneity effectsJ, Biomed. Mater. Res. A 86A (3) (2008) 627–636.
[384] A. Vadiraj, M. Kamaraj, Characterization of fretting fatigue damage of PVD TiN coated biomedical titanium alloys, Surf. Coatings Technol. 200 (14–15) (2006) 4538–4542.
[385] P.P. Yicheng, D. Jarlen, P.C. Tsuchin, M. Ajay, Influence of diamond-like carbon coatings on the fatigue behavior of spinal implant rod, in: T. Proulx (Ed.), Time Depend. Const. Behav. Fract. Process., vol. 3, Springer, New York, 2011, pp. 383–389.
[386] K. Sadananda, R.L. Holtz, Review of fatigue of coatings/substrates, in: G.-M. Chow, I.A. Ovid'ko, T. Tsakalakos (Eds.), Nanostructured Film Coatings, Springer, Netherlands, Dordrecht, 2000, pp. 283–295.
[387] R.A. Antunes, M.C.L. de Oliveira, Corrosion fatigue of biomedical metallic alloys: mechanisms and mitigation, Acta Biomater. 8 (3) (2012) 937–962.
[388] J.J. Kruzic, R.M. Cannon, J.W. Ager, R.O. Ritchie, Fatigue threshold R-curves for predicting reliability of ceramics under cyclic loading, Acta Mater. 53 (9) (2005) 2595–2605.
[389] S. Gallops, T. Fett, J.J. Kruzic, Fatigue threshold R-curve behavior of grain bridging ceramics: role of grain size and grain-boundary adhesion, J. Am. Ceram. Soc. 94 (8) (2011) 2556–2561.
[390] M. Härtelt, S. Fünfschilling, T. Schwind, H. Riesch-Oppermann, T. Fett, J.J. Kruzic, Deducing the fatigue crack growth rates of natural flaws in silicon nitride ceramics: role of R-curves, J. Am. Ceram. Soc. 96 (8) (2013) 2593–2597.
[391] R.B. Greene, S. Fünfschilling, T. Fett, M.J. Hoffmann, J.J. Kruzic, Fatigue crack growth behavior of silicon nitride: roles of grain aspect ratio and intergranular film composition, J. Am. Ceram. Soc. 96 (1) (2013) 259–265.
[392] R.B. Greene, S. Fünfschilling, T. Fett, M.J. Hoffmann, J.J. Kruzic, Fatigue threshold R-curves predict fatigue endurance strength for self-reinforced silicon nitride, J. Am. Ceram. Soc. 97 (2) (2014) 577–583.
[393] F. Chevalier, Testing of medical devices, in: H.G. Vogel, J. Maas, F.J. Hock, D. Mayer (Eds.), Drug Discov. Eval. Saf. Pharmacokinet. Assays, Springer, Berlin, Heidelberg, 2013, pp. 1265–1271.
[394] S.M. Bradberry, J.M. Wilkinson, R.E. Ferner, Systemic toxicity related to metal hip prostheses, Clin. Toxicol. 52 (5) (2014) 837–847.
[395] C.H. Lohmann, Metallic debris from metal-on-metal total hip arthroplasty regulates periprosthetic tissues, World J. Orthop. 5 (5) (2014) 660–666.
[396] A.K. Matthies, J.A. Skinner, H. Osmani, J. Henckel, A.J. Hart, Pseudotumors are common in well-positioned low-wearing metal-on-metal hips, Clin. Orthop. Relat. Res. 470 (7) (2012) 1895–1906.
[397] M.G. Zywiel, J.-M. Brandt, C.B. Overgaard, A.C. Cheung, T.R. Turgeon, K.A. Syed, Fatal cardiomyopathy after revision total hip replacement for fracture of a ceramic liner, Bone Jt. J. 95B (1) (2013) 31–37.
[398] E. Yagil-Kelmer, P. Kazmier, M.N. Rahaman, B.S. Bal, R.K. Tessman, D.M. Estes, Comparison of the response of primary human blood monocytes and the U937 human monocytic cell line to two different sizes of alumina ceramic particles, J. Orthop. Res. 22 (4) (2004) 832–838.
[399] R. Ma, T. Tang, Current strategies to improve the bioactivity of PEEK, Int. J. Mol. Sci. 15 (4) (2014) 5426–5445.
[400] J.R. Jones, E. Gentlemen, J. Polak, Bioactive glass scaffolds for bone regeneration, Elements 3 (6) (2007) 393–399.
[401] B. Elliott, T. Goswami, Implant material properties and their role in micromotion and failure in total hip arthroplasty, Int. J. Mech. Mater. Des. 8 (1) (2011) 1–7.
[402] G. Manivasagam, D. Dhinasekaran, A. Rajamanickam, Biomedical implants: corrosion and its prevention—a review, Recent Patents Corros. Sci. 2 (2010) 40–54.
[403] H. Warashina, S. Sakano, S. Kitamura, K.-I. Yamauchi, J. Yamaguchi, N. Ishiguro, Y. Hasegawa, Biological reaction to alumina, zirconia, titanium and polyethylene particles implanted onto murine calvaria, Biomaterials 24 (21) (2003) 3655–3661.
[404] R.G. Munro, Evaluated material properties for a sintered α-alumina, J. Am. Ceram. Soc. 80 (8) (1997) 1919–1928.
[405] J. Melendezmartinez, Creep of silicon nitride, Prog. Mater. Sci. 49 (1) (2004) 19–107.
[406] D.A. Bonnell, T.Y. Tien, M. Ruhle, Controlled crystallization of the amorphous phase in silicon nitride ceramics, J. Am. Ceram. Soc. 70 (7) (1987) 460–465.
[407] P.K. Chu, L. Li, Characterization of amorphous and nanocrystalline carbon films, Mater. Chem. Phys. 96 (2–3) (2006) 253–277.
[408] K.J. Hamelynck, D.J. Woodnutt, R. Rice, G. Bongaerts, Ceramic surface engineering of the articulating surfaces effectively minimizes wear and corrosion of metal-on-metal hip prostheses, in: Tribol. Total Hip Arthroplast, Springer, Berlin, Heidelberg, 2011, pp. 113–119.
[409] G. Wang, H. Zreiqat, Functional coatings or films for hard-tissue applications, Materials (Basel) 3 (7) (2010) 3994–4050.
[410] D. Galusková, M. Hnatko, D. Galusek, P. Šajgalík, Corrosion of structural ceramics under subcritical conditions in aqueous sodium chloride solution and in deionized water. Part I: dissolution of Si_3N_4-based ceramics, J. Am. Ceram. Soc. 94 (9) (2011) 3035–3043.
[411] L. Ćurković, M.F. Jelača, S. Kurajica, Corrosion behavior of alumina ceramics in aqueous HCl and H_2SO_4 solutions, Corros. Sci. 50 (3) (2008) 872–878.
[412] W. Genthe, H. Hausner, Influence of chemical composition on corrosion of alumina in acids and caustic solutions, J. Eur. Ceram. Soc. 9 (6) (1992) 417–425.
[413] D. Shikha, U. Jha, S.K. Sinha, A.K. Singh, P.K. Barhai, K.G.M. Murleedharan Nair, S. Dash, A.K. Tyagi, et al., A comparative study of corrosion resistance in ringer solution of nitrogen-implanted alumina at different energies for orthopedic implants, Int. J. Appl. Ceram. Technol. 7 (2) (2010) 156–163.
[414] K.R. Mikeska, S.J. Bennison, Corrosion of alumina in aqueous hydrofluoric acid, J. Am. Ceram. Soc. 82 (12) (1999) 3561–3566.
[415] K.R. Mikeska, S.J. Bennison, S.L. Grise, Corrosion of ceramics in aqueous hydrofluoric acid, J. Am. Ceram. Soc. 83 (5) (2000) 1160–1164.
[416] K. Oda, T. Yoshio, Hydrothermal corrosion of alumina ceramics, J. Am. Ceram. Soc. 80 (12) (1997) 3233–3236.

[417] M. Schacht, N. Boukis, E. Dinjus, Corrosion of alumina ceramics in acidic aqueous solutions at high temperatures and pressures, J. Mater. Sci. 35 (24) (2000) 6251–6258.
[418] M.G. Lawson, F.S. Pettit, J.R. Blachere, Hot corrosion of alumina, J. Mater. Res. 8 (8) (1993) 1964–1971.
[419] D. Shikha, U. Jha, S.K. Sinha, Improvement in corrosion resistance of biomaterial alumina after 60 keV nitrogen ion implantation, Int. J. Cerem. Technol. 5 (1) (2008) 44–48.
[420] M. Schacht, N. Boukis, E. Dinjus, K. Ebert, R. Janssen, F. Meschke, N. Claussen, Corrosion of zirconia ceramics in acidic solutions at high pressures and temperatures, J. Eur. Ceram. Soc. 18 (1998) 2373–2376.
[421] ZTA Alumina Zirconia Platelet Composite, CeramTec AG Corp. Broch. <www.ceramtec.com> (2014).
[422] M. Herrmann, B. Seipel, J. Schilm, K.G. Nickel, G. Michael, A. Krell, Hydrothermal corrosion of zirconia-toughened alumina (ZTA) at 200 °C, J. Eur. Ceram. Soc. 25 (10) (2005) 1805–1812.
[423] C. ?H. Lin, K. Komeya, T. Meguro, J. Tatami, Y. Abe, M. Komatsu, Corrosion resistance of wear resistant silicon nitride ceramics in various aqueous solutions, J. Cerem. Soc Jpn. 111 (7) (2003) 452–456.
[424] M. Herrmann, J. Schilm, W. Hermel, A. Michaelis, Corrosion behavior of silicon nitride ceramics in aqueous solutions, J. Ceram. Soc. Jpn. 114 (11) (2006) 1069–1075.
[425] T. Sato, Y. Tokunaga, T. Endo, M. Shimada, K. Komeya, M. Komatsu, T. Kameda, Corrosion of silicon nitride ceramics in aqueous hydrogen chloride solutions, J. Am. Ceram. Soc. 71 (12) (1988) 1074–1079.
[426] S.W. Sharkaway, A.M. El-Aslabi, Corrosion of silicon nitride ceramics in aqueous HCL and HF solutions at 27–80 °C, Corros. Sci. 40 (7) (1998) 1119–1129.
[427] T. Sato, Y. Tokunaga, T. Endo, M. Shimada, K. Komeya, K. Nishida, M. Komatsu, T. Kameda, Corrosion of silicon nitride ceramics in aqueous HF solutions, J. Mater. Sci. 23 (1988) 3440–3446.
[428] F. Monteverde, C. Mingazzini, M. Giorgi, A. Bellosi, Corrosion of silicon nitride in sulphuric acid aqueous solution, Corros. Sci. 43 (10) (2001) 1851–1863.
[429] B. Seipel, K.G. Nickel, Corrosion of silicon nitride in aqueous acidic solutions: penetration monitoring, J. Eur. Ceram. Soc. 23 (4) (2003) 595–602.
[430] J. Schilm, M. Herrmann, G. Michael, Kinetic study of the corrosion of silicon nitride materials in acids, J. Eur. Ceram. Soc. 23 (4) (2003) 577–584.
[431] M. Herrmann, J. Schilm, G. Michael, J. Meinhardt, R. Flegler, Corrosion of silicon nitride materials in acidic and basic solutions and under hydrothermal conditions, J. Eur. Ceram. Soc. 23 (4) (2003) 585–594.
[432] N. Uchida, K. Uematsu, T. Kurita, K. Yoshimoto, Y. Suzuki, Corrosion of silicon nitride ceramics by nitric acid, in: Mater. Res. Symp. Proc., Cambridge University Press, Cambridge, UK, 1992, pp. 533–538.
[433] K. Oda, T. Yoshio, Y. Miyamoto, M. Koizumi, Hydrothermal corrosion of pure, hot isostatically pressed silicon nitride, J. Am. Ceram. Soc. 76 (5) (1993) 1365–1368.
[434] D.S. Fox, N.S. Jacobson, Molten-salt corrosion of silicon nitride: I, sodium carbonate, J. Am. Ceram. Soc. 71 (2) (1998) 128–138.
[435] N.S. Jacobson, D.S. Fox, F. Si, Molten-salt corrosion of silicon nitride: II, sodium sulfate, J. Am. Ceram. Soc. 71 (2) (1988) 139–148.
[436] M. Herrmann, Corrosion of silicon nitride materials in aqueous solutions, J. Am. Ceram. Soc. 96 (10) (2013) 3009–3022.
[437] L. Van Leaven, M.N. Alias, R. Brown, Corrosion behavior of ion plated and implated films, Surf. Coatings Technol. 53 (1) (1992) 25–34.
[438] Y. Massiani, A. Medjahed, J.P. Crousier, Corrosion of sputtered titanium nitride films deposited on iron and stainless steel, Surf. Coatings Technol. 45 (1–3) (1991) 115–120.
[439] U.K. Whala, L.M. DPenttinen, A.S. Korhonen, Improved corrosion resistance of physical vapour deposition coated TiN and ZrN, Surf. Coatings Technol. 41 (2) (1990) 191–204.
[440] H.W. Wang, M.M. Stack, Corrosion of PVD TiN coatings under simultaneous erosion in sodium carbonate/bicarbonate buffered slurries, Surf. Coatings Technol. 105 (1–2) (1998) 141–146.
[441] I. Milošev, B. Navinšek, A corrosion study of TiN (physical vapour deposition) hard coatings deposited on various substrates, Surf. Coatings Technol. 63 (3) (1994) 173–180.
[442] S.D. Chyou, H.C. Shih, T.T. Chen, On the corrosion characterization of titanium nitride in sulfuric acid solution, Corros. Sci. 35 (1–4) (1993) 337–347.
[443] W.-J. Chou, G.-P. Yu, J.-H. Huang, Corrosion resistance of ZrN films on AISI 304 stainless steel substrate, Surf. Coatings Technol. 167 (1) (2003) 59–67.
[444] Y. Cheng, Y.F. Zheng, A study of ZrN/Zr coatings deposited on NiTi alloy by PIIID technique, IEEE Trans. Plasma Sci. 34 (4) (2006) 1105–1108.
[445] H.W. Wang, M.M. Stack, S.B. Lyon, P. Hovsepian, W.-D. Münz, The corrosion behaviour of macroparticle defects in arc bond-sputtered CrN/NbN superlattice coatings, Surf. Coatings Technol. 126 (2–3) (2000) 279–287.
[446] F.Y. Zhou, B.L. Wang, K.J. Qiu, W.J. Lin, L. Li, Y.B. Wang, F.L. Nie, Y.F. Zheng, Microstructure, corrosion behavior and cytotoxicity of Zr–Nb alloys for biomedical application, Mater. Sci. Eng. C 32 (4) (2012) 851–857.
[447] I.-V. Branzoi, M. Iordoc, F. Branzoi, Evaluation of electrochemical behaviour and surface properties for oxinium-like Zr–Nb biomedical alloys, Key Eng. Mater. 415 (2009) 13–16.
[448] G. Singh, S. Singh, S. Prakash, Characterization and corrosion behavior of plasma sprayed pure and reinforced HA coatings in simulated body fluid, J. Miner. Mater. Charact. Eng. 10 (9) (2011) 765–775.
[449] C.T. Kwok, P.K. Wong, F.T. Cheng, H.C. Man, Characterization and corrosion behavior of hydroxyapatite coatings on Ti6Al4V fabricated by electrophoretic deposition, Appl. Surf. Sci. 255 (13–14) (2009) 6736–6744.
[450] J. Allain, S. Le Mouel, D. Goutallier, M.C. Voisin, Poor eight-year survival of cemented zirconia–polyethylene total hip replacements, J. Bone Jt. Surg. 81Br (5) (1999) 835–842.
[451] J. Chevalier, J.M. Drouin, B. Cales, Low temperature ageing behaviour of zirconia hip joint heads, Bioceramics 10 (October) (1997) 10–12.
[452] J. Chevalier, B. Cales, J.M. Drouin, Low-temperature aging of Y-TZP ceramics, J. Am. Ceram. Soc. 82 (8) (1999) 2150–2154.
[453] S. Chowdhury, Y. Vohra, Accelerating aging of zirconia femoral head implants: change of surface structure and mechanical properties, Mater. Res. Part B Appl. Biomater. 81B (2007) 486–492.
[454] S. Williams, M. Butterfield, T. Stewart, E. Ingham, M. Stone, J. Fisher, Wear and deformation of ceramic-on-polyethylene total hip replacements with joint laxity and swing phase microseparation, Proc. Inst. Mech. Eng. H. 217 (2) (2003) 147–153.
[455] M. Manaka, I.C. Clarke, K. Yamamoto, T. Shishido, A. Gustafson, A. Imakiire, Stripe wear rates in alumina THR-comparison of microseparation simulator study with retrieved implants, J. Biomed. Mater. Res. Part B Appl. Boimater. 69 (2) (2004) 149–157.
[456] T. Sato, M. Shimada, Transformation of yttria-doped tetragonal ZrO_2 polycrystals by annealing in water, J. Am. Ceram. Soc. 68 (6) (1985) 356–359.
[457] X. Guo, T. Schober, Water incorporation in tetragonal zirconia, J. Am. Ceram. Soc. 4887 (4) (2004) 746–748.
[458] M. Keuper, K. Eder, C. Berthold, K.G. Nickel, Direct evidence for continuous linear kinetics in the low-temperature degradation of Y-TZP, Acta Biomater. 9 (1) (2013) 4826–4835.
[459] S. Deville, J. Chevalier, G. Fantozzi, J.F. Bartolomé, J. Requena, J.S. Moya, R. Torrecillas, L.A. Díaz, Low-temperature ageing of zirconia-toughened alumina ceramics and its implication in biomedical implants, J. Eur. Ceram. Soc. 23 (15) (2003) 2975–2982.
[460] D. Gutknecht, J. Chevalier, V. Garnier, G. Fantozzi, Key role of processing to avoid low temperature ageing in alumina zirconia composites for orthopaedic application, J. Eur. Ceram. Soc. 27 (2–3) (2007) 1547–1552.
[461] G. Pezzotti, Toughening vs. environmental aging in BIOLOX® delta: a micromechanics study, in: J.-D. Chang, K. Billau (Eds.), Bioceram. Altern. Bear. Jt. Arthroplast. Proc. 12th Biol. Symp. Sep 7-8, 2007, Steinkopff, New York, 2007, pp. 163–168.
[462] G. Pezzotti, K. Yamada, A.A. Porporati, M. Kuntz, K. Yamamoto, Fracture toughness analysis of advanced ceramic composite for hip prosthesis, J. Am. Ceram. Soc. 92 (8) (2009) 1817–1822.
[463] G. Pezzotti, T. Saito, G. Padeletti, P. Cossari, K. Yamamoto, Nano-scale topography of bearing surface in advanced alumina/zirconia hip joint before and after severe exposure in water vapor environment, J. Ortho. Res. 28 (6) (2010) 762–766.
[464] A.V. Lombardi, K.R. Berend, B.E. Seng, I.C. Clarke, J.B. Adams, Delta ceramic-on-alumina ceramic articulation in primary THA: prospective, randomized FDA-IDE study and retrieval analysis, Clin. Orthop. Relat. Res. 468 (2) (2010) 367–374.
[465] P. Taddei, E. Modena, F. Traina, S. Affatato, Raman and fluorescence investigations on retrieved BIOLOX® delta femoral heads, J. Raman Spectrosc. 43 (12) (2012) 1868–1876.
[466] M. Swain, Stability of Mg-PSZ in high temperature steam environment, J. Mater. Sci. Lett. 4 (7) (1985) 848–850.
[467] T. Sato, S. Sato, A. Okuwaki, S.-I. Tanaka, Corrosion behavior of alumina ceramics in caustic alkaline solutions at high temperatures, J. Am. Ceram. Soc. 74 (12) (1991) 3081–3084.
[468] NIST-JANAF Thermochemical Tables <http://kinetics.nist.gov/janaf/> (2015).
[469] R.C. Dante, C.K. Kajdas, A review and a fundamental theory of silicon nitride tribochemistry, Wear 288 (2012) 27–38.
[470] J. Xu, K. Kato, Formation of tribochemical layer of ceramics sliding in water and its role for low friction, Wear 245 (1–2) (2000) 61–75.
[471] J.M. Calderón?Moreno, Stability of diamond-like carbon in hydrothermal conditions, Diam. Relat. Mater. 15 (4–8) (2006) 958–961.
[472] M.T. Raimondi, R. Pietrabissa, The in-vivo wear performance of prosthetic femoral heads with titanium nitride coating, Biomaterials 21 (9) (2000) 907–913.
[473] A. Šimůnek, J. Vackář, Hardness of covalent and ionic crystals: first-principle calculations, Phys. Rev. Lett. 96 (8) (2006) o85501.
[474] F. Gao, Hardness estimation of complex oxide materials, Phys. Rev. B 69 (9) (2004) o94113.
[475] F. Gao, J. He, E. Wu, S. Liu, D. Yu, D. Li, S. Zhang, Y. Tian, Hardness of covalent crystals, Phys. Rev. Lett. 91 (1) (2003) o15502.
[476] M.C. Galetz, E.W. Fleischmann, C.H. Konrad, A. Schuetz, U. Glatzel, Abrasion resistance of oxidized zirconium in comparison with C–CrMo and titanium nitride coatings for artificial knee joints, J. Biomed. Mater. Res. Part B Appl. Biomater. 93 (1) (2010) 244–251.
[477] H. Minakawa, M.H. Stone, B.M. Wroblewski, J.G. Lancaster, E. Ingham, J. Fisher, Quantification of third-body damage and its effect on UHMWPE wear with different types of femoral head, J. Bone Jt. Surg. 80Br (5) (1998) 894–899.

[478] R. Malikian, K. Maruthainar, J. Stammers, C.P. Wilding, G.W. Blunn, Four station knee simulator wear testing comparing titanium niobium nitride with cobalt chrome, J. Bioeng. Biomed. Sci. 3 (3) (2013) 1000125.
[479] A. Essner, K. Sutton, A. Wang, Hip simulator wear comparison of metal-on-metal, ceramic-on-ceramic and crosslinked UHMWPE bearings, Wear 259 (7–12) (2005) 907–913.
[480] S.C. Scholes, T.J. Joyce, Ceramic-on-ceramic joints: a suitable alternative material combination?, Adv. Biomater. Sci. Biomed. Appl. in: R. Pignatello (Ed.) (2013) 539–558.
[481] L. Mattei, F. Di Puccio, B. Piccigallo, E. Ciulli, Lubrication and wear modelling of artificial hip joints: a review, Tribol. Int. 44 (5) (2011) 532–549.
[482] J.R.T. Jeffers, W.L. Walter, Ceramic-on-ceramic bearings in hip arthroplasty: state of the art and the future, J. Bone Jt. Surg. 94Br (6) (2012) 735–745.
[483] J.J. Halma, J. Señaris, D. Delfosse, R. Lerf, T. Oberbach, S.M. van Gaalen, A. de Gast, Edge loading does not increase wear rates of ceramic-on-ceramic and metal-on-polyethylene articulations, J. Biomed. Mater. Res. Part B Appl. Biomater. 102 (8) (2014) 1–12.
[484] M. Al-Hajjar, L.M. Jennings, S. Begand, T. Oberbach, D. Delfosse, J. Fisher, Wear of novel ceramic-on-ceramic bearings under adverse and clinically relevant hip simulator conditions, J. Biomed. Mater. Res. Part B Appl. Biomater. 101 (8) (2013) 1456–1462.
[485] W. Zhu, L. Puppulin, A. Leto, Y. Takahashi, N. Sugano, G. Pezzotti, In situ measurements of local temperature and contact stress magnitude during wear of ceramic-on-ceramic hip joints, J. Mech. Behav. Biomed. Mater. 31 (2014) 68–76.
[486] M. Al-Hajjar, I.J. Leslie, J. Tipper, S. Williams, J. Fisher, L.M. Jennings, Effect of cup inclination angle during microseparation and rim loading on the wear of BIOLOX® delta ceramic-on-ceramic total hip replacement, J. Biomed. Mater. Res. Part B Appl. Biomater. 95 (2) (2010) 263–268.
[487] L. Puppulin, A. Leto, Z. Wenliang, N. Sugano, G. Pezzotti, Innovative tribometer for in situ spectroscopic analyses of wear mechanisms and phase transformation in ceramic femoral heads, J. Mech. Behav. Biomed. Mater. 31 (2014) 45–54.
[488] B.-J. Kang, Y.-C. Ha, D.-W. Ham, S.-C. Hwang, Y.-K. Lee, K.-H. Koo, Third-generation alumina-on-alumina total hip arthroplasty: 14–16 year follow-up study, J. Arthroplasty 30 (3) (2015) 411–415.
[489] P. Hernigou, S. Zilber, P. Filippini, A. Poignard, Ceramic–ceramic bearing decreases osteolysis: a 20-year study versus ceramic–polyethylene on the contralateral hip, Clin. Ortho. Relat. Res. 467 (9) (2009) 2274–2280.
[490] T.J. Heyse, J. Davis, S.B. Haas, D.X. Chen, T.M. Wright, R.S. Laskin, Retrieval analysis of femoral zirconium components in total knee arthroplasty: preliminary results, J. Arthroplasty 26 (3) (2011) 445–450.
[491] H. Dong, W. Shi, T. Bell, Potential of improving tribological performance of UHMWPE by engineering the Ti6Al4V counterfaces, Wear 225–229 (1999) 146–153.
[492] D. Klaffke, M. Griepentrog, U. Gross, I. Kranz, C. Knabe, Potential of wear resistant coatings on Ti–6Al–4V for artificial hip joint bearing surfaces, Wear 264 (7–8) (2008) 505–517.
[493] A.L. Galvin, L.M. Jennings, J.L. Tipper, E. Ingham, J. Fisher, Wear and creep of highly crosslinked polyethylene against cobalt chrome and ceramic femoral heads, Proc. Inst. Mech. Eng. Part HJ. Eng. Med. 224 (10) (2010) 1175–1183.
[494] J.A. Urban, K.L. Garvin, C.K. Boese, L. Bryson, D.R. Pedersen, J.J. Callaghan, R.K. Miller, Ceramic-on-polyethylene bearing surfaces in total hip arthroplasty: seventeen to twenty-one-year results, J. Bone Jt. Surg. 83Am (11) (2001) 1688–1694.
[495] C. Zietz, D. Kluess, P. Bergschmidt, M. Haenle, W. Mittelmeier, R. Bader, Tribological aspects of ceramics in total hip and knee arthroplasty, Semin. Arthroplasty 22 (4) (2011) 258–263.
[496] B.M. Wroblewski, P.D. Siney, P.A. Fleming, Low-friction arthroplasty of the hip using alumina ceramic and cross-linked polyethylene. A 17-year follow-up report, J. Bone Jt. Surg. 87Br (9) (2005) 1220–1221.
[497] B.M. Spector, M.D. Ries, R.B. Bourne, W.S. Sauer, M. Long, G. Hunter, Wear performance of ultra-high molecular weight polyethylene on oxidized zirconium total knee femoral components, J. Bone Jt. Surg. 83Am (Suppl. 2, Part 2) (2001) 80–86.
[498] Y.-H. Kim, Comparison of polyethylene wear associated with cobalt–chromium and zirconia heads after total hip replacement, J. Bone Jt. Surg. 87Am (8) (2005) 1769–1776.
[499] K.A. Ezzet, J.C. Hermida, N. Steklov, D.D. D'Lima, Comparison of polyethylene wear associated with cobalt–chromium and zirconia heads after total hip replacement, J. Bone Jt. Surg. 87Am (8) (2005) 1769–1776.
[500] T.D. Stewart, J.L. Tipper, M.H. Stone, E. Ingham, J. Fisher, Wear of polyethylene against scratched metallic femoral heads in hip prostheses, in: J.P. Garino, G. Willmann (Eds.), Bioceram. Jt. Arthroplast. Proc. 7th Int. Biol. Symp., Thieme, Stuttgart, New York, 2002, pp. 31–33.
[501] J.G. Bowsher, I.C. Clarke, Thermal conductivity of femoral ball strongly influenced UHMWPE wear in a hip simulator, in: Trans. 53rd Annu. Meet. Orthop. Res. Soc. Orthopaedic Research Society, San Diego, CA, 2007, p. 0278.
[502] I. Clarke, G. Pezzotti, A. Lakshminarayanan, M. Burgett-Moreno, Silicon nitride bearings: an alternative to oxide ceramics in total hip arthroplasty, in: Proc. Annu. Meet. Int. Socieity Technol. Arthroplast., Kyoto, Japan, 2015, p. 2969.
[503] R. Hauert, C.V. Falub, G. Thorwarth, K. Thorwarth, C. Affolter, M. Stiefel, L.E. Podleska, G. Taeger, Retrospective lifetime estimation of failed and explanted diamond-like carbon coated hip joint balls, Acta Biomater. 8 (8) (2012) 3170–3176.
[504] M.K. Harman, S.A. Banks, W.A. Hodge, Case report: wear analysis of a retrieved hip implant with titanium nitride coating, J. Arthroplasty 12 (8) (1997) 938–945.
[505] A. Malviya, S. Lobaz, J. Holland, Mechanism of failure eleven years following a buechel pappas hip resurfacing, Acta Orthop. Belgium 73 (6) (2007) 791–794.
[506] C. van-der-Straeten, Evolution of metal ions from a titanium–niobium coated hip resurfacing up till 5 years, in: Proc. Annu. Meet. Int. Soc. Technol. Arthroplasty, Kyoto, Japan, 2015, p. 2919.
[507] E. Gibon, C. Scemama, B. David, M. Hamadouche, Oxinium femoral head damage generated by a metallic foreign body within the polyethylene cup following recurrent dislocation episodes, Ortho. Traumatol. Surg. Res. 99 (7) (2013) 865–869.
[508] R.W. McCalden, K.D. Charron, R.D. Davidson, M.G. Teeter, D.W. Holdsworth, Damage of an oxinium femoral head and polyethylene liner following 'routine' total hip replacement, J. Bone Jt. Surg. 93Br (3) (2011) 409–413.
[509] A.M. Kop, C. Whitewood, D.J.L. Johnston, Damage of oxinium femoral heads subsequent to hip arthroplasty dislocation: three retrieval case studies, J. Arthroplasty 22 (5) (2007) 775–779.
[510] W.L. Jaffe, E.J. Strauss, M. Cardinale, L. Herrera, F.J. Kummer, Surface oxidized zirconium total hip arthroplasty head damage due to closed reduction effects on polyethylene wear, J. Arthroplasty 24 (6) (2009) 898–902.
[511] W.Y. Matar, S.M. Jafari, C. Restrepo, M. Austin, J.J. Purtill, J. Parvizi, Preventing infection in total joint arthroplasty, J. Bone Jt. Surg. 92Am (Suppl. 2) (2010) 36–46.
[512] S. Senthi, J.T. Munro, R.P. Pitto, Infection in total hip replacement: meta-analysis, Int. Orthop. 35 (2) (2011) 253–260.
[513] M.M. Dowsey, T.N. Peel, P.F.M. Choong, Infection in Primary Hip and Knee Arthroplasty, Recent Adv. Arthroplast. in: S. Fokter (Ed.) Intechopen.com, Published Online (2012).
[514] D. Campoccia, L. Montanaro, C.R. Arciola, A review of the biomaterials technologies for infection-resistant surfaces, Biomaterials 34 (34) (2013) 8533–8554.
[515] K. Bazaka, M.V. Jacob, R.J. Crawford, E.P. Ivanova, Efficient surface modification of biomaterial to prevent biofilm formation and the attachment of microorganisms, Appl. Microbiol. Biotechnol. 95 (2) (2012) 299–311.
[516] L. Esteban-Tejeda, F. Malpartida, L.A. Díaz, R. Torrecillas, F. Rojo, J.S. Moya, Glass-(*n*Ag, *n*Cu) biocide coatings on ceramic oxide substrates, PLoS One 7 (3) (2012) e33135.
[517] A. Martinez, F. Guitián, R. López-Píriz, J.F. Bartolomé, B. Cabal, L. Esteban-Tejeda, R. Torrecillas, J.S. Moya, Bone loss at implant with titanium abutments coated by soda lime glass containing silver nanoparticles: a histological study in the dog, PLoS One 9 (1) (2014) e86926.
[518] B. Cabal, L. Alou, F. Cafini, R. Couceiro, D. Sevillano, L. Esteban-Tejeda, F. Guitian, R. Torrecillas, et al., A new biocompatible and antibacterial phosphate free glass–ceramic for medical applications, Sci. Rep. 4 (2014) 5440.
[519] ISO-22196, Measurement of Antibacterial Activity on Plastics and Other Non-Porous Surfaces (2011).
[520] ASTME2180, Standard Test Method for Determining the Activity of Incorporated Antimicrobial Agent(s) In Polymeric or Hydrophobic Materials (2012).
[521] ASTME2149, Standard Test Method for Determining the Antimicrobial Activity of Antimicrobial Agents Under Dynamic Contact Conditions (2013).
[522] Plastics-Evaluation of the Action of Microorganisms; in ISO 846. ISO Press, Geneva, Switzerland, 1997.
[523] M.-P. Ginebra, C. Canal, M. Espanol, E.B. Montufar, R.A. Perez, Bioceramic materials show reduced pathological biofilm formation, Key Eng. Mater. 631 (2015) 448–453.
[524] F. Hizal, N. Rungraeng, S. Jun, C.-H. Choi, Nano-engineered alumina surfaces for prevention of bacteria adhesions, 9th IEEE Int. Conf. Nano/Micro Eng. Mol. Syst. IEEE (2014) 17–22.
[525] K. Yamane, Y. Ayukawa, T. Takeshita, A. Furuhashi, Y. Yamashita, K. Koyano, Bacterial adhesion affinities of various implant abutment materials, Clin. Oral Implants Res. 24 (12) (2013) 1310–1315.
[526] M. Yoshinari, Y. Oda, T. Kato, K. Okuda, A. Hirayama, Influence of surface modifications to titanium on oral bacterial adhesion in vitro, J. Biomed. Mater. Res. 52 (2) (2000) 388–394.
[527] A.S.D. Al-Radha, D. Dymock, C. Younes, D. o'Sullivan, Surface properties of titanium and zirconia dental implant materials and their effect on bacterial adhesion, J. Dent. 40 (2) (2012) 146–153.
[528] L. Karygianni, A. Jähnig, S. Schienle, F. Bernsmann, E. Adolfsson, R. Kohal, J. Chevalier, E. Hellwig, et al., Initial bacterial adhesion on different yttria-stabilized tetragonal zirconia implant surfaces in vitro, Materials (Basel) 6 (12) (2013) 5659–5674.
[529] B. Grössner-Schreiber, J. Teichmann, M. Hannig, C. Dörfer, D.F. Wenderoth, S.J. ott, Modified implant surfaces show different biofilm compositions under in vivo conditions, Clin. Oral Implants Res. 20 (8) (2009) 817–826.
[530] T. Shida, H. Koseki, I. Yoda, H. Horiuchi, H. Sakoda, M. Osaki, Adherence ability of staphylococcus epidermidis on prosthetic biomaterials: an in vitro study, Int. J. Nanomed. 8 (2013) 3955–3961.
[531] L.D. Renner, D.B. Weibel, Physicochemical regulation of biofilm formation, MRS Bull. 36 (5) (2011) 347–355.

[532] M. Ribeiro, F.J. Monteiro, M.P. Ferraz, Infection of orthopedic Implants with emphasis on bacterial adhesion process and techniques used in studying bacterial–material interactions, Biomatter 2 (4) (2012) 176–194.
[533] K. Wang, C. Zhou, Y. Hong, X. Zhang, A review of protein adsorption on bioceramics, Interface Focus 2 (3) (2012) 259–277.
[534] C.J. Wilson, R.E. Clegg, Mediation of biomaterial-cell interactions by adsorbed proteins: a review, Tissue Eng. 11 (1–2) (2005) 1–17.
[535] K. Kiewetter, Z. Schwartz, D.D. Dean, B.D. Boyan, The role of implant surface characteristics in the healing of bone, Crit. Rev. Oral Biol. Med. 7 (4) (1996) 329–345.
[536] R.A. Gittens, T. McLachlan, Y. Cai, S. Berner, R. Tannenbaum, Z. Schwartz, K.H. Sandhage, B.D. Boyan, The effects of combined micro- submicron-scale roughness and nanoscale features on cell proliferation and differentiation, Biomaterials 32 (13) (2011) 3395–3403.
[537] Y.-T. Sul, B.-S. Kang, C. Johansson, H.-S. Um, C.-J. Park, T. Albrektsson, The roles of surface chemistry and topography in the strength and rate of osseointegration of titanium implants in bone, J. Biomed. Mater. Res. 89A (4) (2009) 942–950.
[538] K. Anselme, P. Davidson, A.M. Popa, M. Giazzon, M. Liley, L. Ploux, The interaction of cells and bacteria with surfaces structured at the nanometre scale, Acta Biomater. 6 (10) (2010) 3824–3846.
[539] A.F. Khan, M. Saleem, A. Afzal, A. Ali, Bioactive behavior of silicon substituted calcium phosphate based bioceramics for bone regeneration, Mater. Sci. Eng. C35 (1) (2014) 245–252.
[540] V.V. Nagineni, A.R. James, M. Alimi, C. Hofstetter, B.J. Shin, I. Njoku, A.J. Tsiouris, R. Härtl, Silicate-substituted calcium phosphate ceramic bone graft replacement for spinal fusion procedures, Spine (Phila. Pa. 1976) 37 (20) (2012) E1264–E1272.
[541] W. Waked, J. Grauer, Silicates and bone fusion, Orthopedics 31 (6) (2008) 591–597.
[542] M. Andreiotelli, H.J. Wenz, R.-J. Kohal, Are ceramic implants a viable alternative to titanium implants? A systematic literature review, Clin. Oral Implants Res. 20 (Suppl. 4) (2009) 32–47.
[543] P.N. De Aza, H. De Aza, S. De Aza, Crystalline bioceramic materials, Bol. Soc. Esp. Ceram. V. 44 (3) (2005) 135–145.
[544] P.N. De Aza, A.H. De Aza, P. Pena, S. De Aza, Bioactive glasses and glass–ceramics, Bol. Soc. Esp. Ceram. V. 46 (2) (2007) 45–55.
[545] A.N. Cormack, A. Tilocca, Structure and biological activity of glasses and ceramics, Philos. Trans. Ser. A Math. Phys. Eng. Sci. 370 (1963) (2012) 1271–1280.
[546] J.D. Bobyn, G.J. Stackpool, S.A. Hacking, M. Tanzer, J.J. Krygier, Characteristics of bone ingrowth and interface mechanics of a new porous tantalum biomaterial, J. Bone Jt. Surg. 81Br (5) (1999) 907–914.
[547] D.M. Findlay, K. Welldon, G.J. Atkins, D.W. Howie, A.C.W. Zannettino, D. Bobyn, The proliferation and phenotypic expression of human osteoblasts on tantalum metal, Biomaterials 25 (12) (2004) 2215–2227.
[548] R.K. Roeder, D. Ph, S.M. Smith, T.L. Conrad, N.J. Yanchak, C.H. Merrill, G.L. Converse, PEEK implants for interbody spinal fusion (October) (2009) 46–48.
[549] L. Meseguer-Olmo, V. Vicente-Ortega, M. Alcaraz-Baños, J.L. Calvo-Guirado, M. Vallet-Regí, D. Arcos, A. Baeza, In-vivo behavior of Si-hydroxyapatite/polycaprolactone/DMB scaffolds fabricated by 3D printing, J. Biomed. Mater. Res. 101A (7) (2013) 2038–2048.
[550] K.A. Hing, Bioceramic bone graft substitutes: influence of porosity and chemistry, Int. J. Appl. Ceram. Technol. 2 (3) (2005) 184–199.
[551] A. Ignatius, M. Peraus, S. Schorlemmer, P. Augat, W. Burger, S. Leyen, L. Claes, Osseointegration of alumina with a bioactive coating under load-bearing and unloaded conditions, Biomaterials 26 (15) (2005) 2225–2332.
[552] K. Schickle, A. Korsten, M. Weber, C. Bergmann, S. Neuss, H. Fischer, Towards osseointegration of bioinert ceramics: can biological agents be immobilized on alumina substrates using self-assembled monolayer technique? J. Eur. Ceram. Soc. 33 (13–14) (2013) 2705–2713.
[553] R. Burgkart, S. Eichhorn, S. Kerschbaumer, B. Theelke, T. Pandorf, J. Boxleitner, T. Obst, R. Gradinger, Mechanical and histological results of a porous ceramic coating based on an alumina composite, in: J.P. Cobb (Ed.), Mod. Trends THA Bear.—Mater. Clin. Perform., Springer, Berlin, Heidelberg, 2010, pp. 245–250.
[554] G. Schierano, F. Mussano, M.G. Faga, G. Menicucci, C. Manzella, C. Sabione, T. Genova, M.M. Von Degerfeld, et al., An alumina toughened zirconia composite for dental implant application: in vivo animal results, Biomed. Res. Int. (2014) 157360.
[555] J.J.P. Jaatinen, R.K. Korhonen, A. Pelttari, H.J. Helminen, H. Korhonen, R. Lappalainen, H. Kröger, Early bone growth on the surface of titanium implants in rat femur is enhanced by an amorphous diamond coating, Acta Ortho. 82 (4) (2011) 499–503.
[556] A. Calzado-Martín, L. Saldaña, H. Korhonen, A. Soininen, T.J. Kinnari, E. Gómez-Barrena, V.-M. Tiainen, R. Lappalainen, et al., Interactions of human bone cells with diamond-like carbon polymer hybrid coatings, Acta Biomater. 6 (8) (2010) 3325–3338.
[557] G. Sovak, A. Weiss, I. Gotman, Osseointegration of Ti6Al4V alloy implants coated with titanium nitride by a new method, J. Bone Jt. Surg. 82Br (2) (2000) 290–296.
[558] M. Rizzi, G. Gatti, M. Migliario, L. Marchese, V. Rocchetti, F. Renò, Effect of zirconium nitride physical vapor deposition coating on preosteoblast cell adhesion and proliferation onto titanium screws, J. Prosthet. Dent. 112 (5) (2014) 1103–1110.
[559] H.S. Khanuja, J.J. Vakil, M.S. Goddard, M.A. Mont, Cementless femoral fixation in total hip arthroplasty, J. Bone Jt. Surg. 93Am (5) (2011) 500–509.
[560] N. Sandiford, C. Doctor, S.S. Rajaratnam, S. Ahmed, D.J. East, K. Miles, A. Butler- Manuel, J.A.N. Shepperd, Primary total hip replacement with a furlong fully hydroxyapatite-coated titanium alloy femoral component: results at a minimum follow-up of 20 years, Bone Jt. J. 95B (4) (2013) 467–471.
[561] S. Bose, M. Roy, A. Bandyopadhyay, Recent advances in bone tissue engineering scaffolds, Trends Biotechnol. 30 (10) (2012) 546–554.
[562] Q. Fu, E. Saiz, M.N. Rahaman, A.P. Tomsia, Toward strong and tough glass and ceramic scaffolds for bone repair, Adv. Funct. Mater. 23 (2013) 5461–5476.
[563] M.N. Rahaman, Bioactive ceramics and glasses for tissue engineering, in: A.R. Boccaccini (Ed.), Tissue Eng. Using Ceram. Polym., Woohead Publishing, Ltd., New York, NY, 2014, pp. 67–114.
[564] C. Gao, Y. Deng, P. Feng, Z. Mao, P. Li, B. Yang, J. Deng, Y. Cao, et al., Current progress in bioactive ceramic scaffolds for bone repair and regeneration, Int. J. Mol. Sci. 15 (3) (2014) 4714–4732.
[565] M. Mravic, B. Péault, A.W. James, Current trends in bone tissue engineering, Biomed Res. Int. 2014 (2014) 865270.
[566] J. Venkatesan, S.K. Kim, Nano-hydroxyapatite composite biomaterials for bone tissue engineering—a review, J. Biomed. Nanotechnol. 10 (2014) 3124–3140.
[567] H. Cao, X. Liu, Plasma-sprayed ceramic coatings for osseointegration, Int. J. Appl. Ceram. Technol. 10 (1) (2013) 1–10.
[568] S. Bose, S. Tarafder, Calcium phosphate ceramic systems in growth factor and drug delivery for bone tissue engineering: a review, Acta Biomater. 8 (4) (2012) 1401–1421.
[569] Google Scholar with Key Search Terms, Hydroxyapatite, and Bone Tissue Engineering <www.scholar.google.com> (accessed 22.03.15) (2015).
[570] L.L. Hench, Chronology of bioactive glass development and clinical applications, New J. Glas. Ceram. 3 (2) (2013) 67–73.
[571] L.L. Hench, J.M. Polak, Third-generation biomedical materials, Science 295 (5557) (2002) 1014–1017.
[572] K. Matsui, H. Yoshida, Y. Ikuhara, Nanocrystalline, ultra-degradation-resistant zirconia: its grain boundary nanostructure and nanochemistry, Sci. Rep. 4 (2014) 4758.
[573] P. Palmero, L. Montanaro, H. Reveron, J. Chevalier, Surface coating of oxide powders: a new synthesis method to process biomedical grade nano-composites, Materials (Basel) 7 (7) (2014) 5012–5037.
[574] R. Torrecillas, J.S. Moya, L.A. Díaz, J.F. Bartolomé, A. Fernández, S. Lopez-Esteban, Nanotechnology in joint replacement, Nanomed. Nanobiotechnol. 1 (5) (2009) 540–552.
[575] C.F. Gutiérrez-González, A. Smirnov, J.F. Bartolomé, Aging effect on the tribological behavior of a novel 3Y-TZP/Nb biocomposite against ultra high molecular weight polyethylene, J. Am. Ceram. Soc. 95 (3) (2012) 851–854.
[576] A. Smirnov, J.F. Bartolomé, Mechanical properties and fatigue life of ZrO_2–Ta composites prepared by hot pressing, J. Eur. Ceram. Soc. 32 (15) (2012) 3899–3940.
[577] E. Fernandez- Garcia, J. Guillem-Marti, C.F. Gutierrez-Gonzalez, A. Fernandez, M.-P. Ginebra, S. Lopez-Esteban, Osteoblastic cell response to spark plasma- sintered zirconia/titanium cermets, J. Biomater. Appl. 29 (2014) 813–823.
[578] M.E. Roy, L.A. Whiteside, B.J. Katerberg, J.A. Steiger, Phase transformation, roughness, and microhardness of artificially aged yttria- and magnesia-stabilized zirconia femoral heads, J. Biomed. Mater. Res. 83A (4) (2007) 1096–1102.
[579] E. Alakoski, V.-M. Tiainen, A. Soininen, Y.T. Konttinen, Load-bearing biomedical applications of diamond- like carbon coatings—current status, Open Orthop. J. 2 (2008) 43–50.
[580] M. Azzi, P. Amirault, M. Paquette, J.E. Klemberg-Sapieha, L. Martinu, Corrosion performance and mechanical stability of 316L/DLC coating system: role of interlayers, Surf. Coatings Technol. 204 (24) (2010) 3986–3994.
[581] LifeLongJoints <http://www.lifelongjoints.eu> (2014).
[582] M. Bahraminasab, B.B. Sahari, K.L. Edwards, F. Farahmand, M. Arumugam, Aseptic loosening of femoral components-materials engineering and design considerations, Mater. Des. 44 (2013) 155–163.
[583] P.J. Rao, M.H. Pelletier, W.R. Walsh, R.J. Mobbs, Spine interbody implants: material selection and modification, functionalization and bioactivation of surfaces to improve osseointegration, Ortho. Surg. 6 (2) (2014) 81–89.
[584] M.P. Arts, J.F.C. Wolfs, T.P. Corbin, The CASCADE trial: effectiveness of ceramic versus PEEK cages for anterior cervical discectomy with interbody fusion; protocol of a blinded randomized controlled trial, BMC Musculoskelet. Disord. 14 (1) (2013) 244.
[585] B. Theelke, M. Kuntz, M. Zipperle, S. Eichhorn, T. Boxleitner, T. Pandorf, R. Burgkart, Development of osseointegrative ceramic coatings based on zpta—mechanical characterization and influence on the substrate, Bioceram. Dev. Appl., (2011) Artcile ID: 101202.
[586] K.S. Ely, A.C. Khandkar, R. Lakshminarayanan, A.A. Hofmann, Hip prosthesis with monoblock ceramic acetabular cup, US Patent 7695521 (2010).
[587] K.C. Laurenti, L.C. de, A. Haach, A.R. dos Santos Jr., J.D. de, A. Rollo, R.B. de, M. Reiff, A.M.M. Gaspar, B. de, M. Purquerio, C.A. Fortulan, Cartilage reconstruction using self-anchoring implant with functional gradient, Mater. Res. 17 (3) (2014) 638–649.
[588] J. Zhao, Z. Shen, W. Si, X. Wang, Bi-colored zirconia as dental restoration ceramics, Ceram. Int. 39 (8) (2013) 9277–9283.

[589] F. Böke, K. Schickle, H. Fischer, Biological activation of inert ceramics: recent advances using tailored self-assembled monolayers on implant ceramic surfaces, Materials (Basel) 7 (6) (2014) 4473–4492.
[590] J.C. Love, L.A. Estroff, J.K. Kriebel, R.G. Nuzzo, G.M. Whitesides, Self-assembled monolayers of thiolates on metals as a form of nanotechnology, Chem. Rev. 105 (4) (2005) 1103–1169.
[591] B. Bujoli, P. Janvier, M. Petit, Application of metal phosphonates to biotechnologies, in: A. Clearfiled, K.D. Demadis (Eds.), Met. Phosphonate Chem.—From Synth. to Appl., The Royal Society of Chemisty, Cambridge, UK, 2012, pp. 420–425.
[592] Orthobond <www.orthobond.com> (2015).
[593] M. Mrksich, G.M. Whitesides, Using self-assembled monolayers to understand the interactions of man-made surfaces with proteins and cells, Ann. Rev. Biophys. Biomol. Struct. 25 (1996) 55–78.
[594] J.E. Raynor, J.R. Capadona, D.M. Collard, T.A. Petrie, A.J. García, Polymer brushes and self-assembled monolayers: versatile platforms to control cell adhesion to biomaterials (review), Biointerphases 4 (2) (2009) FA3–A16.
[595] T. Moro, Y. Takatori, M. Kyomoto, K. Ishihara, M. Hashimoto, H. Ito, T. Tanaka, H. Oshima, et al., Long-term hip simulator testing of the artificial hip joint bearing surface grafted with biocompatible phospholipid polymer, J. Orthop. Res. 32 (3) (2014) 369–376.
[596] Y. Takatori, T. Moro, K. Ishihara, M. Kamogawa, H. Oda, T. Umeyama, Y.T. Kim, H. Ito, et al., Clinical and radiographic outcomes of total hip replacement with poly(2-methacryloyloxyethyl phosphorylcholine)-grafted highly cross-linked polyethylene liners: three-year results of a prospective consecutive series, Mod. Rheumatol. 25 (2015) 286–291.
[597] V. Campana, G. Milano, E. Pagano, M. Barba, C. Cicione, G. Salonna, W. Lattanzi, G. Logroscino, Bone substitutes in orthopaedic surgery: from basic science to clinical practice, J. Mater. Sci. Mater. Med. 25 (10) (2014) 2445–2461.
[598] R.A. Surmenev, M.A. Surmeneva, A.A. Ivanova, Significance of calcium phosphate coatings for the enhancement of new bone osteogenesis –a review, Acta Biomater. 10 (2) (2014) 557–579.
[599] B.-D. Hahn, Y.-L. Cho, D.-S. Park, J.-J. Choi, J. Ryu, J.-W. Kim, C.-W. Ahn, C. Park, et al., Effect of fluorine addition on the biological performance of hydroxyapatite coatings on Ti by aerosol deposition, J. Biomater. Appl. 27 (5) (2013) 587–594.
[600] H.-W. Yang, M.-H. Lin, Y.-Z. Xu, G.-W. Shang, R.-R. Wang, K. Chen, Osteogenesis of bone marrow mesenchymal stem cells on strontium-substituted nano-hydroxyapatite coated roughened titanium surfaces, Int. J. Clin. Exp. Med. 8 (1) (2015) 257.
[601] A. Farzadi, F. Bakhshi, M. Solati- Hashjin, M. Asadi- Eydivand, N.A. abu Osman, Magnesium incorporated hydroxyapatite: synthesis and structural properties characterization, Ceram. Int. 40 (4) (2014) 6021–6029.
[602] Y.M.B. Ismail, O. Bretcanu, K.W. Dalgarno, A.J. El Haj, Synthesis and in vitro biocompatibility of multi- substituted hydroxyapatite for bone tissue engineering applications, Eur. Cells Mater. 28 (4) (2014) 4.
[603] A.F. Steinert, L. Rackwitz, F. Gilbert, U. Nöth, R.S. Tuan, Concise review: the clinical application of mesenchymal stem cells for musculoskeletal regeneration: current status and perspectives, Stem Cells Transl. Med. 1 (3) (2012) 237–247.
[604] A. Oyane, X. Wang, Y. Sogo, A. Ito, H. Tsurushima, Calcium phosphate composite layers for surface- mediated gene transfer, Acta Biomater. 8 (6) (2012) 2034–2046.
[605] A. Rajendran, R.C. Barik, D. Natarajan, M.S. Kiran, Synthesis, phase stability of hydroxyapatite–silver composite with antimicrobial activity and cytocompatability, Ceram. Int. 40 (2014) 10831–10838.
[606] E. Marsich, F. Bellomo, G. Turco, A. Travan, I. Donati, S. Paoletti, Nano-composite scaffolds for bone tissue engineering containing silver nanoparticles: preparation, characterization and biological properties, J. Mater. Sci. Mater. Med. 24 (7) (2013) 1799–1807.
[607] S.B.S. Goodman, Z. Yao, M. Keeney, F. Yang, M. Kenney, The future of biologic coatings for orthopaedic implants, Biomaterials 34 (13) (2013) 1–10.
[608] D. Neut, R.J. Dijkstra, J.I. Thompson, C. Kavanagh, H.C. van der Mei, H.J. Busscher, A biodegradable gentamicin–hydroxyapatite-coating for infection prophylaxis in cementless hip prostheses, Eur. Cells Mater. 29 (2015) 42.
[609] G. Wei, P.X. Ma, Structure and properties of nano-hydroxyapatite/polymer composite scaffolds for bone tissue engineering, Biomaterials 25 (2004) (2004) 4749–4757.
[610] J. Venkatesan, I. Bhatnagar, P. Manivasagan, K.-H. Kang, S.-K. Kim, Alginate composites for bone tissue engineering: a review, Int. J. Biol. Macromol. 72C (2014) 269–281.
[611] A.M. Ferreira, P. Gentile, V. Chiono, G. Ciardelli, Collagen for bone tissue regeneration, Acta Biomater. 8 (9) (2012) 3191–3200.
[612] A.R. Costa-Pinto, R.L. Reis, N.M. Neves, Scaffolds based bone tissue engineering: the role of chitosan, Tissue Eng. Part B 17 (5) (2011) 331–347.
[613] K. Sariibrahimoglu, W. Yang, S.C.G. Leeuwenburgh, F. Yang, J.G.C. Wolke, Y. Zuo, Y. Li, J.A. Jansen, Development of porous polyurethane/strontium-substituted hydroxyapatite composites for bone regeneration, J. Biomed. Mater. Res. Part A o0A (2014) 1–10.
[614] M.P. Ginebra, T. Traykova, J.A. Planell, Calcium phosphate cements as bone drug delivery systems: a review, J. Control. Release 113 (2) (2006) 102–110.
[615] S. Panseri, C. Cunha, T. D'Alessandro, M. Sandri, A. Russo, G. Giavaresi, M. Marcacci, C.T. Hung, et al., Magnetic hydroxyapatite bone substitutes to enhance tissue regeneration: evaluation in vitro using osteoblast-like cells and in vivo in a bone defect, PLoS One 7 (6) (2012) e38710.
[616] D. Mata, F.J. Oliveira, M.A. Neto, M. Belmonte, A.C. Bastos, M.A. Lopes, P.S. Gomes, M.H. Fernandes, et al., Smart electroconductive bioactive ceramics to promote in situ electrostimulation of bone, J. Mater. Chem. B 3 (9) (2015) 1831–1845.
[617] D. Mata, F.J. Oliveira, N.M. Ferreira, R.F. Araújo, A.J.S. Fernandes, M.A. Lopes, P.S. Gomes, M.H. Fernandes, et al., Processing strategies for smart electroconductive carbon nanotube-based bioceramic bone grafts, Nanotechnology 25 (14) (2014) 145602.
[618] W. Jiang, J. Cheng, D.K. Agrawal, A.P. Malshe, H. Liu, Improved mechanical properties of nanocrystalline hydroxyapatite coating for dental and orthopedic implants, Mater. Res. Soc. Proc. 1140 (2009) HH03.
[619] V. Badami, B. Ahuja, Biosmart materials: breaking new ground in dentistry, Sci. World J. 986 (2014) 986912.
[620] K. Hashimoto, H. Irie, A. Fujishima, TiO_2 photocatalysis: a historical overview and future prospects, Jpn. J. Appl. Phys. 44 (12) (2005) 8269–8285.
[621] C. Yue, R. Kuijer, H.J. Kaper, H.C. van der Mei, H.J. Busscher, Simultaneous interaction of bacteria and tissue cells with photocatalytically activated, anodized titanium surfaces, Biomaterials 35 (9) (2014) 2580–2587.
[622] J. Parvizi, V. Antoci, N.J. Hickok, I.M. Shapiro, Selfprotective smart orthopedic implants, Expert Rev. Med. Devices 4 (1) (2007) 55–64.
[623] K. Vasilev, J. Cook, H.J. Griesser, Antibacterial surfaces for biomedical devices, Expert Rev. Med. Devices 6 (5) (2009) 553–567.
[624] K. Bruellhoff, J. Fiedler, M. Möller, Surface coating strategies to prevent biofilm formation on implant surfaces, Int. J. Artifical Organs 33 (9) (2010) 646–653.
[625] F. Barrère, T.A. Mahmood, K. de Groot, C.A. van Blitterswijk, Advanced biomaterials for skeletal tissue regeneration: instructive and smart functions, Mater. Sci. Eng. R. 59 (1–6) (2008) 38–71.
[626] U.G.K. Wegst, H. Bai, E. Saiz, A.P. Tomsia, R.O. Ritchie, Bioinspired structural materials, Nat. Mater. 14 (Januray) (2015) 23–36.
[627] R.A. Pérez, J.-E. Won, J.C. Knowles, H.-W. Kim, Naturally and synthetic smart composite biomaterials for tissue regeneration, Adv. Drug Deliv. Rev. 65 (4) (2013) 471–496.
[628] M.M. Porter Dr, J. McKittrick, It's tough to be strong: advances in bioinspired structural ceramic based materials, Am. Ceram. Soc. Bull. 93 (5) (2014) 18–24.
[629] B.M. Holzapfel, J.C. Reichert, J.-T. Schantz, U. Gbureck, L. Rackwitz, U. Nöth, F. Jakob, M. Rudert, et al., How smart do biomaterials need to be? A translational science and clinical point of view, Adv. Drug Deliv. Rev. 65 (4) (2013) 581–603.
[630] G. Daculsi, Smart scaffolds: the future of bioceramic, J. Mater. Sci. Mater. Med. 26 (4) (2015) 1–4.
[631] B. Su, S. Dhara, L. Wang, Green ceramic machining: a top–down approach for the rapid fabrication of complex−shaped ceramics, J. Eur. Ceram. Soc. 28 (11) (2008) 2109–2115.
[632] S. Mohanty, A.P. Rameshbabu, S. Mandal, B. Su, S. Dhara, Critical issues in near net shape forming via green machining of ceramics: a case study of alumina dental crown, J. Asian Cerem. Soc. 1 (3) (2013) 274–281.
[633] F. Gervaso, F. Scalera, S. Kunjalukkal Padmanabhan, A. Sannino, A. Licciulli, High-performance hydroxyapatite scaffolds for bone tissue engineering applications, Int. J. Appl. Ceram. Technol. 9 (3) (2012) 507–516.
[634] L. Yin, H.X. Peng, L. Yang, B. Su, Fabrication of three-dimensional inter-connective porous ceramics via ceramic green machining and bonding, J. Eur. Ceram. Soc. 28 (3) (2008) 531–537.
[635] N. Travitzky, A. Bonet, B. Dermeik, T. Fey, I. Filbert-Demut, L. Schlier, T. Schlordt, P. Greil, Additive manufacturing of ceramic-based materials, Adv. Eng. Mater. 16 (6) (2014) 729–754.
[636] E.M. Sach, J.S. Haggerty, M.J. Cima, P.A. Williams, Three-dimensional printing techniques, US Patent 5204055 (1993).
[637] E. Özkol, Rheological characterization of aqueous 3Y-TZP inks optimized for direct thermal ink-jet printing of ceramic components, J. Am. Ceram. Soc. 96 (4) (2013) 1124–1130.
[638] C. Mota, D. Puppi, F. Chiellini, E. Chiellini, Additive manufacturing techniques for the production of tissue engineering constructs, J. Tissue Eng. Regen. Med. 9 (174–190) (2015).
[639] P. Feng, Y. Deng, S. Duan, C. Gao, C. Shuai, S. Peng, Liquid phase sintered ceramic bone scaffolds by combined laser and furnace, Int. J. Mol. Sci. 150 (8) (2014) 14574–14590.
[640] W. Bian, D. Li, Q. Lian, X. Li, W. Zhang, K. Wang, Z. Jin, Fabrication of a bio-inspired beta-tricalcium phosphate/collagen scaffold based on ceramic stereolithography and gel casting for osteochondral tissue engineering, Rapid Prototyp. J. 18 (1) (2012) 68–80.
[641] F. Melchels, J. Feijen, D. Grijpma, A review on stereolithography and its applications in biomedical engineering, Biomaterials 31 (24) (2010) 6121–6130.
[642] B. Thavornyutikarn, N. Chantarapanich, K. Sitthiseripratip, G.A. Thouas, Q. Chen, Bone Tissue Engineering Scaffolding: Computer-Aided Scaffolding Techniques (2014).
[643] M. Vaezi, H. Seitz, S. Yang, A review on 3D micro-additive manufacturing technologies, Int. J. Adv. Manuf. Technol. 67 (5–8) (2013) 1721–1754.
[644] M. Cronskär, L.E. Rännar, M. Bäckström, Implementation of digital design and solid free-form fabrication for customization of implants in trauma orthopaedics, J. Med. Biol. Eng. 32 (2) (2012) 91–96.

[645] R. van Noort, The future of dental devices is digital, Dent. Mater. 28 (1) (2012) 3–12.
[646] R. Olszewski, Three-dimensional rapid prototyping models in cranio-maxillofacial surgery: systematic review and new clinical applications, Proc. Belgian R. Acad. Med. 2 (2013) 43–77.
[647] H. Kang, S.J. Hollister, F. La Marca, P. Park, C.-Y. Lin, Porous biodegradable lumbar interbody fusion cage design and fabrication using integrated global–local topology optimization with laser sintering, J. Biomech. Eng. 135 (10) (2013) 101013:1–101013:8.
[648] Y. Chen, K. Zhang, Y. Hao, Y. Hu, Research status and application prospects of digital technology in orthopaedics, Orthop. Surg. 4 (3) (2012) 131–138.
[649] Guidance Document For The Preparation of Premarket Notification For Ceramic Ball Hip Systems, FDA Website <http//www.fda.gov/RegulatoryInformation/Guidances/ucm080770.htm> (1995).
[650] L. Gremillard, L. Martin, L. Zych, E. Crosnier, J. Chevalier, A. Charbouillot, P. Sainsot, J. Espinouse, et al., Combining ageing and wear to assess the durability of zirconia-based ceramic heads for total hip arthroplasty, Acta Biomater. 9 (7) (2013) 7545–7555.
[651] D.E. Keyes, L.C. McInnes, C. Woodward, W. Gropp, E. Myra, M. Pernice, J. Bell, J. Brown, et al., Multiphysics simulations: challenges and opportunities, Int. J. High Perform. Comput. Appl. 27 (1) (2012) 4–83.
[652] A. Filippone, Theoretical framework for the simulation of transport aircraft flight, J. Aircr. 47 (5) (2010) 1679–1696.
[653] M.U. Khan, M. Moatamedi, M. Souli, T. Zeguer, Multiphysics out of position airbag simulation, Int. J. Crashworthiness 13 (2) (2008) 159–166.
[654] L. Geris, Regenerative orthopaedics: in vitro, in vivo. . . in silico, Int. Orthop. 38 (9) (2014) 1771–1778.
[655] A. Rajpura, D. Kendoff, T.N. Board, The current state of bearing surfaces in total hip replacement, Bone Jt. J. 96B (2) (2014) 147–156.
[656] V. Uskokovic, "The role of hydroxyl channel in defining selected physicochemical peculiarities exhibited by ydroxyapatite,", RSC Adv. 5 (46) (2015) 36614–36633.

Bryan J. McEntire is currently Chief Technology Officer for Amedica Corporation, a position which he has held since 2012. He previously served as Vice President of Manufacturing from 2004 and Vice President of Research from 2006. He received BS (*cum laude*) and MBA degrees in Materials Science and Engineering and Operations Management from the University of Utah in 1978 and 1982, respectively, and his Ph.D. from the Kyoto Institute of Technology in 2015. Dr. McEntire has more than 35 years of industrial experience in research, development and production of advanced ceramics, including prominent management positions at Ceramatec (Salt Lake City, UT, USA), Saint-Gobain Industrial Ceramics Corporation (Northboro, MA and E. Granby, CT, USA), Applied Materials Corporation (Santa Clara, CA, USA), and now at Amedica Corporation (Salt Lake City, UT, USA). Dr. McEntire is the author or coauthor of 37 peer reviewed publications and holds two patents. He was an invited short-course lecturer to the National Institute of Ceramic Engineers of the American Ceramic Society on the forming of ceramics for a 10-year period from 1986 to 1995. He was nominated and elevated to Fellow of the American Ceramic Society in 2012. His current research interests are in silicon nitride for biomedical applications.

B. Sonny Bal is an orthopaedic surgeon who graduated from Cornell University Medical College in New York City. He is Professor of Orthopaedic Surgery at the University of Missouri, Columbia, Missouri. His research interests relate to investigating silicon nitride ceramics in orthopaedic bearings. Dr. Bal serves as executive for Amedica Corporation in Salt Lake City, a company dedicated to commercializing silicon nitride ceramics for biomedical applications. He has a graduate business degree from the Kellogg School of Management at Northwestern University in Evanston, Illinois; and a law degree from the University of Missouri, Columbia School of Law. He has authored or co-authored more than 110 peer-reviewed journal articles and is a co-applicant in 13 U.S. patents for biomaterials-related research submissions. He became an honorary lifetime member of the International Society for Technology in Arthroplasty in 2013.

Mohamed N. Rahaman is a Professor in the Department of Materials Science and Engineering, Missouri University of Science and Technology (formerly the University of Missouri-Rolla). He received his B.A. and M.A. degrees from the University of Cambridge (UK), and his Ph.D. from University of Sheffield (UK). After holding appointments at the University of Leeds (UK), and the Lawrence Berkeley National Laboratory, Dr. Rahaman joined the University of Missouri in 1986, where he has taught courses in ceramic processing, sintering, and biomaterials. Dr. Rahaman is a Fellow of the American Ceramic Society, author of 4 textbooks on processing and sintering of ceramics, and the author/coauthor of over 250 articles. Dr. Rahaman's research interests include processing and sintering of advanced ceramics, bioceramics and bioactive glasses for bone repair, and engineered regeneration of bone and soft tissues.

Jérôme Chevalier is currently full Professor at the National Institute of Applied Sciences in France. After receiving his PhD in 1996 on the "Mechanical properties of biomedical grade zirconia," Dr. Chevalier was employed by the Saint-Gobain Group as a Ceramic Research Engineer. In 1997, he joined the National Institute of Applied Sciences (INSA) in Lyon. Professor Chevalier is currently Director of the Materials Science Laboratory MATEIS at INSA and oversees the work of 180 persons. He is a member of the Institut Universitaire de France, and Editor of the *Journal of the European Ceramic Society*. His career highlights include extensive work on the fatigue behavior of ceramics and the ageing process in zirconia based ceramics and composites. He has also developed a range of innovative ceramic materials and composites for healthcare applications, such as bi-phasic calcium phosphate porous scaffolds with a hierarchical porosity to allow bone ingrowth and drug release, porous glass-ceramic scaffolds, organic-inorganic composites, and zirconia-based nano-composites for dental and orthopedic applications. Professor Chevalier is currently leading the European LONGLIFE project for advanced multifunctional zirconia ceramics for long-lasting dental and orthopedic (spine) applications. He has authored or coauthored more than 160 papers and holds 10 patents. Professor Chevalier was also recently honored as a recipient of the prestigious "Innovation Medal" by the French Centre National de la Recherche Scientifique (CNRS).

Giuseppe Pezzotti is a full tenured professor and leader of the Ceramic Physics Laboratory at the Kyoto Institute of Technology, Japan, a position he has held since the year 2000. He graduated *summa cum laude* in mechanical engineering from Rome University "La Sapienza", Italy, in 1984 and holds three doctoral degrees in materials engineering (Osaka University), solid state physics (Kyoto University), and medical sciences (Tokyo Medical University), all obtained in Japan, the country where he has lived for the past 28 years. Fluent in Japanese, he was one of the first foreign nationals to obtain a tenured full professor position in a Japanese Government University. From 2002 to 2012, Professor Pezzotti served as the director of the Research Institute for Nanoscience at the Kyoto Institute of Technology. Since 2005, he has been an adjunct professor at the Department of Orthopaedic Research at Loma Linda University, Loma Linda, CA. In 2009, he was honored with an invited professorship from the Department of Medical Engineering at Osaka University, and since 2010 has been a visiting professor in the Department of Molecular Cell Physiology at the Kyoto Prefectural University of Medicine. Professor Pezzotti has published about 570 scientific papers, 1 book as a single author, 13 book chapters, and holds 8 patents, including a world patent regarding nanoscale stress microscopy for scanning electron microscopes. He has licensed his intellectual properties to more than 20 major industrial firms around the world and has served as their consultant. His book entitled "Advanced Materials for Joint Implants" (published in 2013) has quickly become a landmark for scientists and medical doctors working in the field of joint arthroplasty. In 2013, Professor Pezzotti became a Fellow of the Academy of Science of the Bologna Institute in appreciation of his advanced studies linking quantum mechanics to medical sciences.